Fakultät für Medizin

Friedrich-Schiedel Institut für Neurowissenschaften

Functional mapping of primary visual cortex in awake mice

Yonghai Zhang

Vollständiger Abdruck der von der Fakultät für Medizin der Technischen Universität München zur Erlangung des akademischen Grades eines

Doctor of Philosophy (Ph.D.)

genehmigten Dissertation.

Vorsitzender: Prof. Dr. Dr. Stefan Engelhardt

Betreuer: Prof. Dr. Arthur Konnerth

Prüfer der Dissertation:

1. apl. Prof. Dr. Helmuth Adelsberger

2. Prof. Dr. Thomas Misgeld

Die Dissertation wurde am 26.01.2017 bei der Fakultät für Medizin der Technischen Universität München eingereicht und durch die Fakultät für Medizin am 16.03.2017 angenommen.

Abstract

Cortical circuits consist of interconnected excitatory and inhibitory neurons. These neurons have highly diverse morphologies. Even in the same cortical layer, the dendritic and axonal arbors of a given class of inhibitory interneurons, for example, have highly distinct structures. The functional specificity of the various types of cortical neurons is largely unclear. Here, by using electrophysiological recordings combined with two-photon calcium imaging in the *in vivo* mouse brain, we first characterized the response properties of different types of interneurons of the primary visual cortex in awake behaving mice, and then we analyzed the response properties of defined, single neurons during distinct cortical states. The results reveal that the response properties of the three major interneuron groups, that is, parvalbumin (PV), somatostatin (SOM) and 5-hydroxytryptamine3A receptor (5HT3aR) positive interneurons were distinctly different in terms of baseline firing rates, sensory stimulation-evoked firing rates, peak response latencies and orientation selectivity indices. Moreover, we identified a new class of 5HT3aR positive interneurons, which was characterized by a unique and highly distinct activity profile. Morphological analyses demonstrated that this is a new type of giant basket cell (GBC) of the mouse visual cortex, which receives synaptic input from cortical layers 1 and 2/3 and provides synaptic output through a huge axonal arbor exclusively to layer 2/3 neurons. The immunohistochemical analysis demonstrated that GBCs are positive not only for 5HT3aR but also for Vasoactive intestinal peptide (VIP), Reelin and Cholecystokinin (CCK). We demonstrate that GBCs act as inhibitory hub cells that effectively control motions detection in L2/3 of awake animals. In conclusion, this study demonstrates that the structural diversity of inhibitory interneurons is associated with highly distinct functional features. This functional diversity was not anticipated in previous studies and emphasizes the need for systematic structure-function analyses of neurons in awake, behaving animals.

Abstract

Kortikale Netzwerke bestehen aus miteinander verbundenen erregenden und hemmenden Neuronen. Die Morphologie dieser Neuronen ist sehr vielgestaltig. Auch in derselben kortikalen Schicht weisen zum Beispiel die dendritischen und axonalen Verzweigungen einer gegebenen Klasse von inhibitorischen Interneuronen sehr unterschiedliche Strukturen auf. Die funktionelle Spezifität der verschiedenen Arten von kortikalen Neuronen ist weitgehend unklar. In dieser Arbeit wurden zunächst die in-vivo-Antworteigenschaften verschiedener Arten von Interneuronen des primären visuellen Kortex in wachen, sich verhaltenden Mäusen mittels elektrophysiologischer Ableitungen in Kombination mit Zwei-Photonen-Kalzium-Imaging charakterisiert. Danach analysierten wir die Antworteigenschaften definierter einzelner Neuronen im Verlauf verschiedener kortikaler Zustände. Die Ergebnisse zeigen, dass die Antworteigenschaften der drei Hauptgruppen von Interneuronen, nämlich der Parvalbumin- (PV), Somatostatin- (SOM) und 5-Hydroxytryptamin3A-Rezeptor- (5HT3aR) positiven Interneurone sich signifikant hinsichtlich der basalen und der durch sensorische Stimulation hervorgerufenen Aktionspotentialraten, der Latenzzeit bis zum Maximum der Antwort und der Orientierungsselektivitätsindizes unterschieden. Darüber hinaus identifizierten wir eine neue Klasse von 5HT3aR-positiven Interneuronen, die durch ein einzigartiges und sehr ausgeprägtes Aktivitätsprofil gekennzeichnet war. Morphologische Untersuchungen zeigten, dass es sich hierbei um eine neuartige Riesenkorbzelle (giant basket cell; GBC) des visuellen Kortex der Maus handelt, die synaptische Eingänge aus den kortikalen Schichten 1 und 2/3 erhält und einen synaptischen Ausgang über eine großen axonale Verzweigung exklusiv für Neuronen der Schicht 2/3 bereitstellt. Die immunhistochemische Analyse zeigte, dass GBCs nicht nur für 5HT3aR, sondern auch für das vasoaktive intestinale Peptid (VIP), Reelin und Cholecystokinin (CCK) positiv sind. Wir zeigen, dass GBCs als inhibitorische Knotenpunkte wirken, die die Detektion von Bewegung in L2/3 von wachen Tieren wirksam kontrollieren. Zusammenfassend zeigt diese Studie, dass die strukturelle Vielfalt der hemmenden Interneurone mit sehr

unterschiedlichen funktionellen Eigenschaften verbunden ist. Diese funktionelle Vielfalt wurde aufgrund früherer Studien nicht erwartet und betont die Notwendigkeit von systematischen Struktur-Funktions-Analysen von Neuronen in wachen Tieren mit genau definierten Verhaltensmustern.

Abbreviation

CCK: Cholecystokinin

DLGN: Dorsal lateral geniculate nucleus

DMSO: Dimethyl sulfoxide

EGFP: Enhanced Green Fluorescent Protein

5HT3aR+: 5-hydroxytryptamine3A receptor positive

GABA: Gamma-Aminobutyric acid

GBC: Giant Basket Cell

GFP: Green Fluorescent Protein

OGB-1: Oregon Green BAPTA-1

PFA: Paraformaldehyde

PV+: Parvalbumin positive

ROI: Region of Interest

SOM+: Somatostatin positive

VIP+: Vasoactive Intestinal Peptide positive

V1: Primary visual cortex

Table of content

1. Introduction 8

1.1. The mouse visual system 9

1.2. The mouse primary visual cortex 9

1.3. The mouse model in visual research 10

1.4. Cortical interneurons and their diversity 11

1.4.1. The PV+ interneuron group 12

1.4.2. The SOM+ interneuron group 12

1.4.3. The 5HT3aR+ interneuron group 12

1.4.4. Interneurons and their response properties in V1 13

1.5. Effects of brain states on the activity of cortical neuron 14

2. Material and methods 17

2.1. Transgenic and wild-type mice 17

2.2. Head-fixed animal preparation 17

2.3. In vivo loose cell-attached recording 19

2.4. In vivo multi-cell bolus loading 19

2.5. Two-photon targeted single cell electroporation 20

2.6. Two-photon calcium imaging 21

2.7. Post-hoc cell identification 22

2.7.1. Tissue preparation 22

2.7.2. Immunohistochemistry 22

2.7.3. Photo-bleaching of Alexa 647 23

2.7.4. 3D morphological reconstructions 24

2.7.5. DAB staining 24

2.8. Visual Stimulation 25

2.9.1. Analysis of electrophysiology data 25

2.9.2. Analysis of calcium imaging data 27

3. Results 28

3.1. Visual response properties of interneurons in the V1 of awake mouse 28

3.1.1. Visual response properties of 5HT3aR+ interneurons 28

3.1.2. Visual response properties of PV+ interneurons 32
3.1.3. Visual response properties of SOM+ interneurons 34
3.2. Suppressed-response interneurons in the V1 of awake mouse 35
3.2.1. Suppressed responses of 5HT3aR+ interneurons 35
3.2.2. Morphological and immunohistochemical characterization of the suppressed response interneurons 43
3.2.3. Suppressed responses of VIP+ interneurons 49
3.3. Effects of anesthesia on the neuronal activity in mouse V1 52
3.3.1. Effects of anesthesia on the activity of PV+ interneuron 52
3.3.2. Effects of anesthesia on the activity of SOM+ interneuron 54
3.3.3. Effects of anesthesia on the activity of suppressed response interneuron 54
3.3.4. Effects of anesthesia on the activity of pyramidal neurons 56
3.4. Effects of locomotion on the neuronal activity in mouse V1 62
3.4.1. Effects of locomotion on PV+ interneurons 63
3.4.2. Effects of locomotion on 5HT3aR+ interneurons 63
3.4.3. Effects of locomotion on SOM+ interneuron 70
3.4.4. Effects of locomotion on the neuronal activity of pyramidal cells 70
4. Discussion 75
4.1. Impairment of neuronal direction/orientation tuning by anesthesia 76
4.2. Response properties of the interneurons in the V1 of the awake mice 78
4.3. Locomotion-dependent binary responses of the neurons in mouse V1 81
4.4. Outlook 83
5. References 84
6. Acknowledgements 94
7. Publications 95

1. Introduction

The processing of sensory information in the neocortex involves highly specific patterns of firing activity in structurally and functionally diverse neurons. Based on their anatomical and physiological characteristics, cortical neurons can be classified into excitatory neurons, which undertake the signal transmission within and among various cortical areas, and inhibitory neurons, which gate signal flow and sculpt network dynamics (Tremblay et al., 2016). The excitatory neurons have relatively stereotyped properties, while the inhibitory interneurons, by contrast, are highly diverse in terms of their morphology, physiology, and immunohistochemistry (Markram et al., 2004; Tremblay et al., 2016). Many criteria were introduced in order to classify the cortical interneurons based on anatomical and immunohistochemical properties (DeFelipe et al., 2013). However, it is still unclear to which extent interneurons within the 'same group' according to one of those criteria, can also be functionally defined in the 'same group'. Therefore, it is essential to explore the common features of those functionally homologous neurons, which in turn, can help us to classify or manipulate subsets of cortical neurons in a more accurate way. In the studies reported in this thesis, I focused on the following questions:

1) How do different types of interneurons in the mouse primary visual cortex respond to the visual stimuli in the awake state?

2) What are the common morphological and immunohistochemical features of those interneurons with similar response patterns?

3) How do different animal states like anesthesia or locomotion affect the activity of cortical neurons?

1.1. The mouse visual system

The mouse, as a nocturnal animal, relies much on its whisker rather than the visual system to navigate the surrounding world. Some structures like the retina in the mouse visual system are specialized for low light vision. Similarly to the retina of other mammals, the mouse retina contains two kinds of photoreceptors, namely, rods and cons. The rod system has very low visual acuity but is highly sensitive to light. On the contrary, the cone system has very high visual acuity but is relatively insensitive to light (Purves et al., 2004). The mouse retina is rod-dominated with a numerical rod/cone ratio of roughly 35:1 (Jeon et al.,1998), which endows mice with a high sensitivity for low light vision at the expense of a visual acuity. The photoreceptors capture the light and respond with an electrical signal, which is then filtered by the three major classes of retinal interneurons: the horizontal, bipolar and amacrine cells (Jeon et al.,1998). After that, the signal is transmitted to the retinal ganglion cells, which in turn, project to more than 20 subcortical regions (Ling et al., 1998), including the dorsal lateral geniculate nucleus (dLGN) of the thalamus. Finally, the visual signal arrives at the V1 via the projections from the dLGN.

1.2. The mouse primary visual cortex

The primary visual cortex (V1) has been identified in all mammals, including primates, carnivores, and rodents (Krubitzer & Kaas, 2005). There are many similarities as well as diversities between the V1 regions of different species (Van Hooser, 2007). Previous studies have found that basic response properties of V1 neurons, like orientation or direction selectivity, the temporal and spatial frequency tuning, the presence of both simple and complex cells and the contrast-invariant tuning in the visual cortex of higher mammals like cats (Hubel and Wiesel, 1959) or monkeys (Hubel & Wiesel, 1968) are also found in the mouse V1 (Drager, 1975; Metin et al., 1988; Niell & Stryker, 2008). There are also many distinct differences between the V1 of the mouse and the V1 of other mammalian species. First, the preferred spatial frequency is different between mouse and other species. The preferred spatial frequency in the mouse ranged from 0.02 to 0.08 (median of 0.036) cycles per degree (cpd) (Niell & Stryker, 2008), which is much smaller

compared to 0.9 cpd in the cat and 1.5–4.2 cpd in macaques (Van Hooser 2007). Second, as shown in Figure1.1, the functional architecture in the visual cortex of carnivores and most primates (Hubel and Wiesel, 1962; Hubel et al., 1977), that is characterized by a columnar organization has not been detected in rodent V1 (Ohki et al., 2005; Ohki & Reid, 2007). Third, the response properties of the inhibitory interneurons in the mouse V1 are different from the other species. In the visual cortex of cats, which have a pinwheel-like orientation map (Bonhoeffer et al.,1991; Ohki et al., 2006), most layer 2/3 interneurons exhibit a clear preference for orientation (Azouz et al., 1997; Cardin et al., 2007). On the contrary, in the visual cortex of mice, which lack orientation columns, interneurons exhibit only weak to moderate selectivity (Kerlin et al., 2010; Niell & Stryker, 2008).

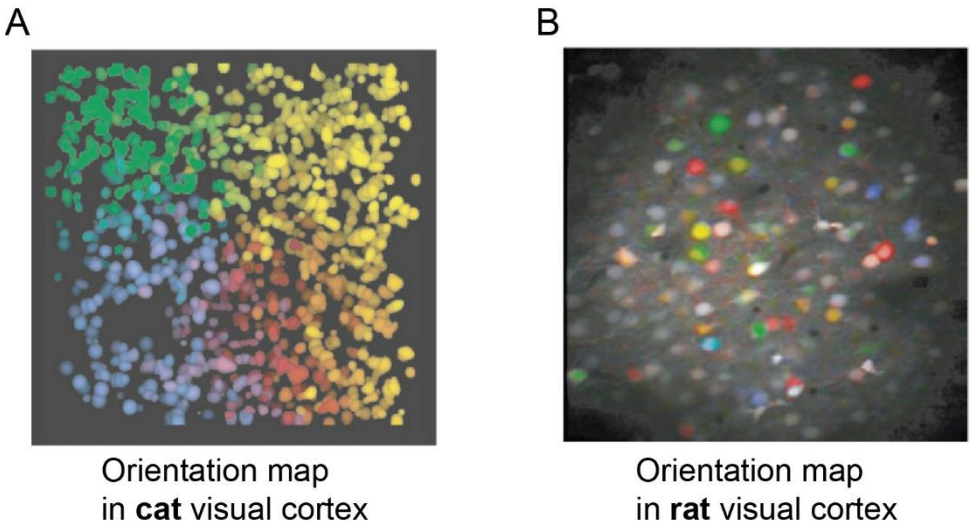

Figure 1.1. Single-cell resolution orientation maps from (**A**) a pinwheel in cat visual cortex and (**B**) rat visual cortex obtained with *in vivo* two-photon calcium imaging. Cells are colored according to their preferred orientation. In (**A**), ~1000 cells from nine different depths are overlaid. Cells are arranged up to the very center of the pinwheel in cat visual cortex. In (**B**), cells in one depth of rat visual cortex are displayed. Even neighboring cells are tuned to different orientations. (Modified from Ohki & Reid, 2007).

1.3. The mouse model in visual research

Experiments on the visual cortex have typically used carnivores or primates, mainly because these animals have a more refined visual system, including a much larger cortical region for visual processing, higher acuity, and their central visual pathways

display many of the same features found in humans (Issa et al.,2000; Nassi & Callaway, 2009; Van Hooser, 2007). In the past two decades, the mouse has become the dominant species in visual research for the following reasons. First, as mentioned before, the mouse V1 shares many fundamental properties with other species. Second, genetic tools provide good opportunities to facilitate new molecular, anatomical, and physiological approaches for investigating the brain (Fenno et al., 2011; Deisseroth & Schnitzer, 2013). Third, the smaller overall size of the mouse V1 spans only several millimeters across the cortical surface (Wang & Burkhalter, 2007), potentially allowing the entire system to be visualized simultaneously via two-photon mesoscopic imaging (Sofroniew et al., 2016). Lastly, due to the small body size, awake recordings are relatively stable in mice. We can, thus, use mice to study the effects of active wakefulness, like locomotion or whisking on the cortical neuronal activity using extracellular recording (Niell & Stryker, 2010), whole-cell recording (Gentet et al.,2012; Polack et al., 2013) and two-photon calcium imaging (Fu et al., 2014; Pakan et al., 2016).

1.4. Cortical interneurons and their diversity

Inhibitory interneurons account for 10-15% of all cortical neuron in rodents (Meyer et al., 2011) and use GABA (γ-aminobutyric acid) as their neurotransmitter. Different from excitatory cells in the cortex, neocortical interneurons are highly diverse regarding their morphology, intrinsic electrophysiological properties, molecular properties, laminar distribution, development and origin (Anderson et al., 1997; Xu et al., 2004; Tremblay et al., 2016). Due to these diversities, the task for the nomenclature and in particular, the classification of the interneurons is complicated and challenging (Ascoli et al., 2008; DeFelipe et al.,2013). Currently, the most efficient way to classify interneurons is based on three non-overlapping molecular markers, that is, parvalbumin (PV), somatostatin (SOM) and 5-hydroxytryptamine3A receptor (5HT3aR). The interneuron classes according to the expression of these three markers are named as parvalbumin-positive (PV+), somatostatin-positive (SOM+) and 5-hydroxytryptamine3A receptor positive (5HT3aR+) interneurons (Rudy et al., 2010; Tremblay et al., 2016).

1.4.1. The PV+ interneuron group

The PV+ interneuron group includes basket and chandelier cells and accounts for ~40% of the cortical interneuron population. The basket cells form axo-somatic synapses on the pyramidal cell somata with a basket-like appearance. Chandelier cells, also known as axo-axonic neurons, are characterized by a short vertical row of axon boutons resembling a chandelier. Unlike the basket cells, chandelier cells synapse on the axonal initial segment of their pyramidal targets. Both PV+ basket cells and chandelier cells are characterized by a fast spiking firing pattern. This electrophysiological property enables PV+ interneurons to show a quick reaction to the excitatory inputs and in turn, provide a feedforward inhibition.

1.4.2. The SOM+ interneuron group

SOM+ interneurons account for ~30% of the cortical interneuron population and can be subdivided into the Martinotti cells and non-Martinotti cells. Martinotti cells have distinct morphological features, that is, they project axons to layer 1 and spread horizontally across neighbor columns (Wang et al., 2004; Ma et al., 2006). Non-Martinotti cells are referred to as SOM+ interneurons lacking such morphological feature. SOM+ interneurons showed a clear laminar specificity, for example, SOM+ interneurons in layer 2/3 and layer 5 are mostly Martinotti cells and target on pyramidal cells. In the layer 4, SOM+ interneurons are non-Martinotti cells and target on PV+ interneurons in the same layer. In the layer 6, SOM+ interneurons consist of long-projecting GABAergic cells that can make either cortico-cortical or corticofugal projections (Yavorska & Wehr, 2016). Unlike PV+ interneurons, SOM+ interneurons are dendrite-targeting interneurons and thus act as a gate for input integration.

1.4.3. The 5HT3aR+ interneuron group

The 5HT3aR+ interneuron group, which accounts for ~30% of the cortical interneuron population, is the largest group of GABAergic interneurons in the superficial layers of neocortex (Lee et al., 2010; Miyoshi G et al., 2010). All 5HT3aR+ interneurons express functional 5HT3a and nicotinic receptors (Lee et al., 2010). Moreover, according to their

expression of the vasoactive intestinal peptide (VIP), 5HT3aR interneurons can be divided into VIP-positive cells and non-VIP positive cells. VIP+ cells attracted an increasing attention in the recent years because studies have shown that this type of interneurons is involved in specific inhibition-disinhibition circuits that consist of interconnected VIP+ interneurons and SOM+ interneurons (Lee et al., 2013; Pi et al.,2013; Fu et al., 2014).

1.4.4. Interneurons and their response properties in V1

In general, interneurons in the rodents' V1 are broadly tuned to the orientation of visual stimuli (Sohya et al., 2007; Kerlin et al.,2010), although some subtypes also have a sharp orientation selectivity (Runyan et al., 2010; Ma et al.,2010). Moreover, the functional inputs to distinct types of inhibitory interneurons are laminar specific (Xu et al., 2009; Ji et al., 2016). For example, PV+ interneurons in layer 2/3 receive inputs from pyramidal cells in the same layer as well as inputs from layer 4 while SOM+ interneurons in layer 2/3 mainly receive inputs from pyramidal cells in the same layer (Xu et al., 2009). On the other hand, 5HT3aR+ interneurons received a relative weak direct thalamocortical synaptic input (Lee et al., 2010), but strong inputs from higher cortical areas (Zhang et al., 2014). These differences in the synaptic input will, in turn, affect interneuron's response properties. For example, the spiking responses of the SOM+ and VIP+ interneurons show longer onset delays of responses to visual stimuli compared to PV+ interneurons and pyramidal cells (Ma et al., 2010; Mesik et al.,2015). Moreover, the SOM+ interneurons also showed weaker but more selective responses to drifting gratings than PV+ interneurons (Ma et al., 2010), although both PV+ and SOM+ showed robust and broadly tuned responses in the awake state (Polack et al.,2013).

So far, studies on response properties of interneurons in the visual cortex were mostly performed in the anesthetized state (but see Polack et al.,2013). To which extent, the tuning properties in the anesthetized state can reflect those in the natural state remained so far unclear. To fill this knowledge gap, it is necessary to carry out experiments in the awake state.

1.5. Effects of brain states on the activity of cortical neuron

Cortical activity is largely dependent on the behavioral states, for example, during wakefulness, cortical activity is characterized by low-amplitude fast oscillations (Gray et al., 1989; Steriade et al., 1996). In contrast, during slow-wave sleep and anesthesia, the brain shows low-frequency (<1 Hz) oscillations (Steriade et al. 1993, Stern et al. 1997). The differences in cortical activity in different behavioral states should affect sensory responses of cortical neurons. In the past, most of the experiments were done in the anesthetized animals. During anesthesia, the animal's state is relatively stable and easy to control. Moreover, anesthesia enables experimenters to perform stable and long-lasting recordings. However, the brain network dynamics are indeed altered by the anesthetic agents via various mechanisms (Franks, 2006). Therefore, it is important to determine how anesthesia alters the neuronal responses in the cortex. This was tested previously in the visual cortex of awake monkey which showed similar neuronal responses, comparing to the previous results from anesthetized animals. Recently, due to significant technical advancements, it became feasible to perform experiments on head-fixed or freely moving mice (Dombeck et al., 2007; Goldey et al., 2014). Inspired by the pioneering work from primates, similar comparisons of neuronal responses in the mouse visual cortex were performed. It was observed that, compared to the responses in the awake state, anesthesia increased the duration of sensory-evoked responses, reduced functional cortico-cortical connections (Sellers et al., 2015), and shortened the response latencies (Wang et al., 2014). Besides, the responses of inhibitory interneurons increased and became more reliable (Kimura et al., 2014) and, thus, generated an inhibition dominated brain state in awake mice (Haider et al., 2013). However, the receptive field properties were considered to be unchanged (Durand et al., 2016; Niell & Stryker, 2010).

One major concern here is that in these studies (except for Kimura et al., 2014), two datasets from different animals were used for the comparison between the two states. In other words, this comparison can only reflect the difference between two populations in

the different states. However, it can't reflect the functional status of the same neuron in the different states.

Wakefulness can be divided into quiet and active awake periods, depending on whether animals are resting or exhibiting exploratory movements (e.g. whisking or locomotion). The cortical neurons' performances are very different in these two states. In the somatosensory cortex, for example, Gentet et al., (Gentet et al., 2010) found that the membrane potentials of three different kinds of interneurons are different during whisking periods. Moreover, they found that the SOM+ interneuron's activity was suppressed in the active awake state (Gentet et al., 2012). In the visual cortex, locomotion can enhance neuronal responses to visual stimulus (Niell & Stryker, 2010). This enhancement is often mediated by an inhibition-disinhibition circuit consisting of VIP+ and SOM+ interneurons (Fu et al., 2014). However, recent studies by Pakan et al., (Pakan et al., 2016) challenged this model. They found that the interneuron's activity during locomotion is context-dependent. Interestingly, in the somatosensory cortex, Reimer et al. (Reimer et al., 2014) found two types of responses to locomotion, that is, type I cells showed depolarization to locomotion, while type II cells showed hyperpolarization to the locomotion. Together, these results reveal cell-type specific effects of locomotioin. So far, it is unclear whether such cell-type specific effects of locomotion exist in the same interneuron groups of the V1.

Using electrophysiological recordings, combined with two-photon calcium imaging in the in vivo mouse brain, we first characterized the response properties of different types of interneurons of the primary visual cortex in awake behaving mice and then we analyzed the response properties of defined, single neurons during distinct cortical states. The results reveal that the response properties of the three major interneuron groups were distinctly different in terms of baseline firing rates, sensory stimulation-evoked firing rates, peak response latencies and orientation selectivity indices. Moreover, we identified a new class of 5HT3aR positive interneurons, which was characterized by a unique and highly distinct activity profile. Morphological analyses demonstrated that this is a new type of giant basket cell (GBC) of the mouse visual cortex, which are positive not only for 5HT3aR

but also for VIP, Reelin and CCK. We demonstrate that GBCs act as inhibitory hub cells that effectively control motions detection in L2/3 of awake animals. In conclusion, this study demonstrates that the structural diversity of inhibitory interneurons is associated with highly distinct functional features. This functional diversity was not anticipated in previous studies and emphasizes the need for systematic structure-function analyses of neurons in awake, behaving animals.

2. Material and methods

All experimental procedures were performed in accordance with institutional animal welfare guidelines and were approved by the state government of Bavaria, Germany.

2.1. Transgenic and wild-type mice

Four transgenic mouse lines and C57BL/6 mice (wild type) were used in the current study. Transgenic mouse lines include: 1) PV-EGFP mice, in which the enhanced green fluorescent protein (EGFP) is expressed in parvalbumin-positive interneurons (Meyer et al., 2002). 2) GIN mice, in which Green Fluorescence Protein (GFP) is expressed in somatostatin-positive interneurons (Oliva et al.,2000). 3) 5HT3aR-EGFP mice, in which the Enhanced Green Fluorescent Protein (EGFP) is expressed in 5HT3aR-positive interneurons (Inta et al., 2008). 4) VIP-tdtomato mice, which are the result of interbreeding between homozygous Vip-ires-cre mice (The Jackson Laboratory) and homozygous Ai14 mice (The Jackson Laboratory). Offspring heterozygous for VIPcre/tdTomato, were used in this study.

2.2. Head-fixed animal preparation

Mice aged 7 to 10 weeks of both sexes were used in this study. A custom-made carbon fiber head-plate was implanted on the animal's skull several days before a recording session. Mice were anesthetized with isoflurane (3% induction, 1.0-1.5% maintenance) and then placed on a heating pad after reaching deep anesthesia level (no reflex to tail pinch). Body temperature was monitored and kept in a range of 37.0 to 37.5°C during surgery. Eye ointment (Bepanthen, Bayer, Germany) was applied on both eyes to prevent dehydration. Local anesthetic (Xylocaine,2%) was injected under the scalp, and a short-acting analgesic (Metamizole,200mg/kg) was subcutaneously injected to relieve the pain of the surgery. Skull was exposed by removing the scalp with a surgical scissor and periosteum on the skull was cleared with a scalpel blade. A thin layer of self-etch dental adhesive (OptiBond™ All-In-One™, Kerr Dental, USA) was brushed over the exposed skull and dried by dental curing light (MEGALUX soft-start, Mega-Physik, Germany),

which provides a substrate to which the other dental materials could adhere. The head-plate was then mounted on the top of the skull with a flowable composite (Tetric EvoFlow, Ivoclar Vivadent, Liechtenstein) covering most of the skull but keeping the skull above the primary visual cortex area exposed. The composite was then dried by dental curing light (MEGALUX soft-start, Mega-Physik, Germany). The gaps (unconnected parts between tetric evoflow and head-plate) were filled with dental cement (Paladur, Heraeus Kulzer, Germany). The exposed skull was covered by silicone elastomer (Kwik-Sil, WPI, USA). After the implantation, the anesthesia was stopped, and a long-acting analgesic was injected subcutaneously (Metacam, 1.5mg/kg). Animals were transferred back to the cage to recover when they became fully awake.

After the 3-days' recovery period, mice were habituated to the head-fixation on a free-spinning circular treadmill on which mice can rest or run freely. Animals underwent two sessions of 30 min in each day for two days. The movement of the treadmill was detected by a retroreflective sensor (Reflexions-Lichtschranke MRL 601, Germany) and acquired by a high-speed data acquisition digitizer (PXIe 5122, National Instruments) running at 20 MHz. Data acquisition was controlled by a custom-written software based on LabVIEW (LabVIEW 2012, National Instruments).

On the day of recording, mice were anesthetized with isoflurane (3% induction, 1.0-1.5% maintenance) and after reaching deep anesthesia level (no reflex to tail pinch), the mice were put on a heating pad. Body temperature was monitored and kept in a range of 37.0 to 37.5°C during surgery. A custom-made chamber was attached on the head-plate with cyanoacrylic glue (UHU, Buhl-Baden, Germany) to allow solution perfusion during recording. The silicone elastomer on the skull was removed, and a craniotomy of ~ 1 mm^2 above the monocular region of the primary visual cortex was made using a high-speed dental drill. The exposed cortical area was covered with 1.5% agarose dissolved in normal saline to increase recording stability. After surgery, the mouse was transferred to the recording setup and placed on the treadmill. The posterior part of the head-plate was tightly clamped with a mechanical clamper to fix the animal's head. The recording chamber was perfused with warm (36.5^{o}C) ACSF containing (in mM): 125 NaCl, 4.5 KCl,

26 $NaHCO_3$, 1.25 NaH_2PO_4, 2 $CaCl_2$, 1 $MgCl_2$, 20 glucose, pH 7.4, bubbled with 95% O_2 and 5% CO_2. To normalize recording situations and utilize comparisons between different animals, we started the awake recording at least 1 h after the termination of anesthesia. For the recording in the anesthetized state, animal's body temperature was kept at 37-37.5^{o}C, and the breathing rate was controlled to 90-110 beat per minute.

2.3. In vivo loose cell-attached recording

Somatic cell-attached recordings were obtained using an EPC10 amplifier (USB Quadro Amplifier; HEKA Elektronik, Germany) by the "shadow-patching" procedure (Kitamura et al. 2008). The patch pipette solution contained 50 μM Alexa Fluor 488 hydrazide sodium salt (Invitrogen) dissolved in ACSF. The pipettes had resistances of 4–6 MΩ. Once the tip of the pipette reached the target cell, a seal of 20-50 MΩ was achieved for loose patch recording. Electrophysiological data were filtered at 10 kHz and sampled at 20 kHz using Patchmaster software (HEKA Elektronik, Germany).

2.4. In vivo multi-cell bolus loading

The staining solution was prepared by following the protocols described before (Stosiek et al., 2003; Garaschuk et al., 2006). The calcium indicator dye Oregon Green BAPTA-1, AM (Molecular Probes™, USA) or Cal 520 AM (AAT Bioquest, USA), which is a recently developed calcium indicator dye with enhanced sensitivity and significantly higher signal to noise ratio (Tada et al., 2014), 50 μg was dissolved in 4 μL DMSO + 20% pluronic-127 and diluted to a final concentration of 1 mM with a solution containing (in mM) 150 NaCl, 2.5 KCl, 10 HEPES and Alexa 488 fluorescent dye (20 μM; Invitrogen) at pH 7.4. Pipettes (2-3 MΩ) were pulled from borosilicate glass capillaries (Hilgenberg GmbH) with a vertical puller (PC-10; Narishige).

To label neurons in the primary visual cortex of wild-type mice with the AM dye, a pipette filled with 1mM Cal520 AM or OGB-1 AM was inserted into the cortex and advanced 150-250 μm below the brain surface, and then the dye was pressure-ejected (1-2 min, 0.5-0.7 bar). Calcium imaging was performed 1h after the dye ejection.

For the different transgenic mouse lines that expressed EGFP in interneurons, a Z-

stack of images (each 90 µm x 90 µm, 80 Hz; step size 1 µm; from the surface to 300 µm below) was acquired before dye injection. Then, with the guidance of two-photon imaging, a pipette filled with the AM dye was inserted into the cortex and advanced to a location around the target area. The dye was pressure-ejected (2-3 min, 100-200 mBar). Calcium imaging was performed 1h after the dye ejection. The Z-stack acquired before was used as a reference to find the matching interneurons after AM staining (Figure 2.1).

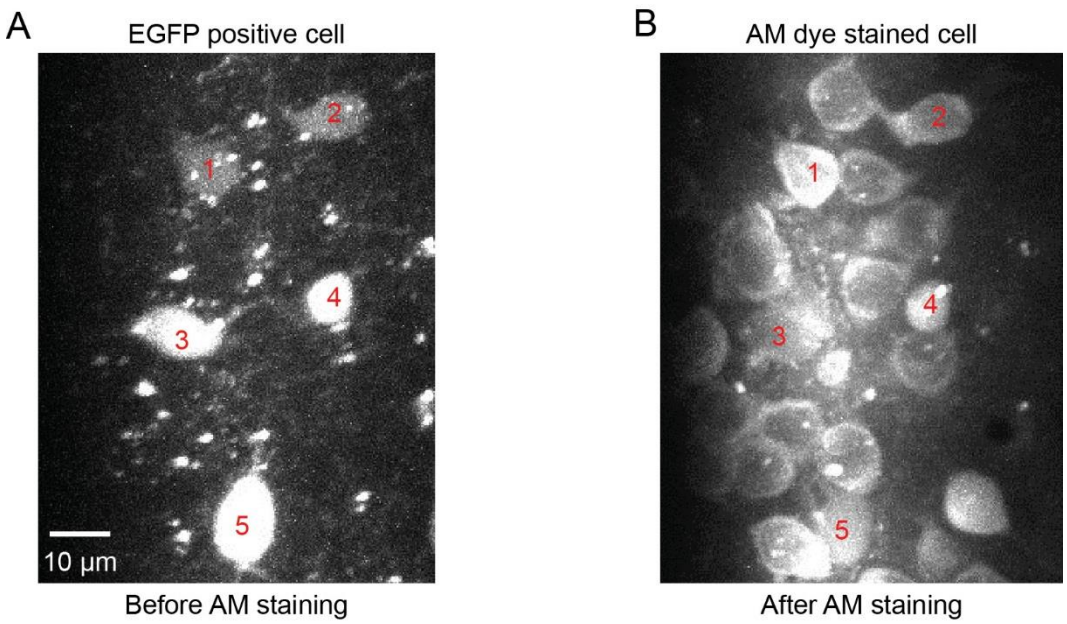

Figure 2.1. Staining of EGFP-expressing interneurons with Cal-520 AM calcium dye. (**A**) *In vivo* two photon image of EGFP-expressing interneurons before AM calcium dye staining. Interneurons were marked with numbers in red. (**B**) Image of EGFP-expressing interneurons after being stained by AM calcium dye (Cal-520 AM).

2.5. Two-photon targeted single cell electroporation

Pyramidal neurons or interneurons in layer 2/3 of primary visual cortex were electroporated with a custom-made electroporation device triggered by a pulse generator (Model 2100, A-M Systems, USA). The electroporation pipettes with resistance of 8-10 MΩ were pulled from borosilicate glass capillaries on a vertical puller (PC10, Narishige, Japan) and were filled with a solution containing (in mM): 135 NaCl, 5.4 KCl, 1.8 $CaCl_2$, 1 $MgCl_2$, 5 HEPES, 10 Oregon Green488 BAPTA-1 hexapotassium salt and 2% biocytin. The pH of the solution was adjusted to 7.2-7.3. Before penetrating the dura, a pressure

of 50-100 mBar was applied to the pipette and the pressure was decreased to ~20 mBar after the dura was penetrated. The pipette was carefully advanced in the brain to reach the target cell, and then the neuron was electroporated with 2-3 negative electrical pulses (pulse duration:50-100 ms, amplitude: 0.1-0.2 µA, pulse interval:1s). The success of the electroporation was judged by spontaneous calcium transients from the dendrite shaft 10-20 min after electroporation (Figure 2.2).

2.6. Two-photon calcium imaging

In vivo calcium imaging was carried out using a custom-built two-photon microscope (Chen et al., 2011). This scanning system consisted of a galvanic mirror (6215HM40, Cambridge Technology) for the slow y-scan and an acousto-optic deflector (AOD) (Crystal Technology Inc. 4150) for the fast x-scan. The AOD and galvanic mirror were controlled by signal generators (PXI 5412, National Instruments), synchronized by a high-speed data acquisition digitizer (PXIe 5122, National Instruments) running at 20 MHz. The data acquisition was controlled by a custom-written software based on LabVIEW (LabVIEW 2012, National Instruments). The scanning system was mounted on a standard upright microscope (BX51WI, Olympus) equipped with a water immersion objective (x40/0.8 NA/3.5WD, Nikon). The excitation wavelength was 925 nm. The average power delivered to the brain was in the range of 5–39 mW. In general, 5–10 trials (each trial had a recording period of 40–56 s) were recorded for each neuron.

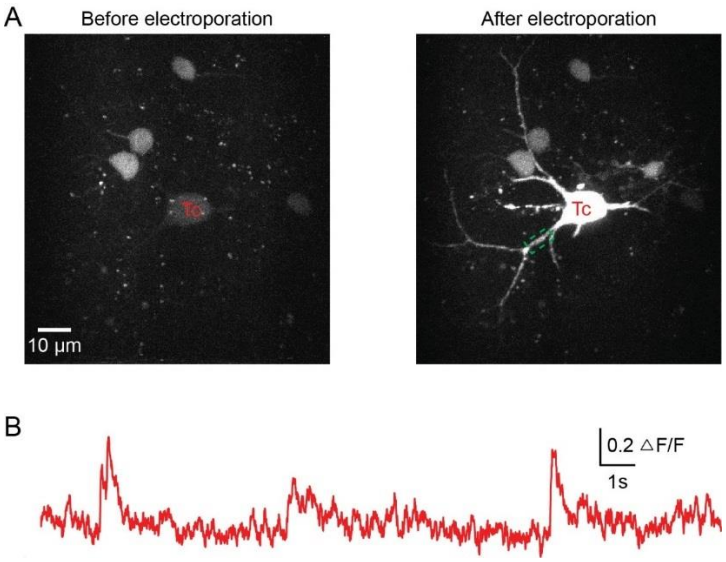

Figure 2.2. Targeted single-cell electroporation of an EGFP-expressing interneuron (**A**) Left: *In vivo* two photon image of EGFP-expressing interneurons in the primary visual cortex. Tc: Target cell for electroporation. Right: z-projection of the target cell after electroporation with 10 mM OGB-1. (**B**) Spontaneous calcium transients from a dendrite segment marked by a green dashed rectangle in (A), imaging was performed 10 min after electroporation.

2.7. *Post-hoc* cell identification

This part of the experiment was performed by Dr. Valérie Bonfardin (AG Arthur Konnerth, Institute of Neuroscience, TU Munich) and Dr. Monika Brill (AG Thomas Misgeld, Institute of Neuronal Cell Biology, TUM).

2.7.1. Tissue preparation

After the electroporation of the target cell with biocytin (2%), mice were fixed by 30 ml transcardiac perfusion of phosphate buffered saline 0.15 M (PBS), pH 7.4, followed by 100 ml paraformaldehyde 4 % containing picric acid 0.2 % and glutaraldehyde 0.1 %. Dissected brains were post-fixed overnight and then kept in PBS at 4° C prior slicing. Using a vibratome (Leica VT1000S), 70 µm coronal sections of the visual cortex were collected in PBS.

2.7.2. Immunohistochemistry

Sections were washed in PBS three times for 15 min each time. The biocytin was visualized after incubation overnight (4° C) with Streptavidin conjugated to Alexa 568 (S11226, Thermo Fisher Scientific, 1:200). Sections containing biocytin-positive 5HT3-interneurons were washed in PBS and incubated 4 days (at 4° C) in the following primary antibodies diluted in blocking solution (10 % normal goat serum, 1% BSA and 1 % Triton X-100 in PBS): anti-vasoactive intestinal peptide (VIP) (rabbit polyclonal, 1:1200; 20077, ImmunoStar), anti-reelin (mouse monoclonal IgG1, 1:1500; CR-50, MBL), anti-cholecystokinin (CCK) (mouse monoclonal IgG2a, 1:3000; ab37274, ABCAM), anti-neuropeptide Y (NPY) (rabbit polyclonal, 1:5000; N9528 Sigma), anti-calretinin (CR)

(guinea pig polyclonal, 1:1000; 214104, Synaptic Systems). An anti-EGFP primary antibody (chicken polyclonal, 1:2000; ab13970, ABCAM) was used to enhance the visibility of EGFP expression in 5HT3aR+ interneurons and to verify the identity of the electroporated cells; This antibody was incubated with the secondary antibodies overnight (at 4° C). Sections were washed with PBS 3 times, incubated overnight with suitable secondary antibodies as follows, and washed again : Anti-rabbit Dylight 405-conjugated (1 :1000 ; 111-475-144, Jackson ImmunoResearch), anti-mouse IgG1 Alexa 647-conjugated (1 :2000 ; A21240, Thermo Fisher Scientific), anti-guinea pig DyLight 405-conjugated (1 :500 ; 706-475-148, Jackson ImmunoResearch), anti-mouse IgG2a Alexa 647-conjugated (1:500; 115-607-186, Jackson ImmunoResearch). Sections were mounted in Vectashield (Vector Laboratories) and stacks of images were acquired for the immuno-identification of the electroporated cells using a confocal microscope (Olympus FV1000 on an upright stand) equipped with x10/0.40 N.A. air-, x20/0.85 N.A., x40/1.35 and x60/1.42 N.A. oil-immersion objectives. Maximum intensity projections were generated using the open source software ImageJ/Fiji (http://fiji.sc). Of note, two antibodies were first tested: Reelin and VIP, because these two peptides are expressed in the vast majority of 5HT3aR+ interneurons. When a cell was negative for one marker, then another marker could be tested.

2.7.3. Photo-bleaching of Alexa 647

Since hippocampal VIP-positive basket cells also express CCK (Hajos et al., 1996; Mátyás et al., 2004), we sought to determine this expression pattern in giant basket cell (GBC) we found in the visual cortex. To this end, we photo-bleached the Reelin (Alexa 647), as GBCs were also immunoreactive for VIP (405 nm), 5HT3-GFP (488 nm) and Biocytin-Streptavidin (568 nm). For photo-bleaching, we used a confocal microscope (FV1000, Olympus) equipped with an oil immersion objective (x60/N.A. 1.42). A rectangular ROI around the soma of the electroporated cell was drawn. The 635 nm laser beam was placed in the respective area, and this area was bleached at maximum power by slow line scanning (20 µs/pixel) in one plane for 10 min, repeating this for several

confocal planes. This procedure was repeated two times until the Alexa 647 fluorescence intensities were drastically reduced. We acquired a confocal image stack before and after photo-bleaching to ensure that the anti-Reelin staining could not be detected anymore. The photobleached slice was stained with an anti-CCK antibody and stacks of images were taken again at the confocal microscope.

2.7.4. 3D morphological reconstructions

Neuronal structures were traced manually using the Filament Editor of the software named 'AMIRA'. 3D image stacks typically 0.6 mm*0.6mm*0.07mm were acquired in the visual cortex at a resolution of 0.120*0.120*0.42 µm per voxel, using a confocal microscope (Olympus FV2000 on an upright stand) equipped with a x60/1.42 N.A. oil-immersion objective.

2.7.5. DAB staining

In some experiments, biocytin-filled cells were stained following a DAB staining protocol (Horikawa & Armstrong, 1988). In brief, after brain perfusion and fixation, 70 µm (for interneurons) or 100 µm (for pyramidal neurons) coronal sections of the visual cortex were collected in PBS. Then the following procedures were carried out on the slices:

1) Rinsed with 0.1M PB (4x10 min)
2) Rinsed with 1% H_2O_2 (in 0.1M PB) to block endogenous peroxidase activity (25 min).
3) Rinsed with 0.1M PB (4x10 min)
4) Incubated 1h in 2% TritonX-100 (in 0.1M PB).
5) Incubated overnight in 50ml 1% TritonX-100 (in 0.1M PB) containing a mixture of 10 drops Reagent A and 10 drops of Reagent B from ABC Kit (Vector Laboratory, USA)
6) Rinsed with 0.1M PB (4x10 min)
7) Incubated 5-10 min in 50ml 0.1M PB solution containing 0.05% of 3,3-diaminobenzidine and 0.003% H_2O_2.
8) Rinsed with 0.1M PB (4x10 min)

9) Slices were embedded in Mowiol and the biocytin-labeled cells were examined with an upright microscope (Axioplan; Zeiss, Germany) connected to the computerized reconstruction system Neurolucida (Microbrightfield, Colchester, VT). Neurons were digitally photographed by using the capability of Neurolucida with the x40/1.3 N.A. oil-immersion objective.

2.8. Visual Stimulation

Visual stimuli were generated by Matlab^{TM} (release 2007b; Mathworks Inc.) with the "Psychtoolbox" add-on package. From our preliminary data set recorded from the awake mice, we found a considerable portion of neurons in primary visual cortex that showed responses to the standing grating (indicated by visual stimulus without an arrow in Figure 2.3). Because of this, in the main part of study in this thesis, we used a visual stimulus protocol as follows: Each visual stimulation sequence started with a gray screen (mean luminance) for 4s, then, the drifting grating was presented at eight different directions (separated by 45°, 0.03 cpd, 1 Hz, contrast 80%,). Each drifting grating lasted for 2-4 seconds, followed by a mean luminance gray screen with the same amount of presenting time before the next grating. In each measurement, evoked activities were recorded from 5 to10 trials.

2.9. Data analysis

2.9.1. Analysis of electrophysiology data

Electrophysiology data were analyzed off-line by using custom-written procedures in Igor Pro based on the following calculations: 1) Baseline firing rate: baseline firing rate was calculated by averaging of cell's firing rate during gray screen periods. 2) Evoked

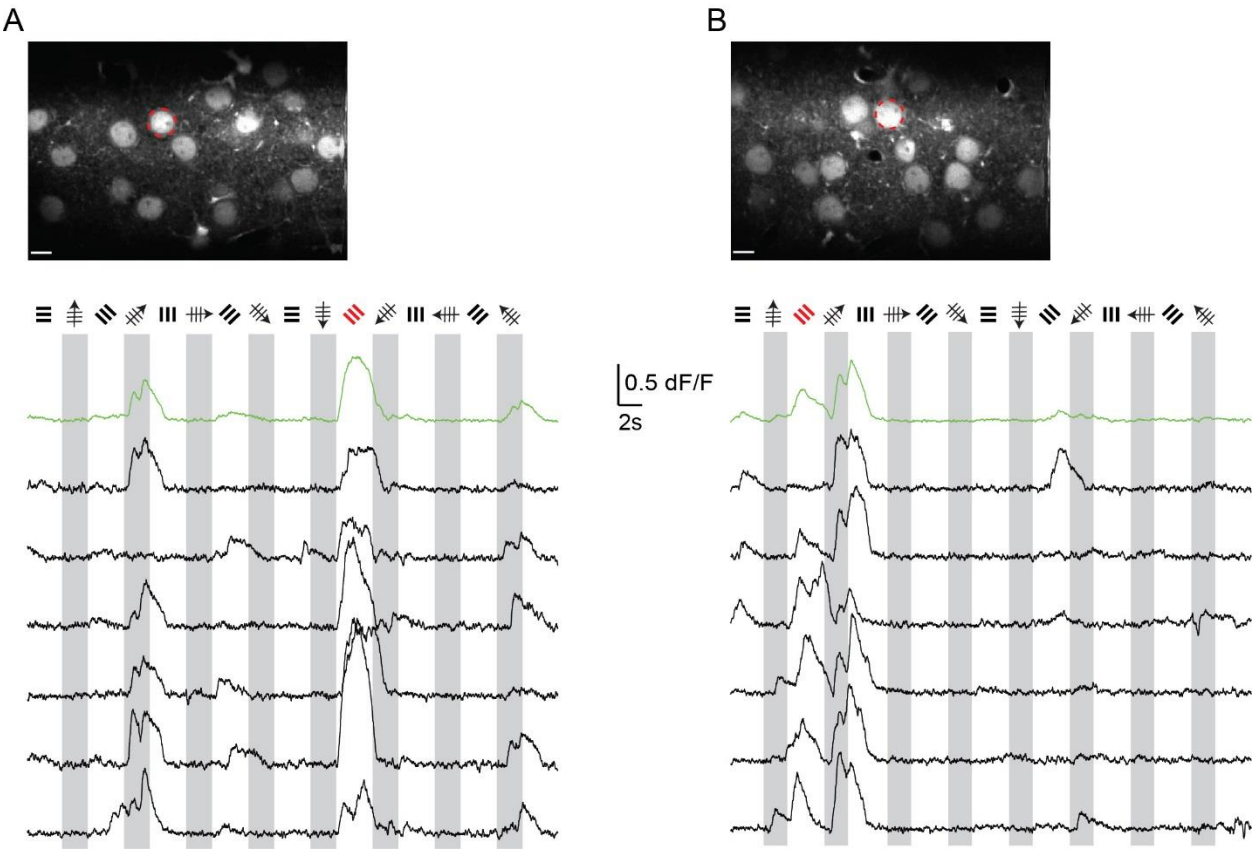

Figure 2.3. Standing grating responsive cells in the V1 of awake mouse

(**A**) Upper: In vivo two photon image of cortical layer 2/3 neurons labeled by AM calcium dye (OGB-1 AM). Lower: visual stimulus evoked calcium transient of the cell marked in the upper panel with a red dashed circle. The cell responded to one drifting grating direction and one standing grating direction (marked in red) (**B**) Upper: In vivo two photon image of cortical layer 2/3 neurons labeled with AM calcium dye (OGB-1 AM). Lower: visual stimulus-evoked calcium transient of the cell marked in the upper panel with a red dashed circle. The cell responded to one standing grating direction (marked in red) and one following drifting grating direction. Scale bar: 10 μm in both (A) and (B).

firing rates: evoked firing rates of the drifting grating were calculated by subtracting baseline firing rate from the averaged firing rate during the drifting grating period. The preferred direction for a cell was defined as the direction of drifting grating evoking the highest firing rate. 3) Orientation selective index (OSI) was calculated to quantify the tuning level of the neurons with regard to the orientation of the drifting grating. The OSI was defined as (Rpref - Rortho)/ (Rpref + Rortho), where Rpref, the response in the

preferred orientation, was the response with the largest magnitude. Rpref was determined as the mean of the evoked firing rates for the two corresponding opposite directions. Rortho was similarly calculated as the response evoked by the orthogonal orientation. 4) Peak response latency: Peak response latency was defined as the time between onset of the visual stimulus and onset of the peak in PSTH generated from spikes evoked by preferred direction (bin size=100ms).

2.9.2. Analysis of calcium imaging data

Calcium signals were expressed as relative fluorescence changes (ΔF/F) corresponding to the mean fluorescence from all pixels within specified ROIs. For each ROI, a transient was accepted as a signal when its amplitude was greater than three times the standard deviation of the noise band. Neurons were defined as responsive to drifting gratings when their activity during the presentation of at least one of the eight directions was significantly higher than their activity during the gray screen period (ANOVA test). The activity was evaluated by the peak amplitude of the calcium transients within the stimulus periods. Polar plots were used to show a neuron's response function to oriented drifting gratings. The responses to each of the eight tested directions were normalized with respect to the maximal response. Then, the function was constructed by connecting lines between the eight values. Statistical analyses were performed using paired or unpaired Student's t-tests in SPSS (version 18, IBM, USA).

3. Results

3.1. Visual response properties of interneurons in the V1 of awake mouse

3.1.1. Visual response properties of 5HT3aR+ interneurons

To study the orientation tuning of 5HT3aR+ interneurons, we recorded their visually evoked responses from 5HT3aR-EGFP transgenic mice, in which EGFP was expressed in 5HT3aR+ interneurons (Inta et al., 2008) by performing *in vivo* two-photon guided loose-patch recording, and in some experiments, two-photon calcium imaging. Drifting gratings at eight different directions were presented to the contralateral eye of the animal while performing recording or imaging. In addition, due to the effects of locomotion on neural activity (Niell & Stryker,2010), here we included only data recorded during stationary periods into the analysis. Neuronal activity during locomotion periods will be shown and discussed in a separate part later. We have 23 cells from 19 mice showing evoked responses (2 cells from calcium imaging and 21 cells from cell-attached recordings). We measured the baseline firing rate, evoked firing rate, peak response latency and orientation selectivity index (OSI) to analyze response properties of recorded neurons. An example cell-attached recording of 5HT3aR+ interneuron is shown in Figure 1A. The cell showed a low baseline firing rate and only a few spikes were detected during the gray screen period (Figure 1B). Besides, it showed evoked responses to all directions of the drifting grating but the response to one orientation (135^{o} and 315^{o}) was stronger than to the other orientations (Figure 1B). This neuron had an OSI of 0.25, indicating a weak orientation selectivity (Figure 1C). In addition to a broadly tuned response property, this neuron also showed a delayed response to all directions of the drifting grating. We measured the peak response latency from PSTH (bin size:100ms) of the preferred direction in a time window of 3s (Figure 1B and 1D). We found that this interneuron showed extremely late peak response to the visual stimulus with a value of 1.99 s.

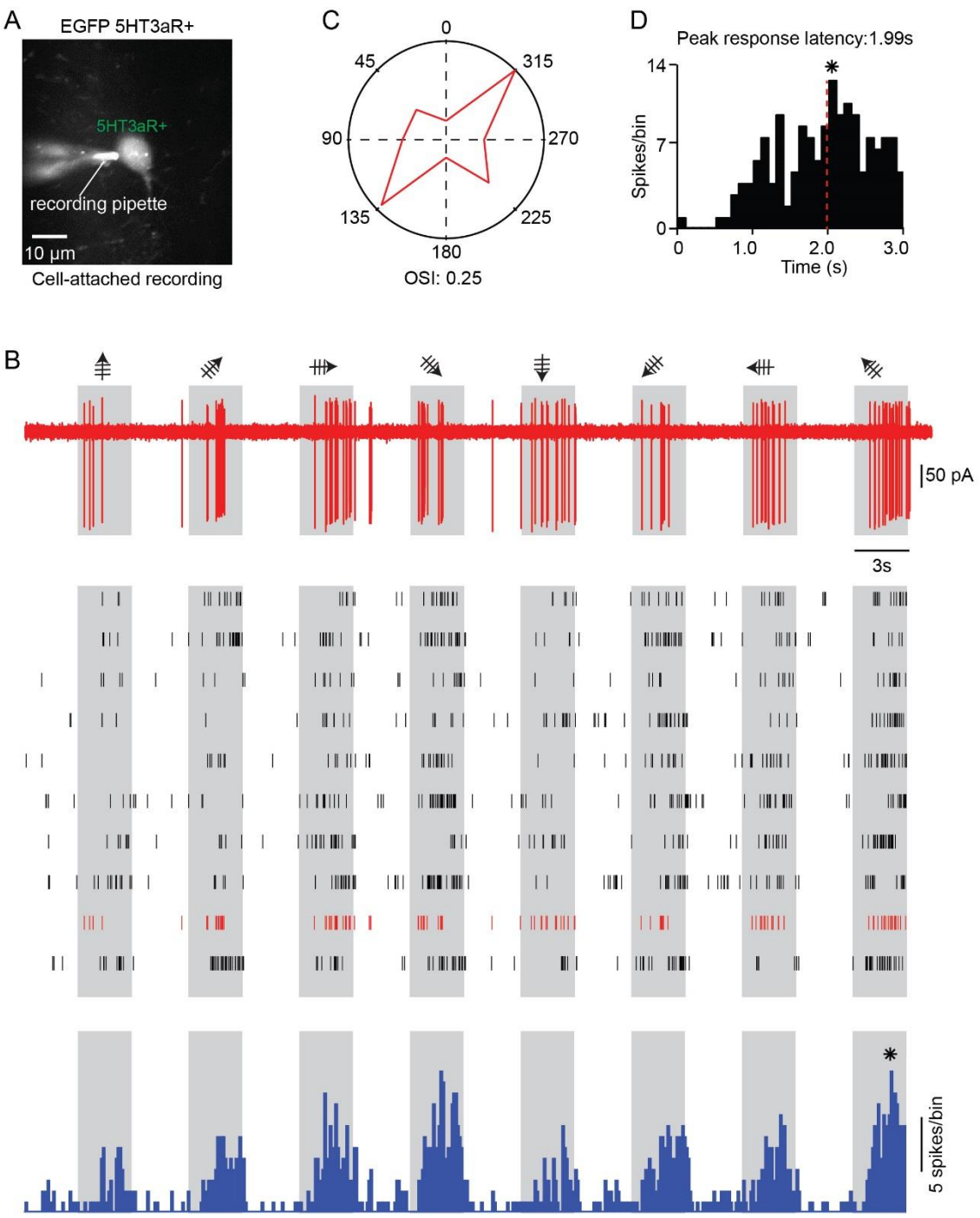

Figure 1. Broadly-tuned response of 5HT3aR+ interneuron in the awake mouse

(**A**) *In vivo* cell-attached recording from a EGFP-expressing 5HT3aR+ interneuron under two-photon imaging guidance. The recording pipette was filled with 50 μM Alexa 488 dissolved in normal Ringer solution. (**B**) Top: Spike responses of the interneuron in figure (A) to the drifting grating at eight different directions. Middle: Raster plot from 10 repeats of recording, the example trace in top panel was displayed in red. Bottom: Peri-stimulus

time histogram from 10 repeats of recording. Asterisk marks the response peak of the preferred direction. Bin size: 100ms. (**C**) Polar plots of the interneuron's response to drifting gratings for eight directions. Responses were normalized with respect to the maximal response. The orientation-selectivity index (OSI) was indicated below the plot. (**D**) PSTH (Bin size: 100ms) of the interneuron's responses to preferred direction indicated by asterisks in (B). The onset of the drifting grating is at time 0 and the response peak was marked with a red dash line. The value of peak response latency was indicated above the plot.

Figure 2 displays calcium imaging data from a 5HT3aR+ interneuron electroporated with Cal-520 (Figure 2A). Consistent with data from electrophysiological recordings, this cell showed a broadly tuned and delayed response to the visual stimulus. It showed evoked responses to most directions of the drifting grating, and the peaks of the evoked calcium transients appeared near the end of the stimulus (Figure 2B). Due to the small amount of samples (n=2 cells), however, these results from calcium imaging were not included in the final statistical analysis.

At the population level, the baseline firing rates of these 21 interneurons from the 5HT3aR group, ranged from 0.41 to 9.29 Hz, the mean value was 2.65 ± 0.48 Hz (Mean ± SEM). The evoked firing rate at the preferred direction ranged from 0.61 to 10.48 Hz, and the mean value was 4.10 ± 0.52 Hz. These interneurons had a weak orientation selectivity, the OSI ranged from 0.04 to 0.48 and the mean value was 0.18 ± 0.03. In addition, these interneurons showed strikingly delayed peak responses. In 19 cells, the peak response latencies at the preferred directions were longer than 1s, and in six cells, the peak response latencies at preferred directions were even longer than 2s. The peak response latencies of all cells ranged from 0.14 to 2.73 s and the mean value was 1.66 ± 0.15 s.

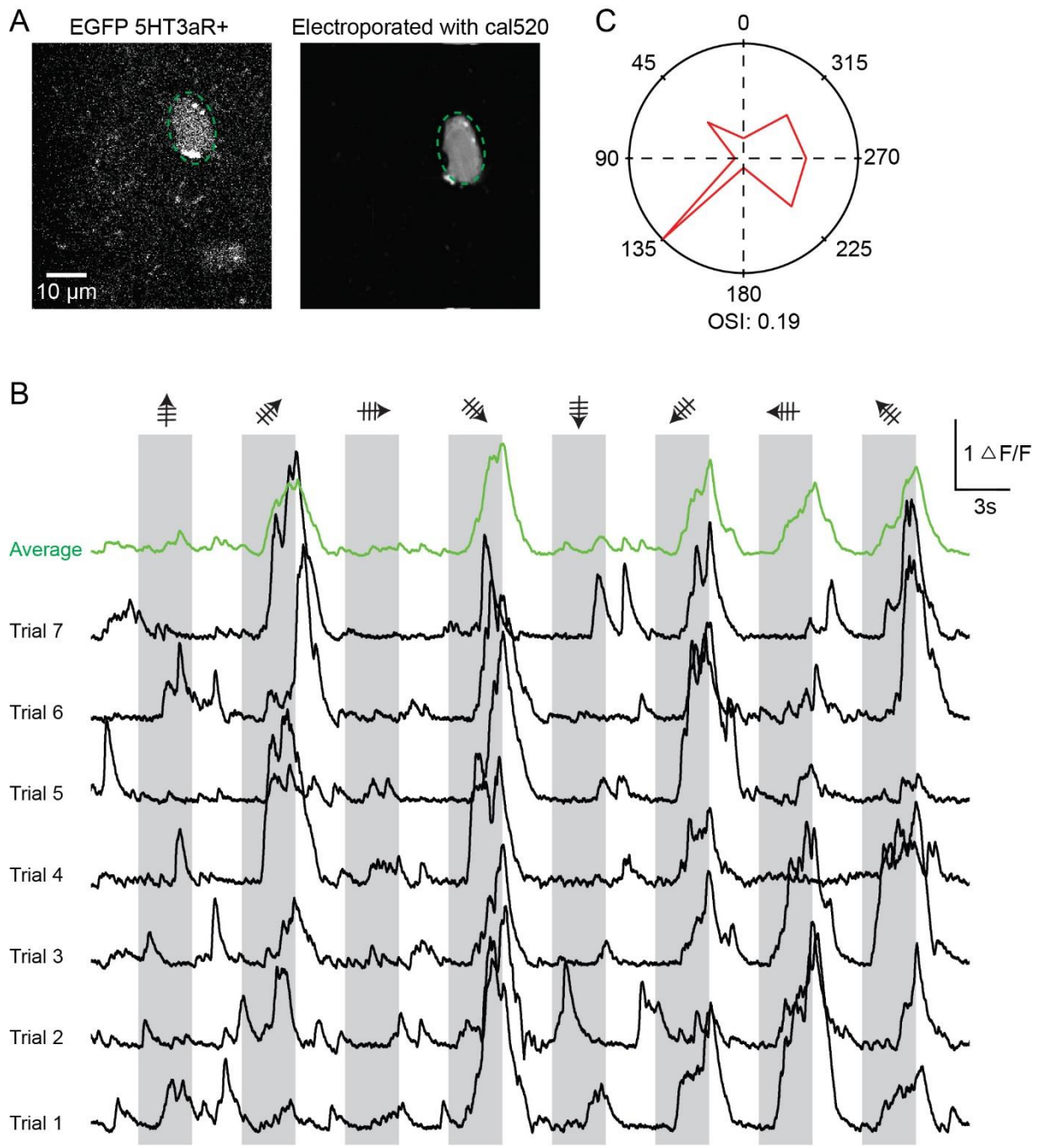

Figure 2. Two-photon calcium imaging of broadly-tuned 5HT3aR+ interneuron in the awake state.

(**A**) Left: Two-photon image of EGFP-expressing 5HT3aR+ interneuron before electroporation. Right: Two-photon image of EGFP-expressing 5HT3aR+ interneuron after electroporation with 10 mM Cal-520 potassium salt solution. (**B**) Visual stimulus-evoked calcium transients from the soma of a 5HT3aR+ interneuron indicated by a green dashed line. Single trials are represented with black lines and the average from all trials

is shown in green. (**C**) Polar plots of interneuron's responses to drifting gratings at eight directions.

3.1.2. Visual response properties of PV+ interneurons

PV+ and SOM+ interneurons are another two major interneuron groups in the cortex. To compare awake response properties of 5HT3aR+ interneurons with PV+ and SOM+ interneurons, we performed cell-attached recordings on another two transgenic mouse lines, in which the Enhanced Green Fluorescent Protein (EGFP) was expressed in PV+ (Meyer et al., 2002) and SOM+ (Oliva et al., 2000) interneurons respectively.

For the PV+ interneurons, we recorded ten cells showing evoked responses from seven PV-EGFP transgenic mice. Figure3 shows the recording of a PV+ interneuron in an awake mouse (Figure 3A). Compared to 5HT3aR+ interneurons, PV+ neurons showed a higher baseline firing rate, and also a higher evoked firing rate with no apparent preference to any directions of the drifting grating (Figure 3B and 3C). The OSI value of the cell was 0.01 indicating this cell was unselective to any orientations. Besides, the PV+ interneuron showed a fast and transient response to the visual stimulus, with the peak response latency of 0.13 s at preferred direction (Figure3D).

At the population level, the baseline firing rate of ten PV+ interneurons ranged from 6.19 to 16.88 Hz, and the mean value was 11.01 ± 1.33 Hz (Mean ± SEM). The evoked firing rate at the preferred direction ranged from 3.82 to 19.56 Hz, and the mean value was 8.16±1.52Hz. All of these PV+ interneurons showed only a weak or no orientation selectivity, with OSI ranging from 0.01 to 0.28 and mean value of 0.10 ± 0.02. In addition, as shown in the example cell, PV+ interneurons showed a fast and transient response to visual stimulus. The peak response latency ranged from 0.13 to 0.42 s and the mean value was 0.24 ± 0.03 s.

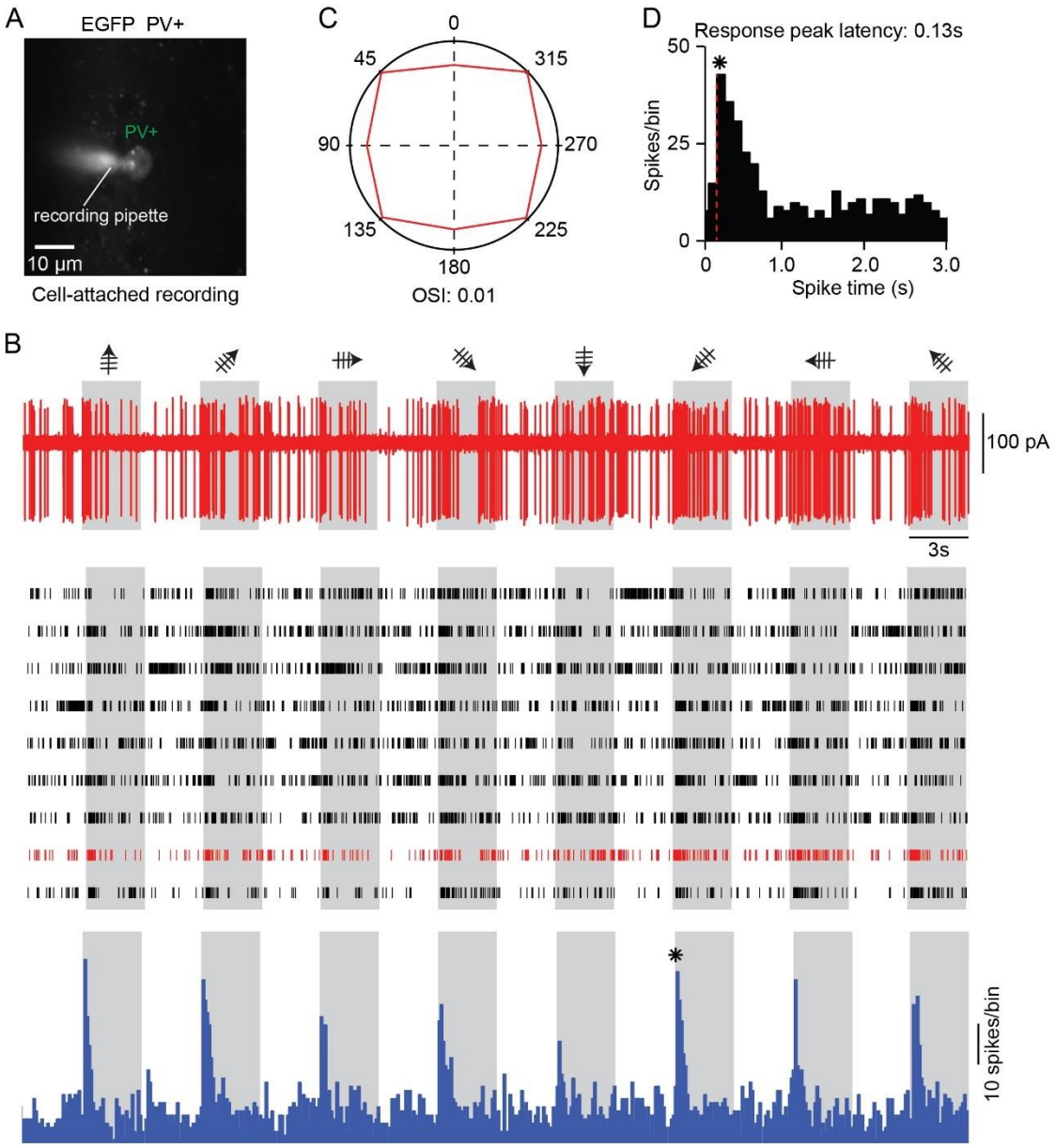

Figure 3. Broadly-tuned response of PV+ interneuron in the awake mouse

(**A**) *In vivo* cell-attached recording of EGFP-expressing PV+ interneuron under two-photon imaging guidance. The recording pipette was filled with 50 µM Alexa 488 dissolved in normal Ringer solution. (**B**) Top: Spike responses of the interneuron in figure (A) to the drifting grating at eight different directions. Middle: Raster plot from 9 repeats of recording. The example trace in top panel was displayed in red. Bottom: Peri-stimulus time histogram from 9 repeats of recording. Asterisk marks the response peak of preferred direction. Bin size: 100ms. (**C**) Polar plots of the interneuron's response to the drifting grating at eight directions. Responses were normalized with respect to the maximal

response. The orientation-selectivity index (OSI) was indicated below the plot. (**D**) PSTH from interneuron's responses to preferred direction indicated by asterisks in (B). the onset of the drifting grating is at time 0 and the beginning of the response peak was marked with a red dashed line. Value of the peak response latency was indicated above the plot.

3.1.3. Visual response properties of SOM+ interneurons

One previous study from anesthetized mice demonstrated that SOM+ interneurons showed weak but delayed responses to the visual stimuli (Ma et al., 2010). In contrast to these findings, we observed strong responses to the drifting grating in SOM+ interneurons in awake mice. We recorded evoked responses in 11cells from 5 SOM-GFP transgenic mice. The example cell in Figure 4A responded to all of the directions of drifting grating with a predominant response amplitude for one direction (Figure 4B and 4C). At the population level, SOM+ interneurons showed relatively low baseline firing rate which ranged from 0.61 to 6.44 Hz with a mean value of 3.89 ± 0.61 Hz (SEM). The evoked firing rate was higher than that in the two other interneuron groups. In SOM+ interneurons, the evoked firing rate ranged from 2.57 to 30.16 Hz with a mean value of 13.93 ± 2.48 Hz. The SOM+ interneurons also showed a sharper orientation tuning than the two other interneuron groups. The mean OSI of SOM+ interneuron was 0.26 ± 0.04 and ranged from 0.03 to 0.45. In addition, the peak responses of SOM+ interneurons at their preferred directions appeared earlier than that of 5HT3aR+interneuorns but later than that of PV+ interneurons. The peak response latency in SOM+ interneurons ranged from 0.26 to 0.74 with a mean value of 0.53 ± 0.05 s.

By comparison of the response properties of these three interneuron groups, we found that the baseline firing rate of the PV+ interneurons is significantly higher than that in the two other groups (Unpaired t-tests: PV versus SOM, $p < 0.001$; PV versus 5HT3aR, $p < 0.001$; Figure 5A). The baseline firing rate of SOM+ interneuron seems to be slightly higher than that of 5HT3aR+ group. However, there is no significant difference between these two groups ($p = 0.12$, Figure 5A). Of all three types of interneurons, the highest

sensory-evoked firing rate was measured in SOM+ interneurons. However, there is no significant difference between PV+ and SOM+ group ($p = 0.06$, Figure 5B). Whereas evoked firing rates in both groups are significantly higher than that in 5HT3aR+ interneurons (PV versus 5HT3aR, $p < 0.05$; SOM versus 5HT3aR, $p < 0.01$). The 5HT3aR+ interneurons showed the weakest and also the most delayed responses to the drifting grating. The peak response latency of 5HT3aR+ interneuron was significantly longer than that in the two other groups (PV versus 5HT3aR, $p < 0.001$; SOM versus 5HT3aR, $p < 0.001$, Figure 5C). Furthermore, the peak response latency of SOM+ interneurons is also significantly longer than in PV+ interneurons (PV versus SOM, $p < 0.001$, Figure 5C). When comparing the orientation selectivity indices between the three groups, we detected that the OSI of SOM+ interneuron was significantly higher than the OSI of PV+ interneurons ($p < 0.01$, Figure 5D). There is no significant difference between SOM+ and 5HT3aR+ group as well as between PV+ group and 5HT3aR+ group (PV versus 5HT3aR, $p = 0.07$; SOM versus 5HT3aR, $p = 0.13$ Figure 5D). Taken together, our data demonstrate that subtypes of interneurons in the visual cortex are functionally different regarding their role in visual information processing.

3.2. Suppressed-response interneurons in the V1 of awake mouse

3.2.1. Suppressed responses of 5HT3aR+ interneurons

Within the group of 5HT3aR+ interneurons, we found that a small portion showed a response to the visual stimulus with an entirely different pattern from those ‘broadly tuned’ interneurons in the awake state.

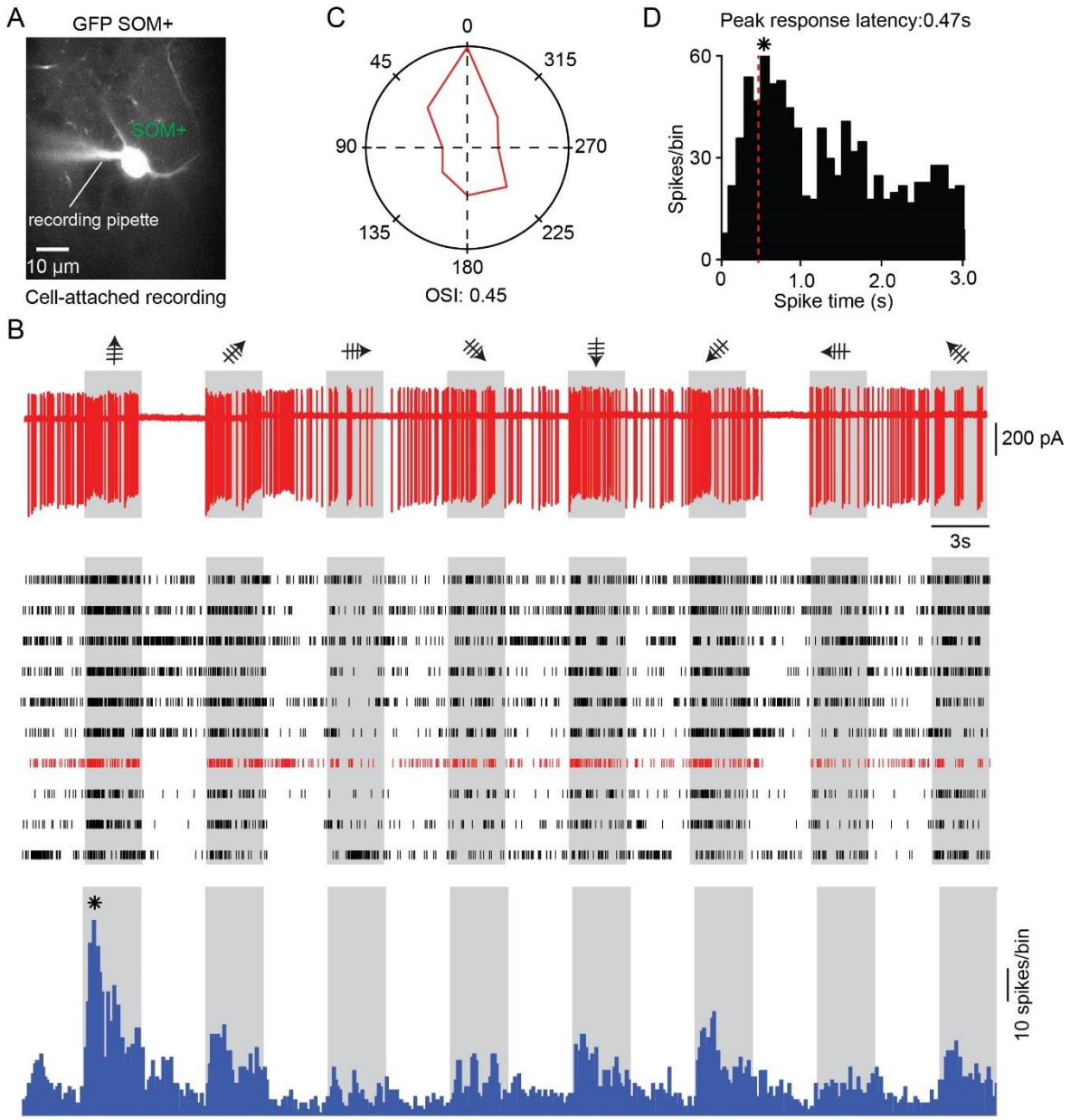

Figure 4. Broadly-tuned response of SOM+ interneuron in the awake mouse

(**A**) *In vivo* cell-attached recording of GFP-expressing SOM+ interneuron under two-photon imaging guidance. The recording pipette was filled with 50 µM Alexa 488 dissolved in normal Ringer solution. (**B**) Top: Spike responses of the interneuron in figure (A) to the drifting grating at eight different directions. Middle: Raster plot from 10 repeats of recording, the example trace in the top panel was displayed in red. Bottom: Peri-stimulus time histogram from 10 repeats of recording. Asterisk marks the response peak of the preferred direction. Bin size: 100ms. (**C**) Polar plots of the interneuron's response to drifting gratings at eight directions. Responses were normalized with respect to the

maximal response. The Orientation-selectivity index (OSI) was indicated below the plot. (**D**) PSTH from the interneuron's responses to preferred direction indicated by asterisks in (B). Onset of drifting grating is at time 0 and the response peak was marked with a red dashed line. The Value of peak response latency is indicated above the plot.

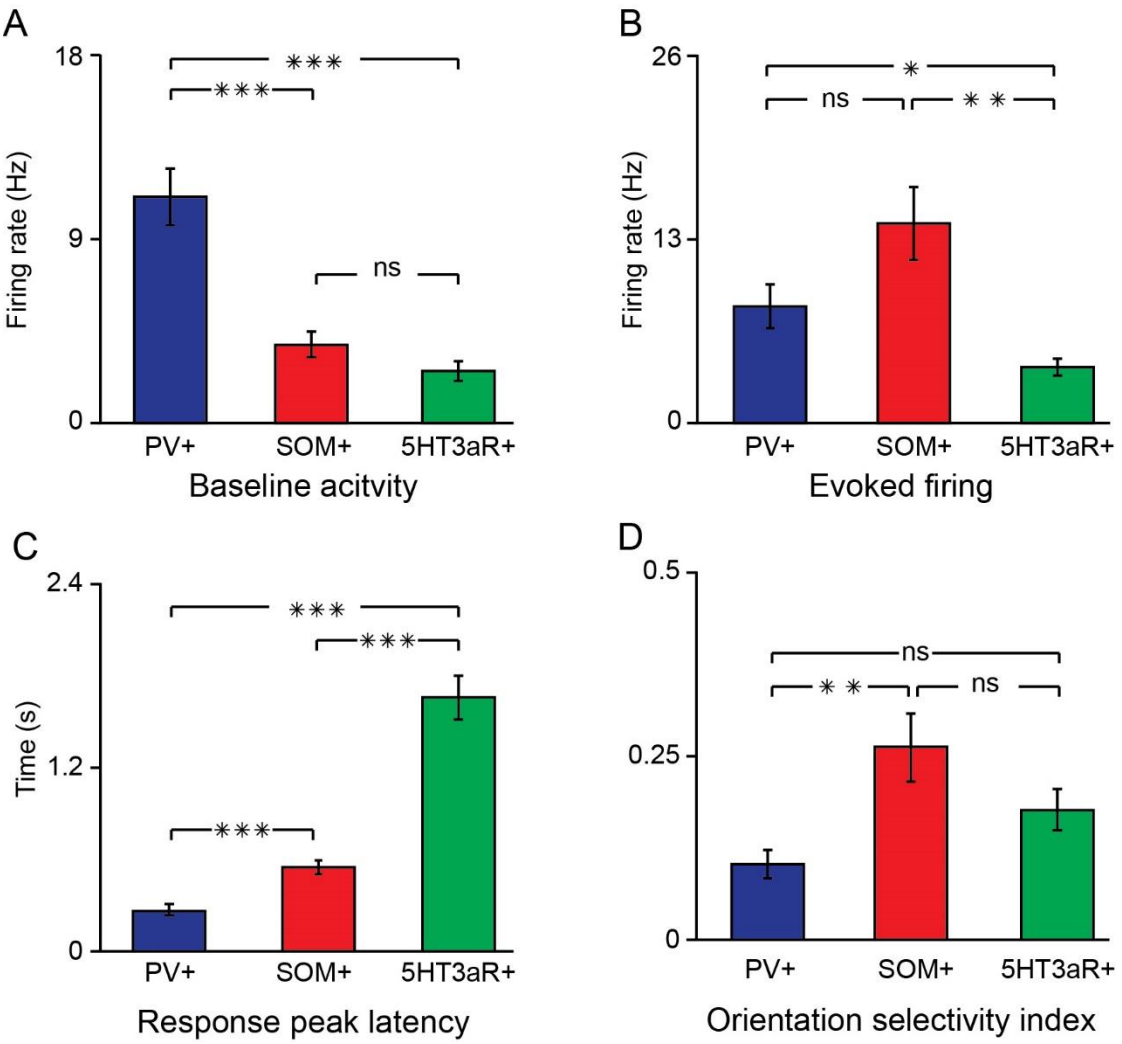

Figure5. Response properties of different types of interneurons in the awake mice (**A**) Baseline activity of different types of interneurons. (**B**) Evoked firing at the preferred direction. (**C**) Peak response latency at preferred direction. (**D**) Orientation selectivity index of different types of interneurons. Error bar, SEM. N=10, 11, 21 for PV+, SOM+ and 5HT3aR+ interneurons respectively, ns: no significant difference, * p<0.05,** p< 0.001, *** p< 0.0001. Unpaired t test.

In contrast to the evoked response, the activity in these cells was suppressed by drifting gratings. As an example of cell-attached recording shown in Figure 6A, the cell firing was suppressed once the drifting grating appeared no matter in which direction the grating moved. In some case, the firing even stopped during the phase of the drifting grating (Figure 6B). Since in these neurons the activity during the visual stimulation was lower than the baseline activity, we called this type of interneurons as 'suppressed response interneuron' (Figure 6C). To quantify response properties of the suppressed response interneuron, we measured the baseline firing rate and the suppressed firing rate by subtracting the baseline firing rate from the firing rate during the drifting grating period. It should be noted here that the value of the suppressed firing rate is negative, so we used the absolute value of the suppressed firing rate to calculate the OSI and for comparisons with the activity of other types of interneurons. In addition, we defined the preferred orientation of these suppressed response interneuron as the orientation of drifting grating that generated maximum suppression of the cell's activity. Response properties of 16 suppressed response interneurons were examined. The baseline firing rate of these cells ranged from 1.27 to 14.86 Hz and the mean value was 5.43 ± 0.93 Hz (Mean±SEM) which was significantly higher than the baseline firing rate of the 5HT3aR+ 'broadly tuned' interneuron (Broadly tuned (n = 21 cells) versus Suppressed response (n = 16 cells), $p < 0.05$, unpaired t-test). The orientation selectivity index of suppressed response interneuron ranged from 0.01 to 0.18, and the mean value was 0.09 ± 0.01 which was significantly lower than the OSI of the broadly tuned interneuron (Broadly tuned (n = 21 cells) versus Suppressed response (n = 16 cells), $p < 0.01$, unpaired t-test). This indicates that those suppressed response cells showed no preference to any directions of the drifting gratings.

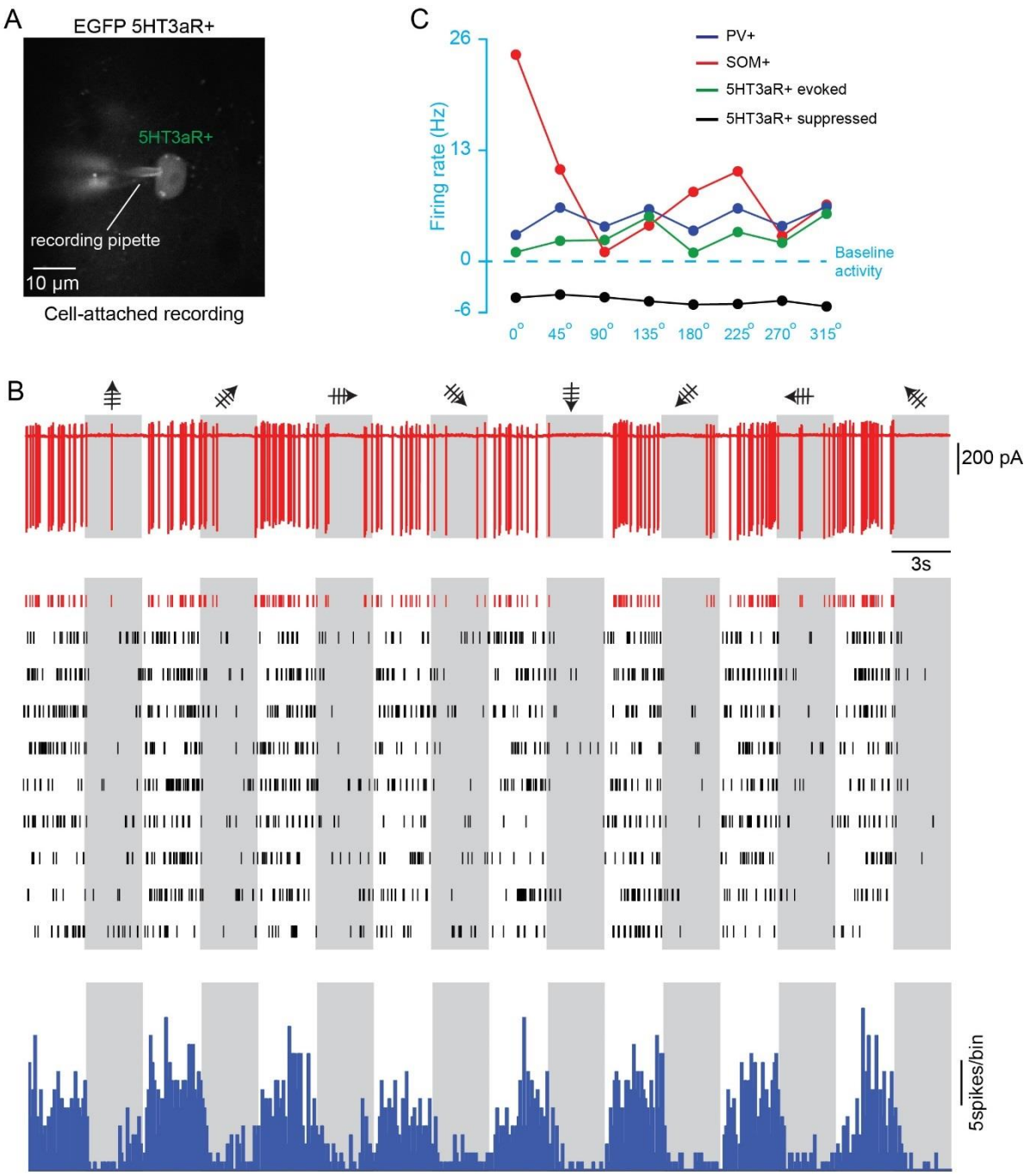

Figure 6. Suppressed response of 5HT3aR+ interneuron in the awake state

(**A**) *In vivo* cell-attached recording of EGFP-expressing 5HT3aR+ interneuron under two-photon imaging guidance. The recording pipette was filled with 50 μM Alexa 488 dissolved in normal Ringer solution. (**B**) Top: Spike responses of the interneuron in figure (A) to drifting grating at eight different directions. Middle: Raster plot from 10 repeats of recording. The example trace in top panel was displayed in red. Bottom: Peri-stimulus time histogram from 10 repeats of recording. Bin size: 100ms. (**C**) Response curve of the

interneuron to drifting grating at eight directions. The curve was constructed by connecting the value of firing rate at each angle of drifting grating. The light blue dashed line indicates the level of baseline activity. The response curve of the cell in (A) was indicated by black line. The curves of the other cells from Figure 2,3 and 4 were displayed in green, blue and red respectively.

The absolute value of suppressed firing rate ranged from 0.72 to 11.57 Hz, the mean value was 4.28 ± 0.74 Hz, which showed no significant difference from the evoked firing rates of the 5HT3aR+ broadly tuned interneuron (Broadly tuned (n = 21 cells) versus Suppressed response (n = 16 cells), p = 0.84, unpaired t-test).

In order to simultaneously monitor the activity from the neuronal network of the suppressed response interneuron, we used multi-cell bolus loading with the Ca^{2+} sensitive fluorescent dye Cal520 AM dye. As shown in Figure 7, Cal520 AM dye labels 5HT3aR-EGFP positive interneurons as well as the EGFP negative cells in the vicinity (Figure 7A). Consistent with our data from cell-attached recording, calcium transients of the suppressed response cell decrease during drifting period indicating a suppression of spike activity and recovered during the period of the gray screen indicating an increase in spike activity (Figure 7B, left panel). In contrast to this, calcium transients from EGFP negative cells increase during one specific direction of the drifting grating indicating a 'sharp tuned' response (Figure 7B, right panel). Interestingly, in some experiments (n = 4 cells from 4 experiments), we found an out-phased responding cell near the suppressed response 5HT3aR+ interneuron. As shown in Figure 8, the out-of-phase responding cell (marked with a red circle in Figure 8A) does not express EGFP which means it most probably does not belong to the 5HT3aR+ interneuron group. In addition, the evoked response during the drifting period of this cell matched well to the descending phase of calcium transients from suppressed response 5HT3aR+ interneuron (Figure 8B). It is currently unclear if these two cells had functional connections or not. More experiments need to be done to clarify this issue.

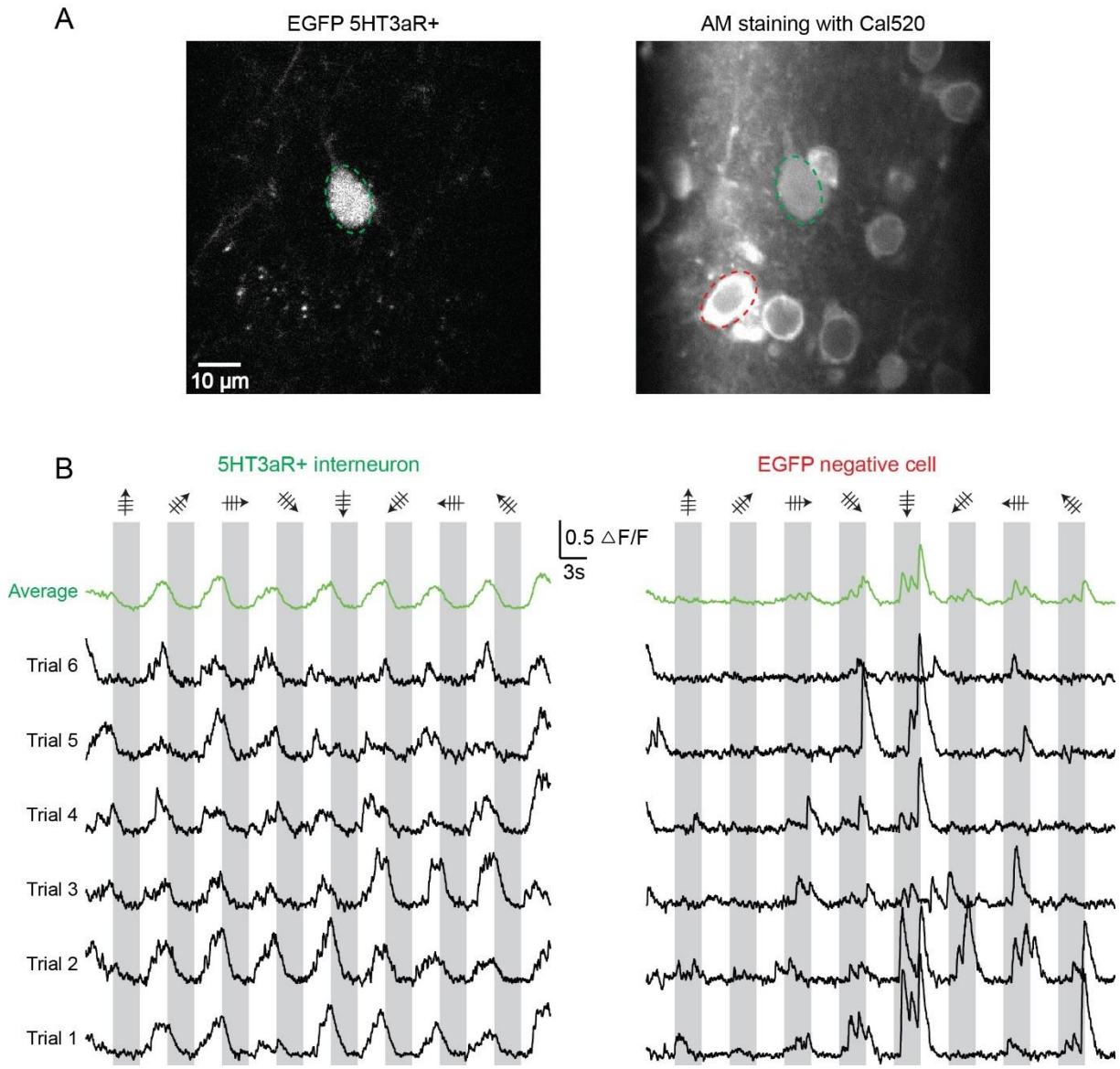

Figure 7. Two-photon calcium imaging of the suppressed response interneuron

(**A**) Two-photon image of EGFP-expressing 5HT3aR+ interneuron before (left panel) and after Cal-520 AM staining (right panel). Interneuron was indicated by green dashed circle in both panels. An EGFP negative cell was indicated by red dashed circle in right panel. (**B**) Visual stimulus-evoked calcium transients of the 5HT3aR+ interneuron (left panel) and the EGFP negative cell (right panel). Single trials are represented with black lines and the average of all trials is shown in green.

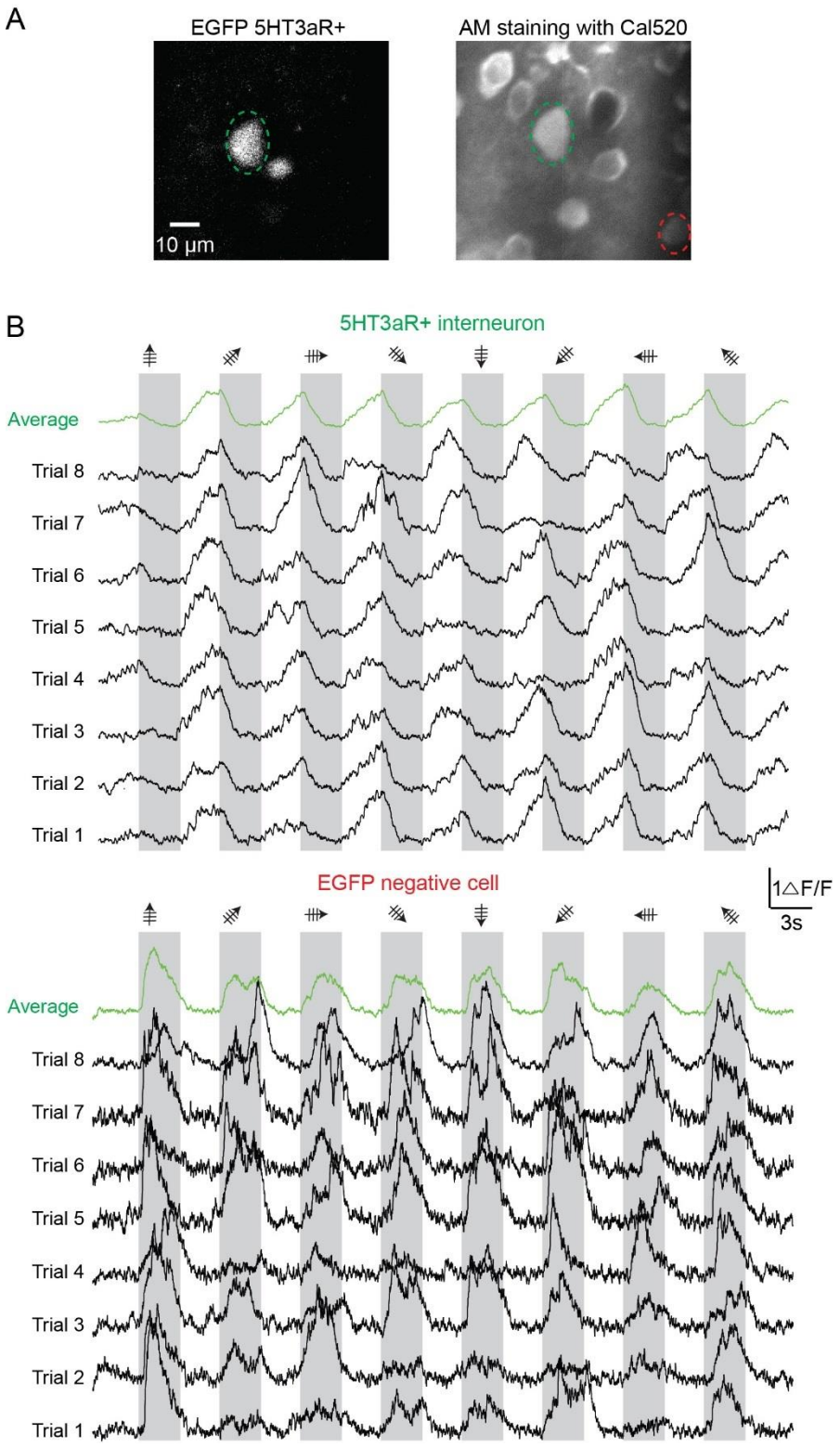

Figure 8. Out-phased response cell near the suppressed response interneuron

(**A**) Two-photon image of EGFP-expressing 5HT3aR+ interneuron before (left panel) and after Cal-520 AM staining (right panel). The 5HT3aR+ cell was indicated by green dashed circle in both panels. An EGFP negative cell was indicated by red dashed circle in right

panel. (**B**) Calcium transients evoked by visual stimulation of the 5HT3aR+ cell (upper panel) and the EGFP negative cell (bottom panel). Single trials are represented with black lines and the average of all trials is shown in green.

3.2.2. Morphological and immunohistochemical characterization of the suppressed response interneurons

This part of the experiment was performed by Dr. Valérie Bonfardin (AG Arthur Konnerth, Institute of Neuroscience, TU Munich) and Dr. Monika Brill (AG Thomas Misgeld, Institute of Neuronal Cell Biology, TUM).

To identify the cell type of these suppressed-response interneurons, we characterized them regarding two aspects, namely, morphological characteristics, including the axonal arborization and the immunohistochemical markers that they expressed. To do this, we electroporated seven cells (one from electrophysiological recording and six from calcium imaging experiments respectively) with an OGB-1 potassium salt (10mM) and biocytin (2%) contained solution. The morphology of the soma and the dendrite can be visualized in fluorescent Z-projection images obtained with two-photon microscopy or images under confocal microscopy after perfusion, slicing of the brain and the streptavidin staining of the biocytin (See more details in Materials and methods section). Figure 9A shows the Z-projection image of one suppressed response cell. This cell has four dendrites, and one of them is much thicker than the others. Moreover, there are some spines sparsely distributed on the dendritic shafts (Figure 9B). The confocal images from another example cell show similar dendritic characteristics: 3 dendrites including one thick dendrite and sparsely distributed spines on the dendritic shafts (Figure 9C and 9D).

Since the dendritic morphology cannot reliably define the type of interneurons, we then analyzed the axonal arborization of the suppressed response interneurons. A typical example cell is shown in Figure 10. The soma of the cell is located on the boundary between layer 1 and layer 2/3, the dendrites of the cell are located in layer1 but also in layer 2/3. The axon starts from one of the dendrite and branches extensively mostly in

layer 2/3. Interestingly, the axon of the cell envelops somata of layer 2/3 neurons in a baskets-like appearance (Figure 11).

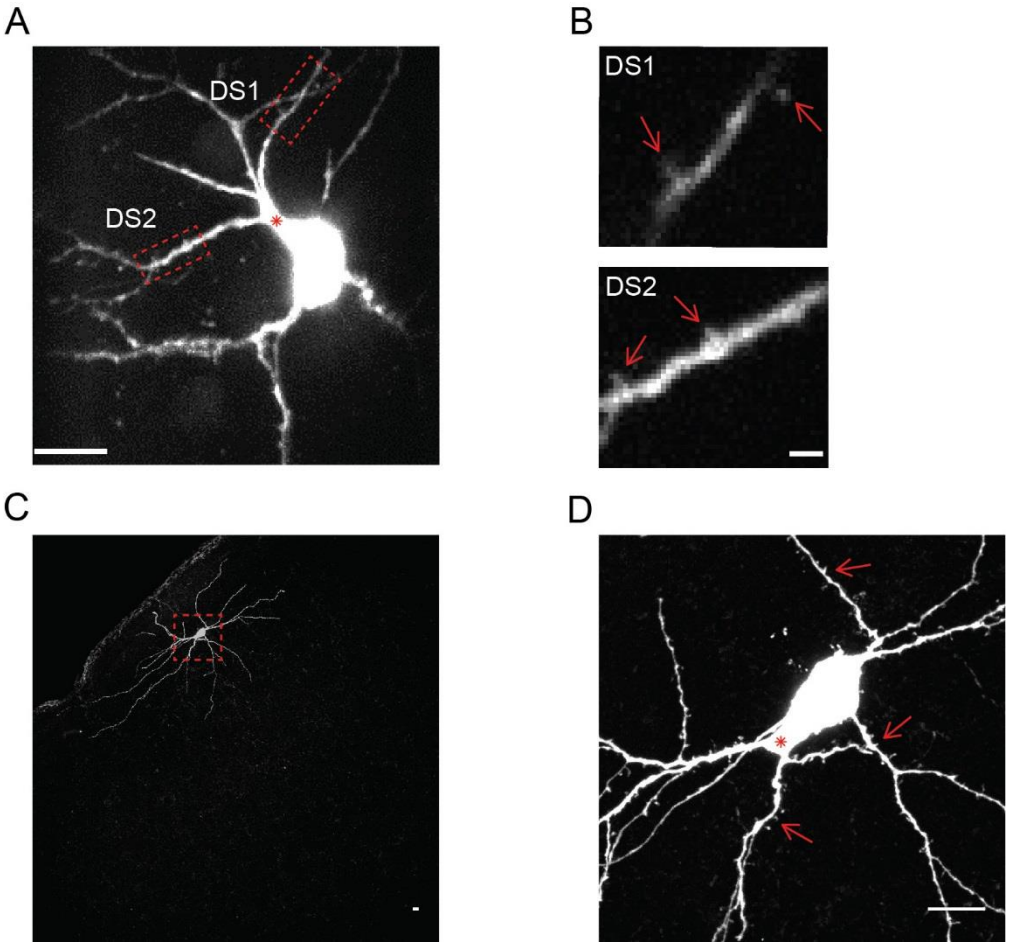

Figure 9. Morphological characteristics of the suppressed response interneuron

(**A**) Z-Projection of a Suppressed response 5HT3aR+ interneuron labeled with OGB-1 via electroporation. The red dashed line indicates the area magnified in (B). (**B**) The image at high magnification of the dendritic segment (DS1, DS2) indicated in (A). (**C**) and (**D**) Example of another suppressed response 5HT3aR+ interneuron in confocal images obtained using 20x (C) and 60x (D) objectives, respectively. Spines on dendritic shafts are indicated by the red arrow, and the thick dendrites are indicated by red asterisks in (B) and (D). Scale bar: 10 µm in (A), (C) and (D), 2µm in (B).

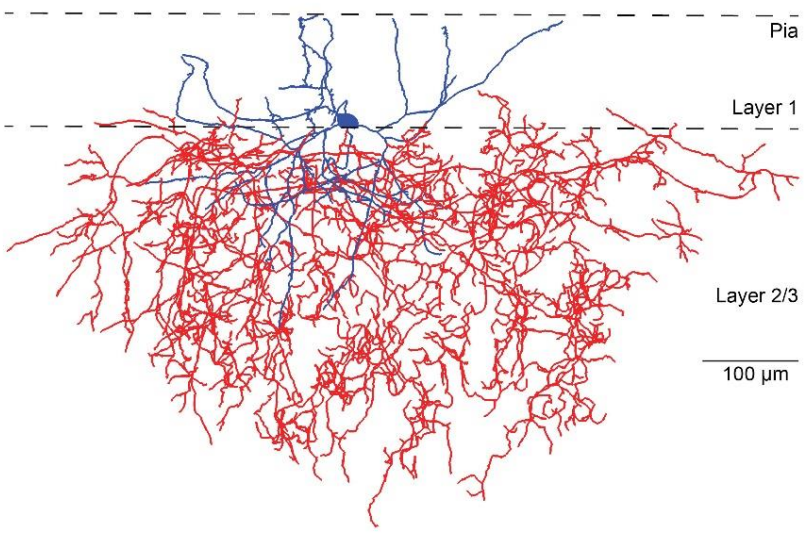

Figure 10. Three-dimensional reconstruction of a suppressed response interneuron in the mouse visual cortex. The cell was labeled with biocytin using electroporation at the end of the experiment. Biocytin was visualized after incubation with Streptavidin conjugated to Alexa 568. The soma and the dendrites of the cell were located at the end of layer 1 (in blue), but some of the dendrites were also in layer 2/3. The axon is mostly located in layer 2/3 and starts from one of the dendrite (in red); Scale bar: 100 µm.

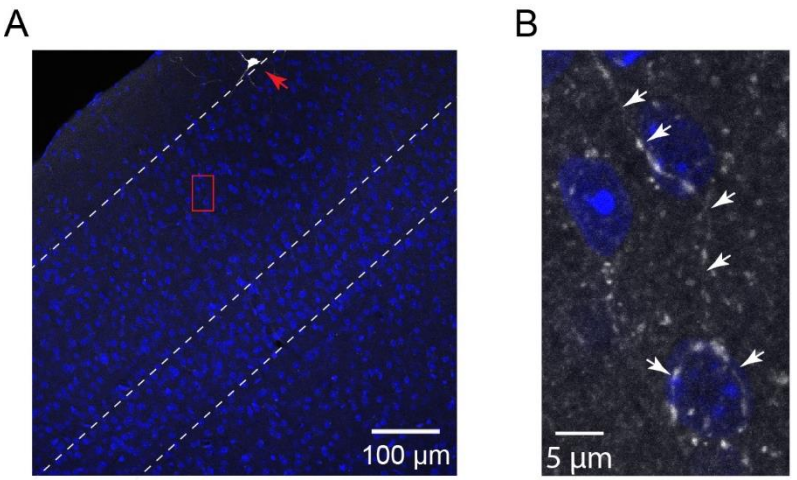

Figure 11. Axonal boutons of a suppressed response interneuron terminating in the perisomatic region of nearby cells.

(**A**) The cell used for recordings was filled with biocytin (red arrow), and, the coronal section was counterstained with Dapi (Blue, 405 nm): The dashed lines demonstrate five

layers of the visual cortex. (**B**) The area marked with the red box in (A) is shown with higher magnification. Note that the axon (white) is wrapping the somata of two cells (white arrows).

To further characterize this type of interneurons, we next performed immunohistochemical analyses to assess the expression of neurochemical markers. We first tested if these cells expressed Reelin or VIP, two markers which are expressed in the majority of 5HT3aR+ interneurons. By using double immunofluorescence staining on these electroporated cells (n=7). We found that all of these interneurons co-expressed VIP and Reelin. An example cell is shown in Figure 12.

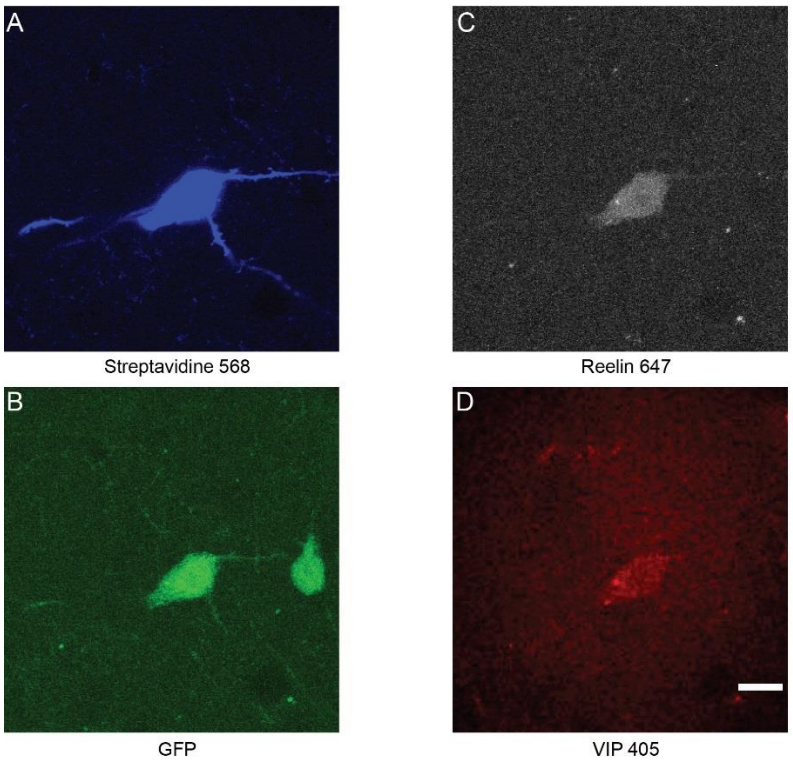

Figure 12. Suppressed response interneuron is expressing VIP and Reelin. This cell displayed fluorescence for biocytin (**A**) and immunoreactivity for GFP (**B**, green, 488 nm), Reelin (**C**, gray, 647 nm) and VIP (**D**, red, 405 nm); Scale bar: 10 µm.

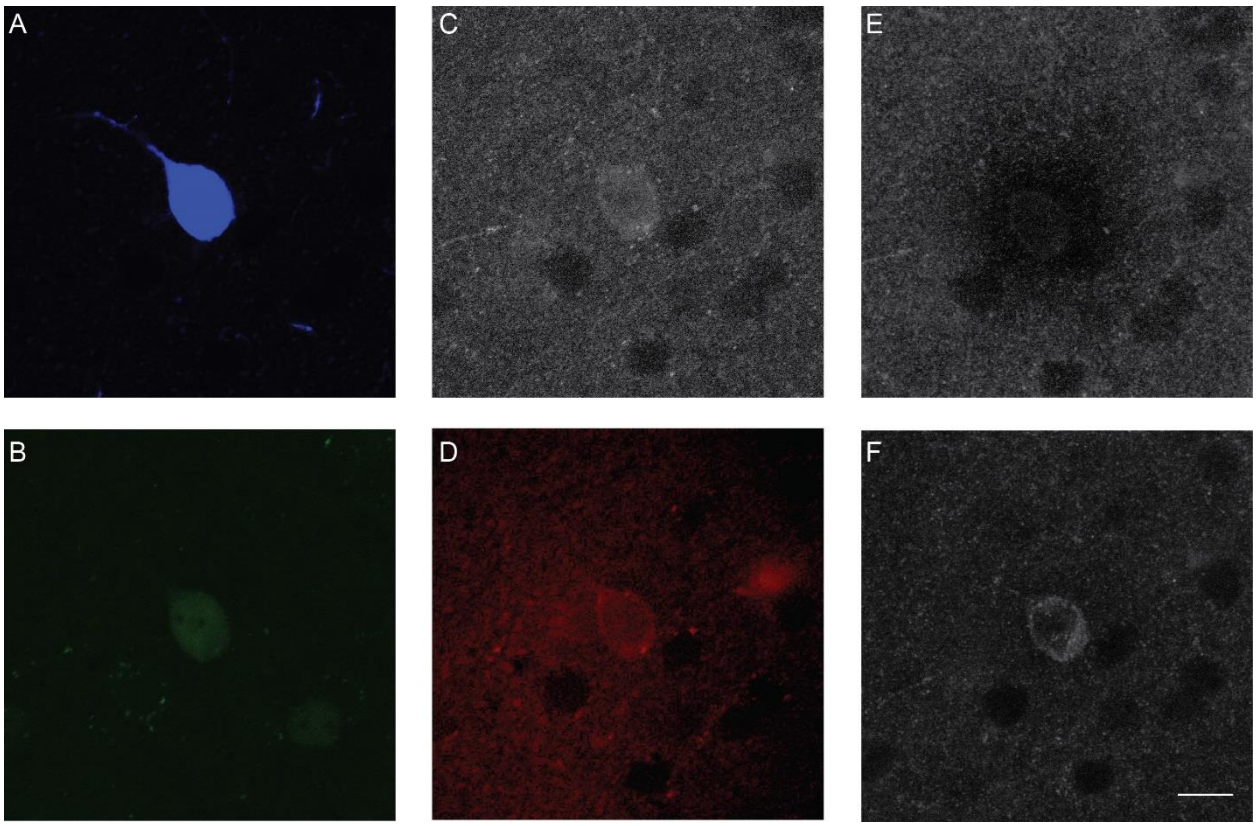

Figure 13. Suppressed response interneuron is expressing CCK

(**A**) Cell filled with biocytin (blue, Streptavidin, 568 nm). This cell was immunoreactive for GFP (**B,** green, 488 nm), CCK (**C,** gray, 647 nm) and VIP (**D**, red, 405 nm). After photo-bleaching of the CCK staining (Alexa 647) (**E**, gray, 647 nm), immunostaining for Reelin was done, and the cell was found to be positive for Reelin (**F**, gray, 647 nm); Scale bar: 10 µm.

These results from the immunohistochemistry together with the morphological characteristics described before indicate that the suppressed response interneuron belongs to the VIP-basket cell subgroup of interneurons which was found to exist in the dentate gyrus of rats in a previous study (Hajos et al., 1996). Since hippocampal VIP-positive basket cells also express CCK (Hajos et al., 1996; Mátyás et al., 2004), we sought to determine whether CCK is also present in the basket cells newly identified

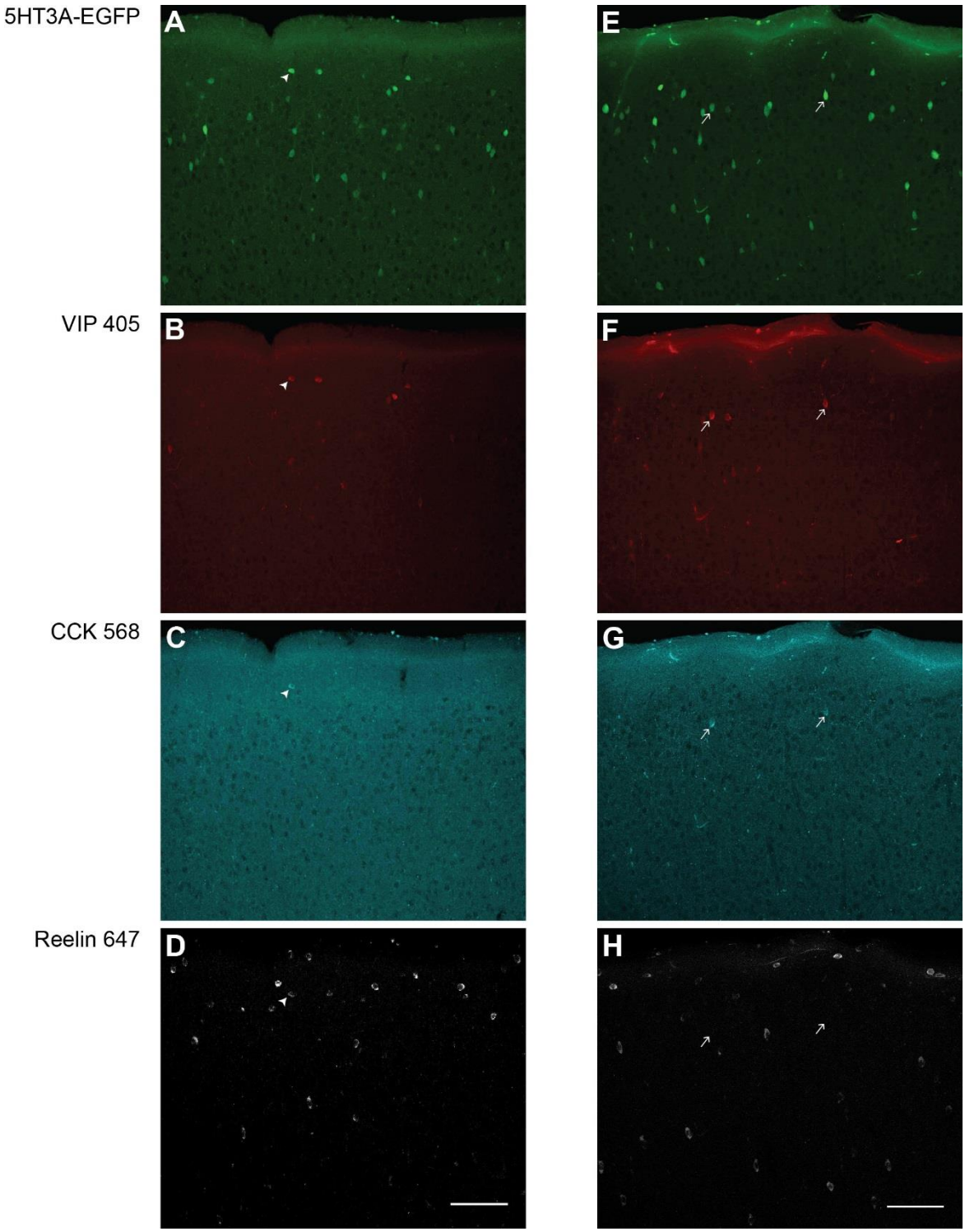

Figure 14. Sparse distribution of 5HT3aR+ cells co-expressing VIP, CCK and Reelin in layer 1 and 2/3 of the visual cortex (**A, E**) EGFP positive cells from a 5-HT3aR EGFP transgenic mouse showing the distribution of 5-HT3A interneurons in layer 1 and 2/3 of the visual cortex (green, 488 nm). (**B, F**) VIP-positive cells in the same corresponding sections (A, E) (Red, 405 nm); (**C, G**) CCK-positive cells (Cyan, 568 nm); (**D, H**) Reelin-

positive cells (Gray, 647 nm). (A, B, C, D) showed one 5-HT3A interneuron expressing VIP, CCK and Reelin (white arrowhead). (E, F, G, H) showed two 5-HT3A interneurons expressing only VIP and CCK (white arrows). The proportion of cell expressing only VIP and CCK is 2 to 3 time higher than that of cells expressing VIP, Reelin and CCK. Scale bars: 100 µm.

by us. To this end, we first photo-bleached the Reelin (Alexa 647) using a confocal microscope (FV1000, Olympus) equipped with an oil immersion objective (x60/N.A. 1.42). The 635 nm laser beam was placed on the targeted cell, and the cell was bleached at maximum power by slow line scanning (20µs/pixel) until the intensity of Alexa 647 fluorescence was drastically reduced. We acquired confocal image stacks before and after photo-bleaching to ensure that the staining against Reelin disappeared. These stacks then were compared with the one showing the staining against CCK. We found that all Reelin-positive cells tested also express CCK (n=7). Thus, the suppressed response cells were VIP-basket cells, that co-expressed Reelin and CCK. However, how large the proportion of these cells in the 5HT3aR+ group was unknown. In order to answer this question, we did triple Immunohistochemistry staining on slices from the primary visual cortex of 5HT3aR+ EGFP-expressing transgenic mice and found triple-positive cells very sparsely distributed in the preparation (Figure 14).

3.2.3. Suppressed responses of VIP+ interneurons

In addition, we also tested the VIP-positive interneurons from the VIP-tdtomato mice, and we found suppressed response cells both from electrophysiology (Figure 15) and calcium imaging experiments (Figure 16), further confirmed our results from 5HT3aR+ interneuron experiments which demonstrated that the suppressed response cells belonged to the VIP-positive subgroup.

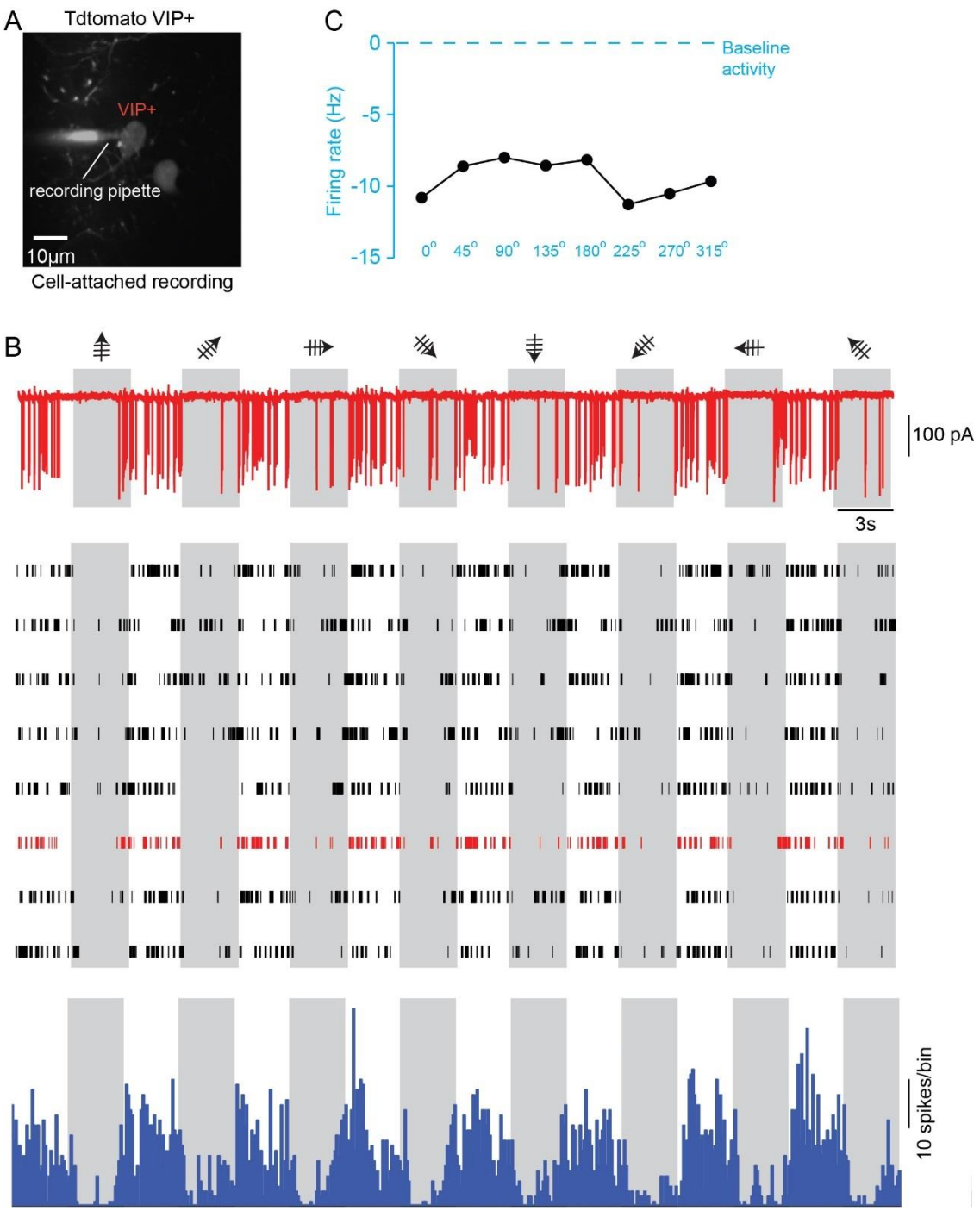

Figure 15. Suppressed response of a VIP+ interneuron in the awake state.

(**A**) *In vivo* two-photon image of a Tdtomato-expressing VIP+ interneuron with the attached recording pipette filled with 50 μM Alexa 488 dissolved in normal Ringer solution. (**B**) Top: Spike responses of the interneuron in figure (A) to drifting grating at eight different directions. Middle: Raster plot from 8 repeats of recording, example trace in the top panel was displayed in red. Bottom: Peri-stimulus time histogram from 8 repeats of

recording. Bin size: 100ms. (**C**) Response curve of the interneuron to drifting grating at eight directions. The curve was constructed by connecting the values of evoked firing rates at each angle of the drifting grating. The light blue dashed line indicates the level of baseline activity.

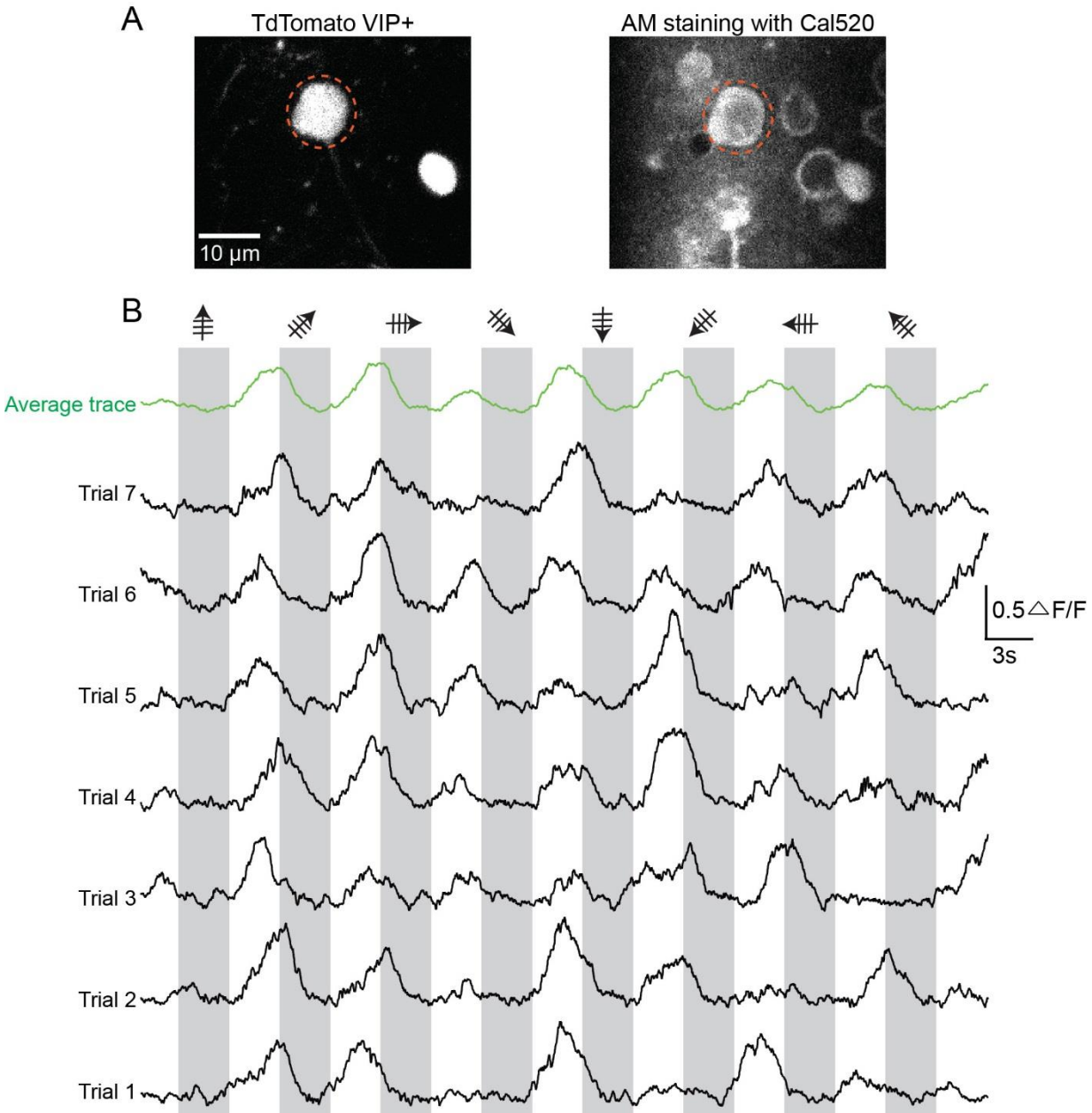

Figure 16. Two-photon calcium imaging of tdtomato expressing VIP+ interneuron. (**A**) Two photon image of a Tdtomato-expressing VIP+ interneuron before (left panel) and after Cal-520 AM staining (right panel). The VIP+ cell is marked by a red dashed circle in

both panels. (**B**) Calcium transients evoked by visual stimulation of the VIP+ interneuron. Single trials are represented with black lines and the average of all trials is shown in green.

3.3. Effects of anesthesia on the neuronal activity in mouse V1

In this part of the thesis, we compared visually-evoked neuronal responses in different cortical states. In the case of electrophysiological recording, we first performed cell-attached recording on an interneuron in the awake state. Then, the recording pipette was gently removed out of the brain while a small positive pressure (15-20 mBar) was applied to the back of the pipette. Following that, the mouse was anesthetized with isoflurane and cell-attached recording was performed on the same neuron in the anesthetized state. In the case of calcium imaging, we first performed population calcium imaging in one focal plane. Following that, the mouse was anesthetized with isoflurane and calcium imaging was performed on the same focal plane in the anesthetized state. Then, the anesthesia was stopped, calcium imaging was performed on the same focal plane when the mouse waked up again.

3.3.1. Effects of anesthesia on the activity of PV+ interneuron

After recording in the awake state, we successfully performed cell-attached recordings on four PV+ cells in the anesthetized state. An example cell is shown in Figure17A. In the awake state, the cell showed high baseline firing activity and also sensory-evoked firing activity (Figure 17B and 17C) as described before in Figure 3. In the anesthetized state, the activity of both baseline firing and evoked firing decreased. Interestingly, the effect of the anesthesia on baseline activity was stronger than that on the sensory-evoked firing activity and thus, the net effect of anesthesia is a better signal to noise ratio in the anesthetized state (Figure 17B and 17C). In addition, the tuning properties of the neurons also changed when the brain state switched from wakefulness to anesthesia (Figure 17D). Our results indicate that isoflurane affects the PV+ cell activity like a ‘filter’ resulting in an increase of the signal to noise ratio.

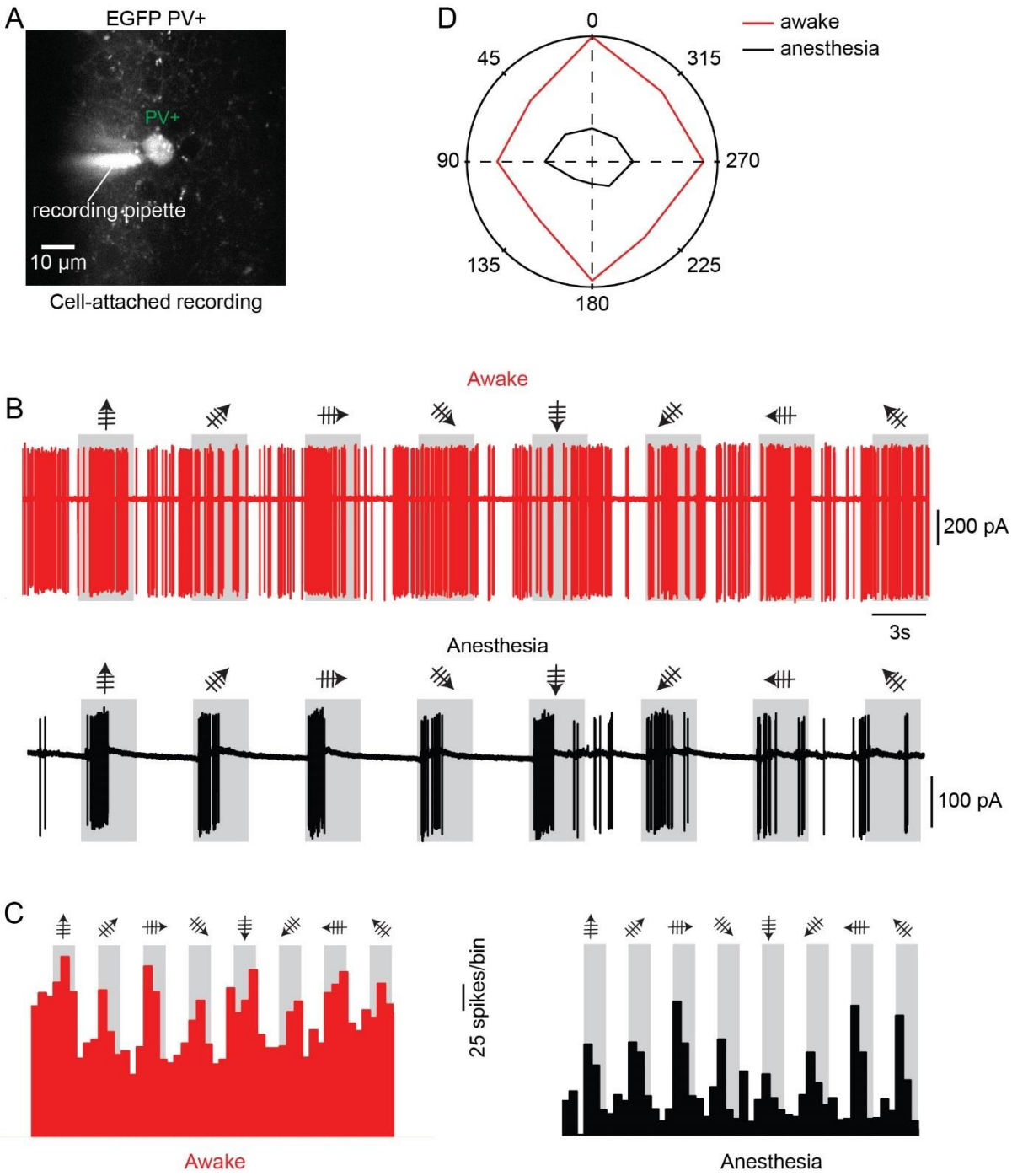

Figure17: Effects of anesthetized on responses of PV+ interneuron

(**A**) *In vivo* two-photon image of an EGFP-expressing PV+ interneuron. The recording pipette was filled with 50 µM Alexa 488 dissolved in normal Ringer solution. (**B**) Top: Response of the interneuron to drifting grating at eight different directions in the awake state. Bottom: Responses of the interneuron to the drifting grating at eight different directions in the anesthetized state. (**C**) Peri-stimulus time histogram of 9 repeats from

the recording in the awake (left panel) and anesthetized (right) states respectively. Bin size: 1s. (**D**) Polar plots of the interneuron's responses to the drifting gratings at eight directions in the awake (red) and anesthetized (black) states, respectively. Responses were normalized to the respective maximal responses in both states.

3.3.2. Effects of anesthesia on the activity of SOM+ interneuron

Similar to PV+ interneurons, we also compared activities of SOM+ interneurons in different states. For that, we performed cell-attached recordings on six SOM+ cells when the mouse was in awake and anesthetized states. An example cell is shown in Figure18A. In the awake state, the cell showed high baseline activity and also strong and stable responses to all directions of the drifting grating with no clear preference to any specific directions (Figure 18B and 18C). In the anesthesia, the cell was silent and showed no activity irrespective whether the mouse was exposed to the gray screen or the drifting grating (Figure 18B and 18C). All six SOM+ cells from which we obtained recording in both states, showed responses evoked by the drifting grating in the awake state. In the anesthetized state, however, only one cell showed a selective but weak and delayed response consistent with a previous study (Ma et al., 2010). Another five cells showed no activity or only a few spikes during the whole recording period (10~15 min). These data indicated that SOM+ interneuron are quite sensitive to anesthesia and the anesthetic (isoflurane) affects the activity of SOM+ interneurons like a 'silencer'.

3.3.3. Effects of anesthesia on the activity of suppressed response interneuron

In the previous part, we have introduced suppressed response cells which are VIP-basket cell based on our data from morphological reconstructions and immunohistochemical staining. After recording from these cells in the awake state, we performed recording on four such cells (two cells with cell-attached recordings and two cells with calcium imaging) in the anesthetized state to compare differences between these two states. An example

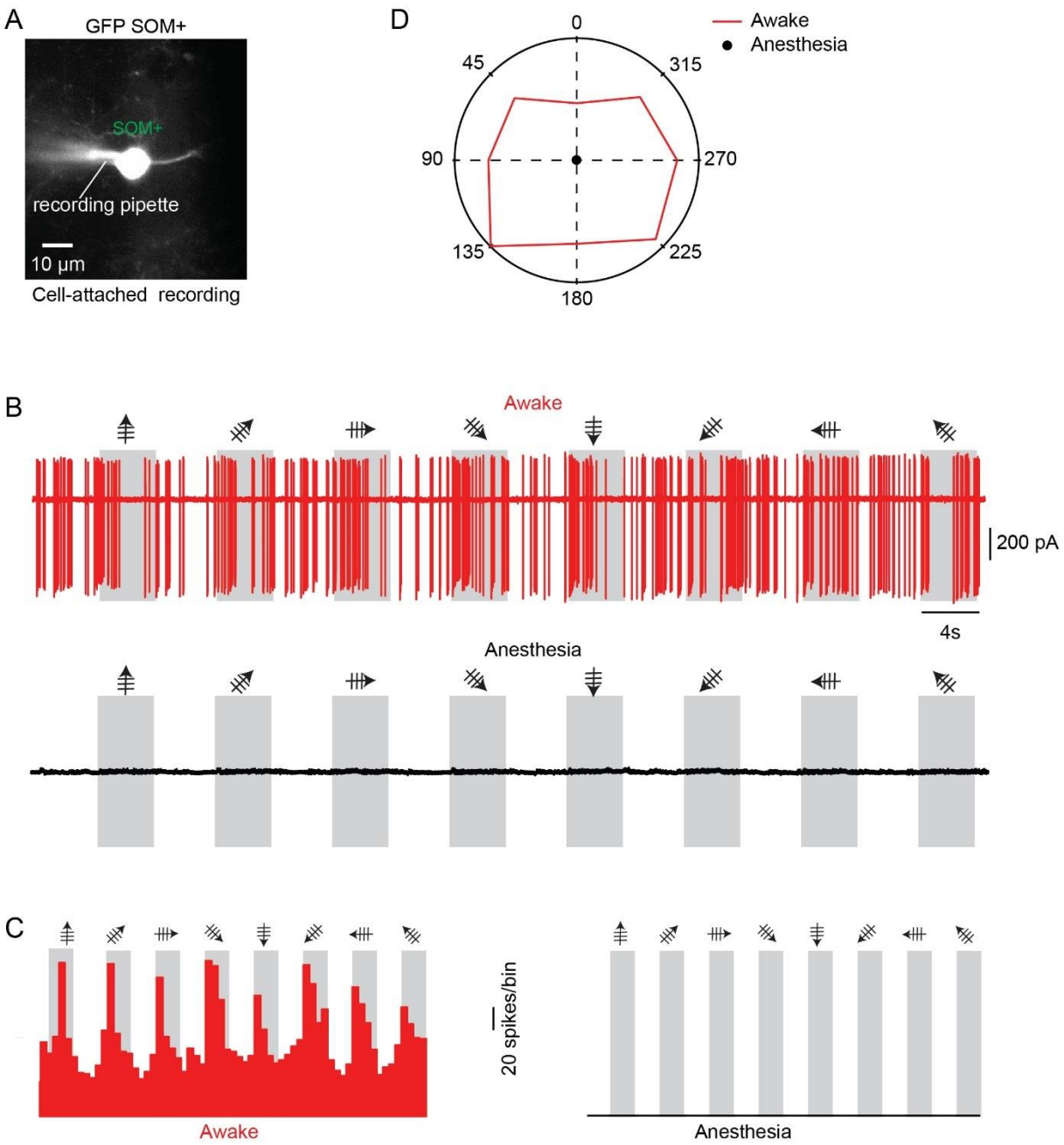

Figure18. Effects of anesthesia on responses of SOM+ interneuron

(**A**) *In vivo* two-photon image of a GFP-expressing SOM+ interneuron with the cell-attached recording pipette that was filled with 50 µM Alexa 488 dissolved in normal Ringer solution. (**B**) Top: Responses of the interneuron to drifting grating at eight different directions in the awake state. Bottom: Responses of the interneuron to the same stimulation when the mouse was anesthetized. (**C**) Peri-stimulus time histogram of 8 repeats from recordings in the awake (left panel) and anesthetized (right) states, respectively. Bin size: 1s. (**D**) Polar plots of the interneuron's responses to drifting gratings

at eight directions under awake (red line) and anesthetized (black dot) states, respectively. Responses were normalized to the maximal responses in each state.

of one such experiment with cell-attached recordings is shown in Figure19A. In the awake state, the cell showed suppressed response pattern, that is, the activity of the cell was suppressed by the drifting grating (Figure 19B and 19C). Interestingly, when the mouse is anesthetized, the suppression of responses to the drifting grating seemed to disappear or became weaker. Instead, the excitation became stronger and thus dominated during the drifting grating periods resulting in the evoked responses to drifting grating and thus changed the cell's visual responses into a 'broadly tuned' pattern (Figure 19B, 19C and 19D). These data suggest that anesthesia affects suppressed response interneuron's activity like a 'converter'.

3.3.4. Effects of anesthesia on the activity of pyramidal neurons

A previous study using extracellular recordings on pyramidal neurons in the primary visual cortex found that tuning properties in the awake animals were similar to those measured in the anesthetized animals (Niell et al., 2010). However, since this comparison was made from two neuronal populations in separate experiments, it is not clear whether this similarity can be confirmed in subsequent recordings performed under both conditions in the same cells. In this part, by using in vivo population calcium imaging, we compared the tuning properties of pyramidal neurons in the awake and the anesthetized states. We analyzed 86 cells, which showed visual responses in one or the other conditions and classified them into three groups based on their response patterns. In the first group, the cells didn't change their preferred orientation or direction when the brain state switched from the awake to the anesthetized state. In the second group, the cells showed responses only in the anesthetized state. In the third group, the cells changed their preferred orientation or direction when the brain state switched from the awake to the anesthetized state.

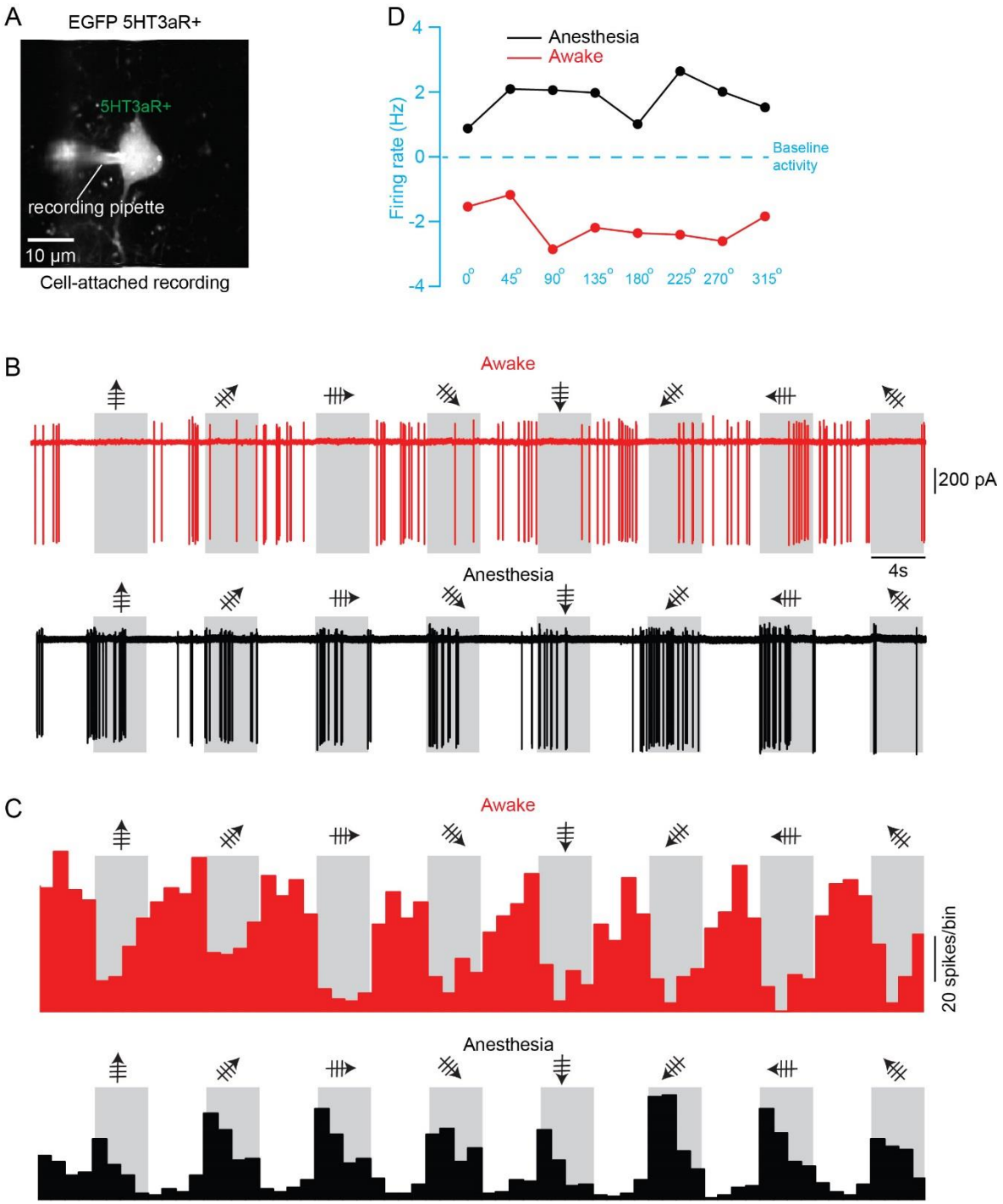

Figure 19. Effects of anesthesia on responses of the suppressed response interneuron.

(**A**) *In vivo* two-photon image of an EGFP-expressing 5HT3aR+ interneuron with the cell-attached pipette that was filled with 50 µM Alexa 488 dissolved in normal Ringer solution. (**B**) Top: Responses of the interneuron to drifting grating at eight different directions in the awake state. Bottom: Responses of the interneuron to drifting grating at eight different

directions in the anesthetized state. (**C**) Peri-stimulus time histogram of 8 repeats from recording in the awake (top panel) and anesthetized (bottom) state. Bin size: 1s. (**D**) Response curve of the interneuron to drifting grating at eight directions in the awake (red) and anesthetized (black) state.

Figure 20A shows an example cell with a tuning response pattern that is not affected by anesthesia. In the awake state, the cell reliably showed responses to one orientation (Figure 20B). In the anesthetized state, the preference for this orientation remained the same, even though response reliability and the amplitude of the response were smaller than in the awake state (Figure 20C). However, these alterations were transient and partially recovered when the mouse returned to wakefulness (Figure 20D). Figure 21A shows an experiment in which the cells' responses to visual stimulation were present under anesthesia only. In the awake state, no responses of the cell to the presentation of the drifting grating were observed, irrespective of the directions of the drifting grating. The only activity observed occurred spontaneously (Figure 21B). However, in the anesthetized state, the cell showed a preferred response to one direction of the drifting grating (Figure 21C). After returning to the awake state the cell's response disappeared again (Figure 21D). An experiment in which a cell changed tuning patterns with the two cortical states tested is shown in Figure 22A. In the awake state, this cell responded strongly and distinctively to one orientation of the drifting grating (Figure 22B, left panel and 22C). Interestingly, when the brain state switched from the awake state to the anesthetized state, the cell shifted its preference to a slightly different orientation (Figure 22B, middle panel and 22C). After returning to the awake state, the cell's response also returned to the initial tuning (Figure 22B, right panel and 22C). To determine the cell type of this neuron, we injected OGB-1 and biocytin into the cell and did a DAB staining. We found that this cell had the typical appearance of a pyramidal cell (Figure 22D).

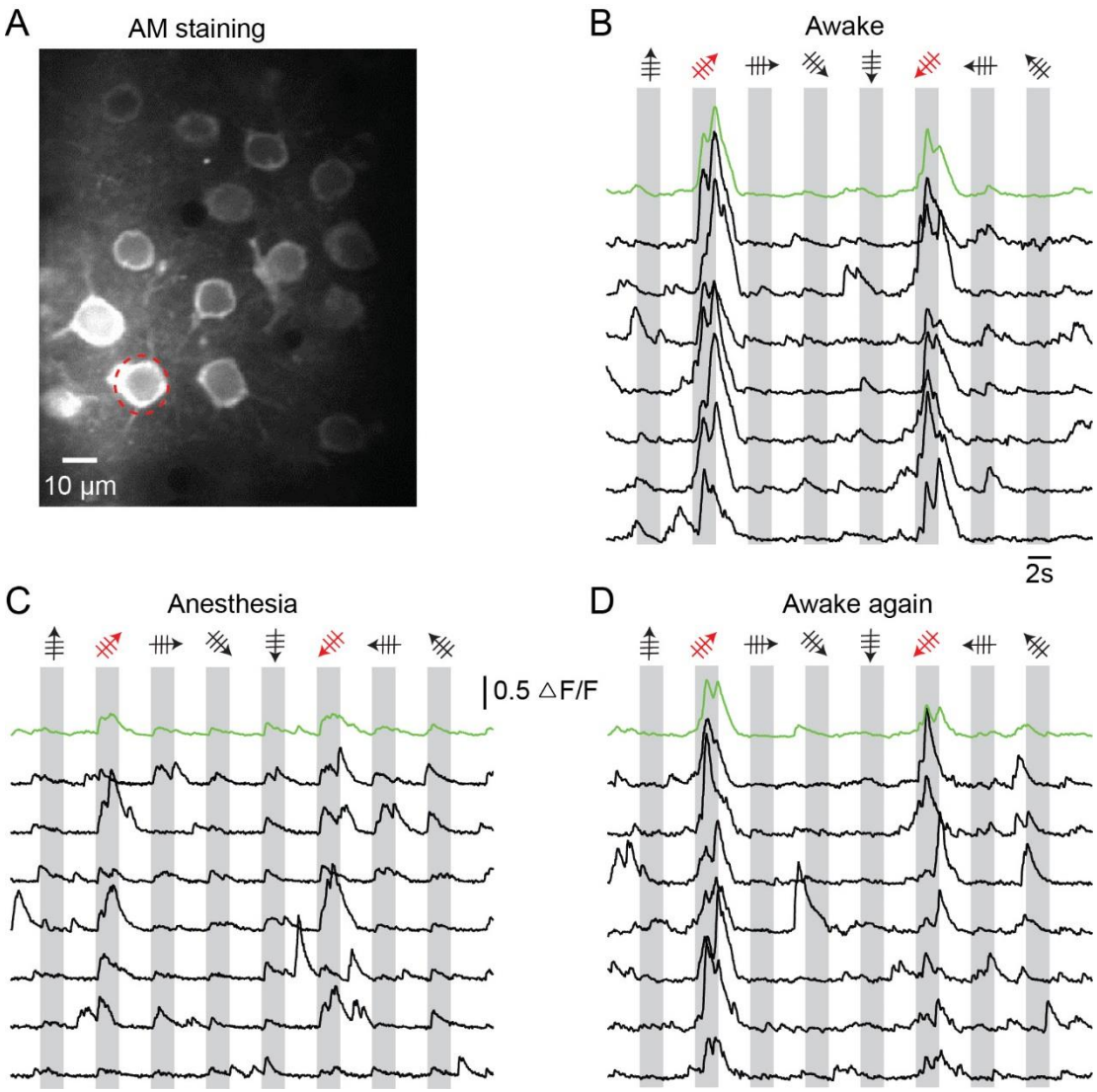

Figure 20. Tuning unchanged response pattern in the anesthetized and awake states.

(**A**) In vivo two-photon image of cortical neurons in layer 2/3 of the V1 stained with Cal-520 AM dye. (**B-C**) Calcium transients evoked by drifting grating of the cell indicated by red dashed circle in (A) showed a decreased amplitude of the response to the preferred direction in anesthetized state (**C**) comparing to the response under awake state (**B, D**). Single trials are represented with black lines and the average of all trials is shown in green. The preferred orientation of the cell in the awake and anesthetized state are marked in red.

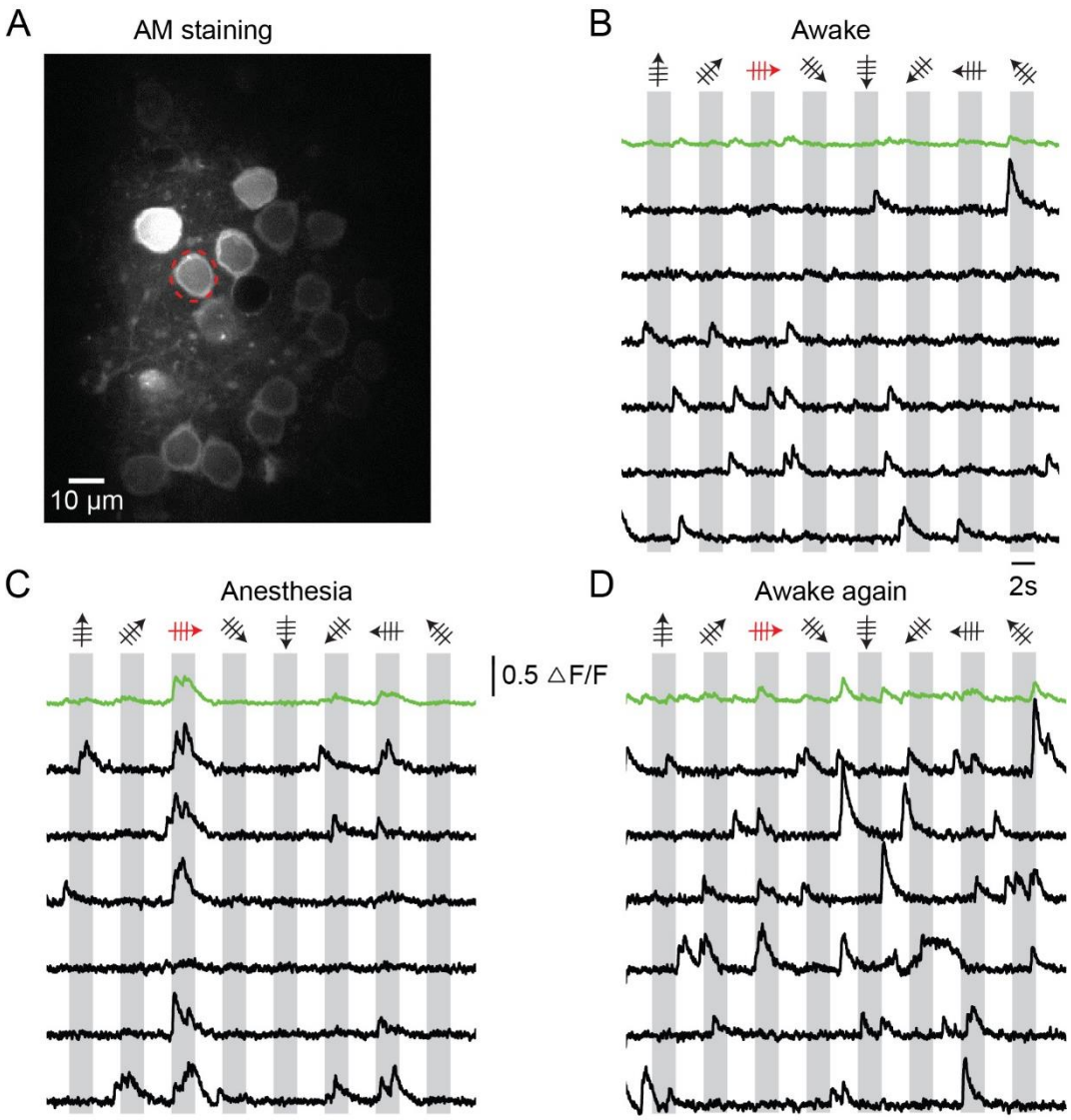

Figure 21. Cell showed response to visual stimulus only in the anesthesia

(**A**) *In vivo* two-photon image of cortical neurons in layer 2/3 of the V1 stained with Cal-520 AM dye. (**B-C**) Calcium transients of the cell indicated by red dashed circle in (A) showed an evoked response only in the anesthetized state (**C**) but not in the awake state (**B, D**). Single trials are represented with black lines and the average of all trials is shown in green. The preferred direction of the cell in the anesthetized state is marked in red.

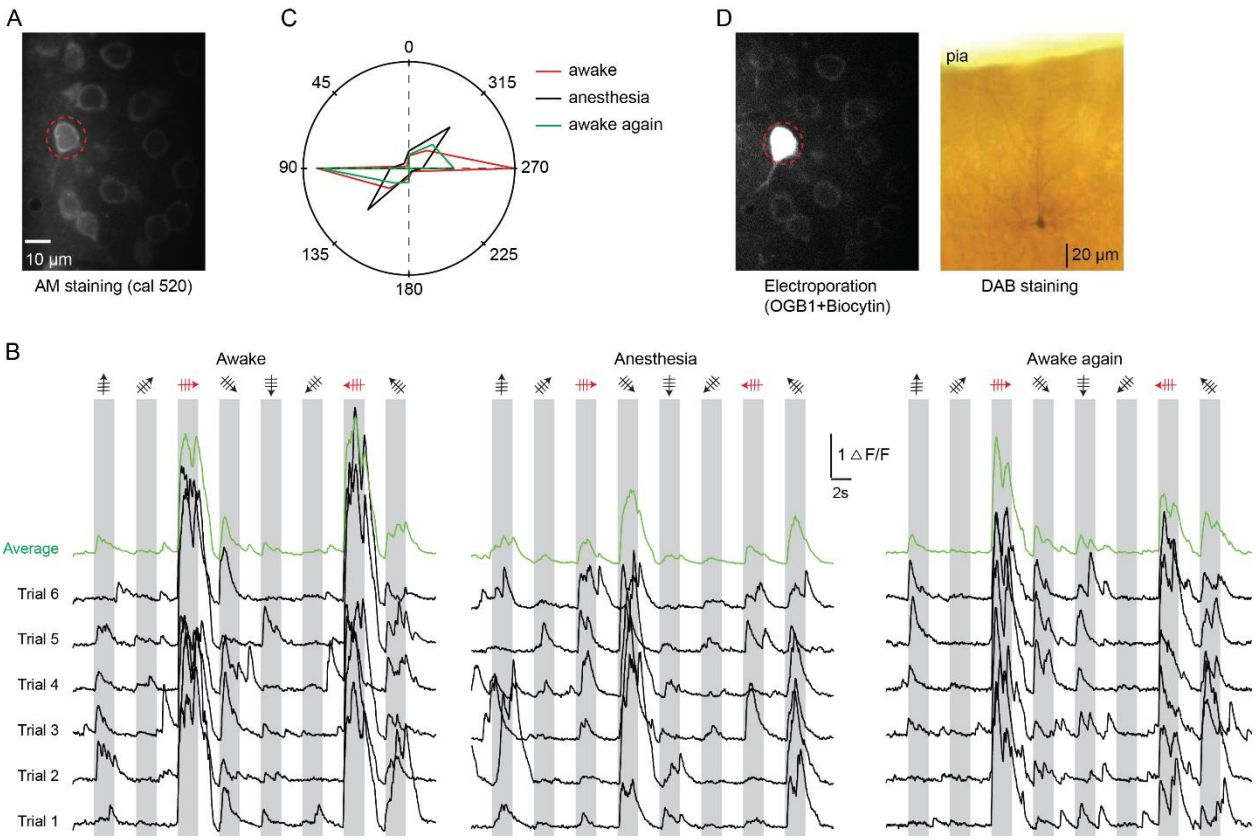

Figure 22. Tuning changed response pattern in the anesthetized and awake states. (**A**) *In vivo* two-photon image of cortical neurons in layer 2/3 of the V1 stained with Cal-520 AM dye. (**B**) Calcium transients evoked by drifting grating of the cell indicated by red dashed circle in (A) showed a change of the preferred orientation in the anesthetized state (Middle panel) comparing to the response in the awake state (left and right panel). Single trials are represented with black lines and the average of all trials is shown in green. The preferred orientation of the cell in the awake is marked in red. (**C**) Polar plots of the neuron's response to drifting gratings at eight directions in the awake (red and green trace) and anesthetized state (black trace). (**D**) Left: The cell indicated by red dashed circle in (A) was electroporated with an OGB-1 and biocytin contained solution after recording. Right: Biocytin-filled cell was visualized by DAB staining.

In summary, nearly 60% of the neurons in our study (51/86) had stable tuning patterns that were insensitive to the anesthetized state. In around one-quarter of the neurons

(21/86), preferred orientation or direction of the drifting grating was affected by anesthesia. Finally, around 16% of the neurons (14/86) were irresponsive to visual stimulation in the awake state but responded under anesthesia (Figure 23). It should be noted here that our assumption that these cells are pyramidal cells depends largely on their tuning properties. We cannot exclude the possibility that some of them are interneurons unless more tests, like morphology reconstruction are done after the recording.

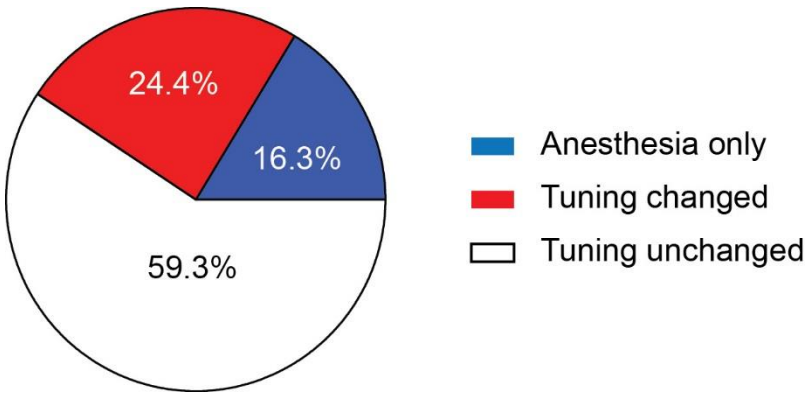

Figure 23: Relative proportions of neurons showing responses in anesthesia only, tuning sensitive to anesthesia and tuning insensitive to anesthesia response patterns.

3.4. Effects of locomotion on the neuronal activity in mouse V1

In the first part of this thesis, we reported visual stimulus-evoked responses of different subtypes of cortical interneurons during immobility of the mouse. In this part of the thesis, we focus on the effects of locomotion on neuronal activity in the V1. It needs to be pointed out that the duration of movement period was different from trial to trial. In some experiments, the mouse movement did not last long enough to match the periods of visual stimulus presentation. In this case, only the effects of locomotion on neurons' spontaneous activity were analyzed. Besides, only data from locomotion periods that lasted for at least 5 seconds were included in the analysis.

3.4.1. Effects of locomotion on PV+ interneurons

We recorded from five PV+ interneurons during running periods and analyzed locomotion effects on the spontaneous activity of these cells. In four of these cells, an increase in firing rate during locomotion was observed. The other cell, on the contrary, showed a decrease firing rate during locomotion. The running periods for those cells in which firing rates increased ranged from 6 to 36 seconds (mean = 15.1 ± 10.5 s). Figure 24A (same cell in Figure3A) depicted an experiment, in which the firing rate increased from ~13Hz when the mouse was stationary (Figure 24B) to ~30Hz when the mouse was running (Figure 24C). It is worth to noting that during the interval between two running periods, the cell's firing rate quickly returned to the stationary level and once the mouse started to move again, its firing increased again (Figure 24C). The averaged spontaneous activity during stationary periods for those four cells was 7.11 ± 2.11 Hz (Mean ± SEM, n = 4 cells) and it significantly increased to 16.44 ± 4.59 Hz during the running periods ($p < 0.05$, n = 4 cells, paired t-test). Interestingly, in the same mouse, we found another cell in which a decrease of the firing during locomotion was observed (Figure 25). We recorded the spontaneous firing of this cell during three running periods lasting for 9, 12, and 15 seconds respectively. In order to compare the responses, we choose three stationary recording periods with the same duration. During stationary periods, the spontaneous firing rate of this cell was 7.31 ± 1.01 Hz (Mean ± SD, n = 3 periods from 1 cell), whereas, when the mouse started running, the cell's firing rate significantly decreased to 0.44 ± 0,51Hz ($p < 0.01$, paired t-test).

3.4.2. Effects of locomotion on 5HT3aR+ interneurons

Locomotion also affected 5HT3aR+ interneurons' spontaneous activity. We recorded 15 cells during running periods. Among them, nine cells showed an increase in their firing rates. The running periods for those cells ranged from 7 to 23 seconds (mean = 14.93 ± 5.09s). For the six other cells, the firing rates decreased. In the experiment showed in Figure 26A, the spontaneous firing rate was 3.42 Hz when the mouse was stationary (Figure 26B). The cell's firing rate increased to 8.75 Hz when the mouse was running

(Figure 26C). The cell's firing rate quickly returned to the stationary level when the animal stopped running (Figure 26C). The averaged spontaneous activity during stationary periods for those nine cells was 4.74 ± 0.91 Hz (Mean ± SEM, n = 9 cells), and it significantly increased to 11.62 ± 2.17 Hz during the running periods ($p < 0.01$, n = 9 cells, paired t-test).

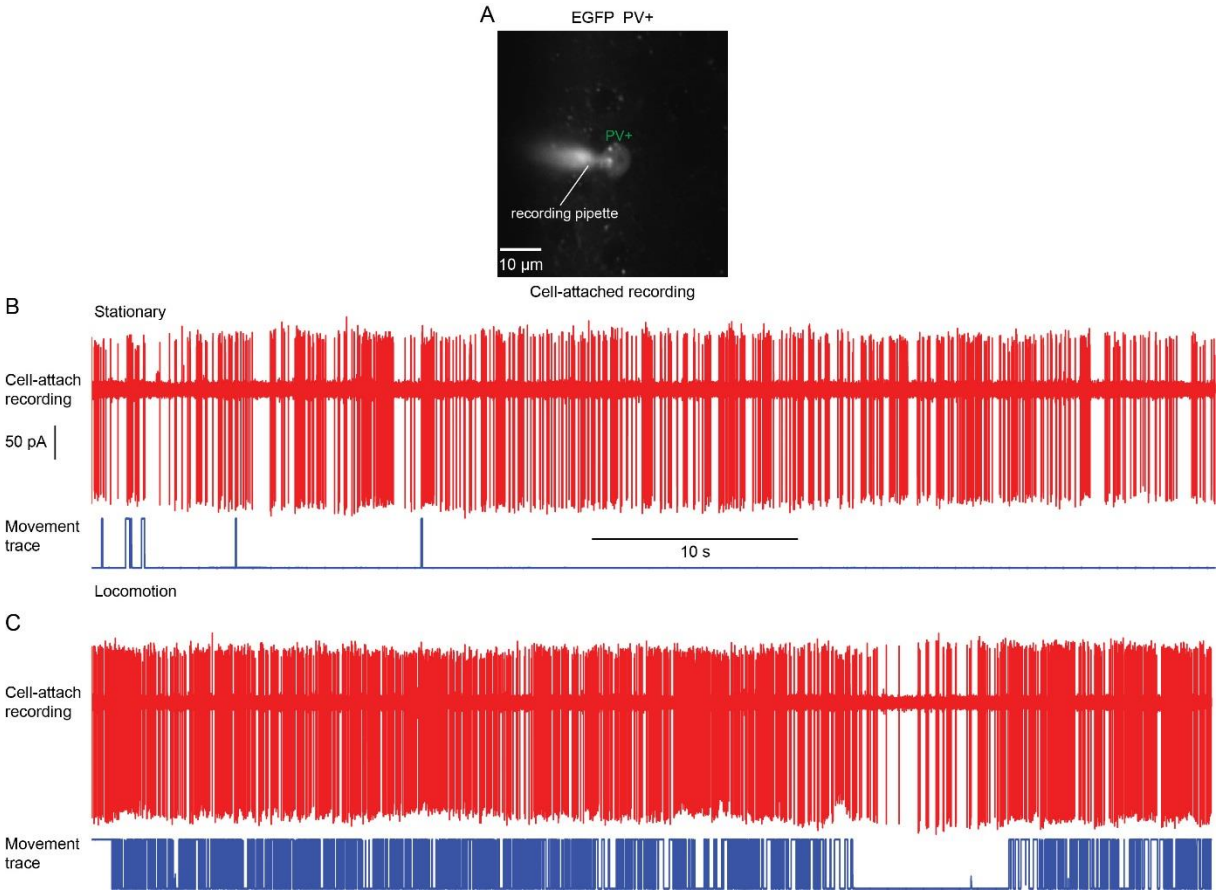

Figure 24. Locomotion increased firing rates of a PV+ interneuron

(**A**) *In vivo* two-photon imaging of an EGFP-expressing PV+ interneuron, (same cell as in Figure 3). The cell-attached recording pipette was filled with 50 µM Alexa 488 dissolved in normal Ringer solution. (**B**) Cell-attached recording from the cell in the stationary state. (C) Firing rates increased when the mouse was running.

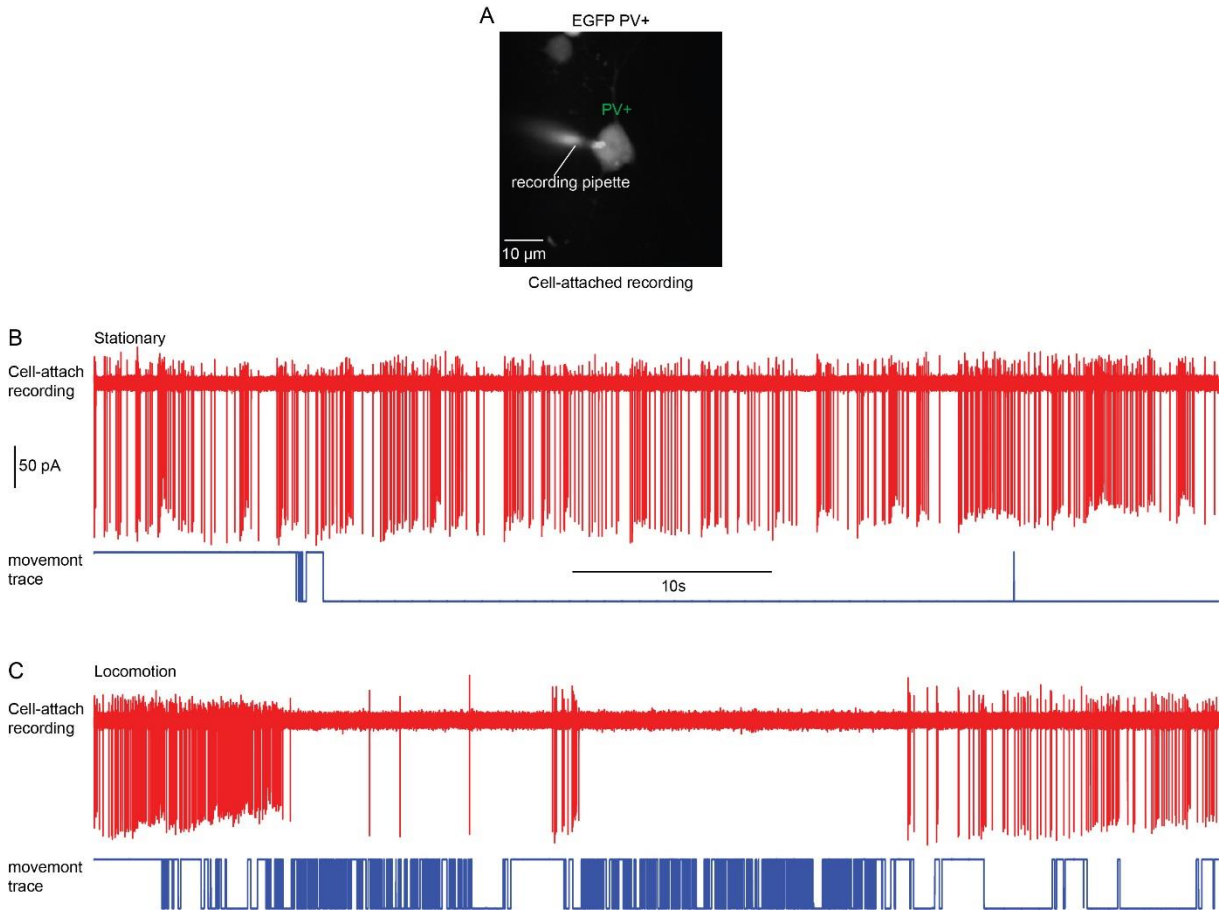

Figure 25. Locomotion decreased the activity of a PV+ interneuron

(**A**) *In vivo* two-photon imaging of a PV+ interneuron. The cell-attached recording pipette was filled with 50 µM Alexa 488 dissolved in normal Ringer solution. (**B**) Cell-attached recording from the cell in the stationary state. The interneuron showed decreasing of firing during locomotion (**C**)**.**

Similar to the results from PV+ interneurons, we found six 5HT3aR+ interneurons that demonstrated a decrease of firing rates during locomotion as shown in Figure 27. When the mouse was stationary, the spontaneous firing rate of the cell was 5.12 Hz (Figure 27B), whereas, when the mouse is running, the cell's firing rate decreased to 0.36 Hz (Figure 27C). The averaged spontaneous activity during stationary periods for these six cells was 6.93 ± 1.51 Hz (Mean ± SEM, n = 6 cells), and it significantly decreased to 1.80 ± 0.49 Hz during the running periods ($p < 0.001$, n = 6 cells, paired t-test).

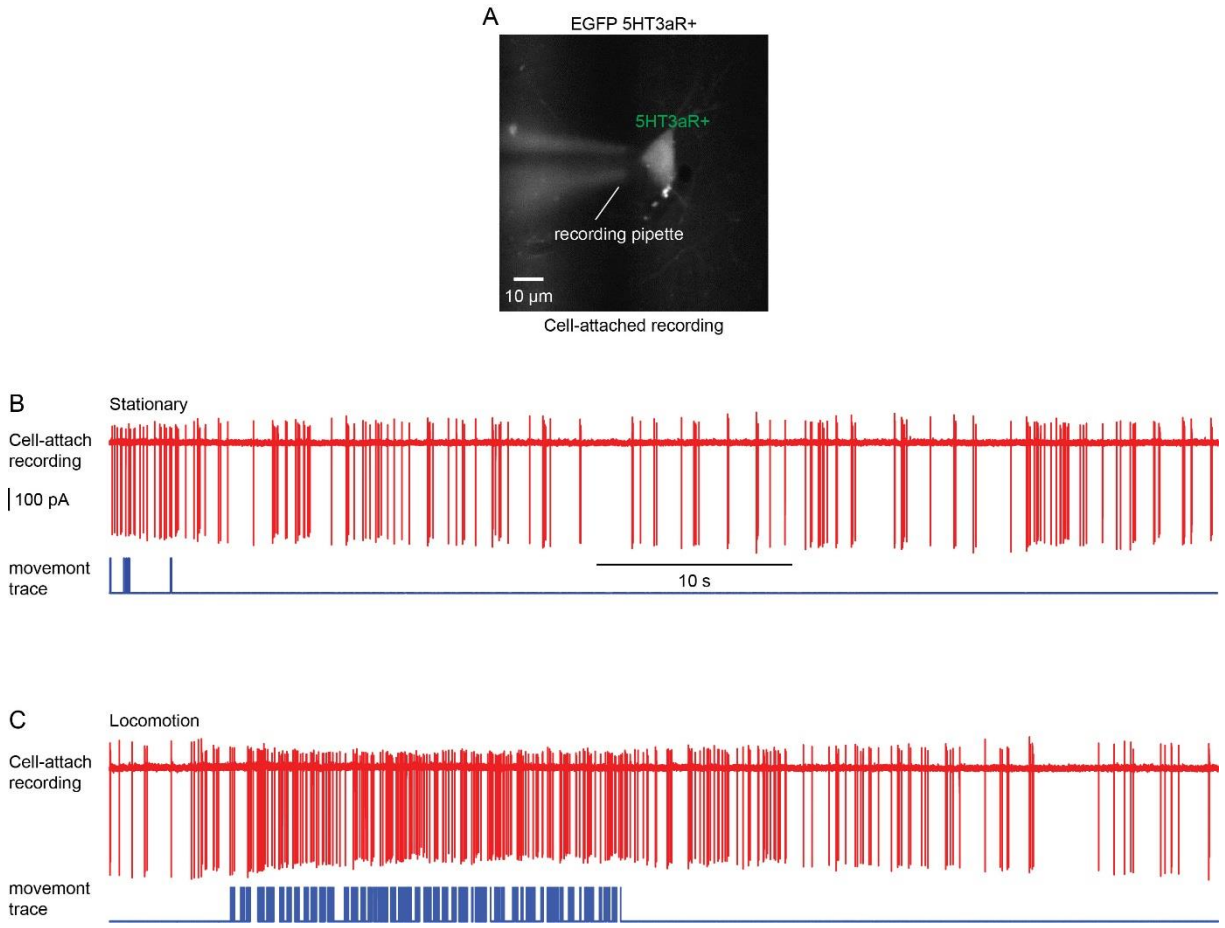

Figure 26. Locomotion increased firing rates of a 5HT3aR+ interneuron

(**A**) *In vivo* two-photon imaging of an EGFP-expressing 5HT3aR+ interneuron. The recording pipette was filled with 50 µM Alexa 488 dissolved in normal Ringer solution. (**B**) Cell-attached recording from the cell in the stationary state, spontaneous firing rates increased during locomotion (**C**).

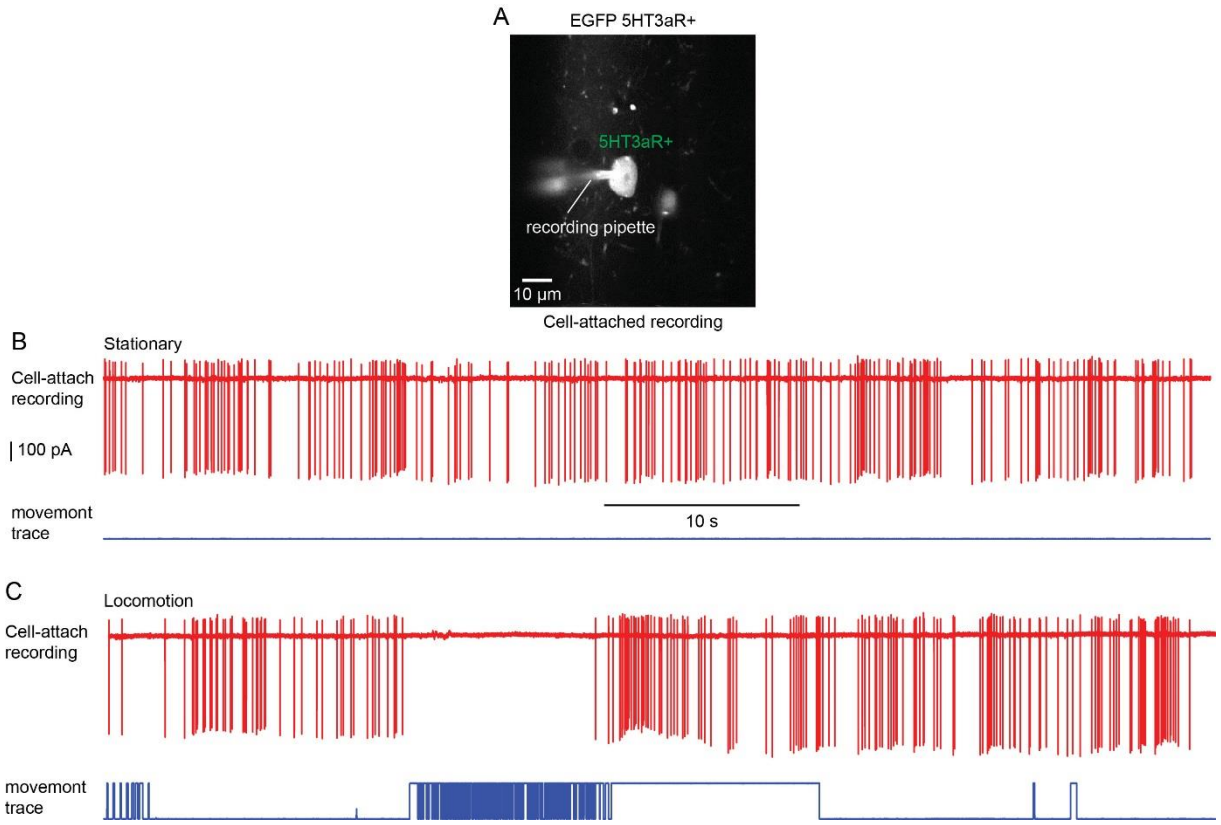

Figure 27. Decreased activity of a 5HT3aR+ interneuron during locomotion

(**A**) *In vivo* two-photon imaging of an EGFP-expressing 5HT3aR+ interneuron. The cell-attached recording pipette was filled with 50 µM Alexa 488 dissolved in normal Ringer solution. (**B**) Cell-attached recording of the cell in the stationary state. (**C**) During locomotion, the firing rate decreased**.**

In order to determine the role of local network activity in the reduction of the firing rate of these interneurons during locomotion, we labeled the 5HT3aR+ interneurons and the neurons that were around with Cal520-AM after the electrophysiological recordings, in three experiments. Then we locally applied glutamate in the vicinity of the 5HT3aR+ interneuron in order to excite its local network (Figure 27A left panel). Interestingly, although the neurons around were activated by glutamate application, the activity of 5HT3aR+ interneuron was suppressed, and once the application stopped, its activity recovered (Figure 27A right panel).

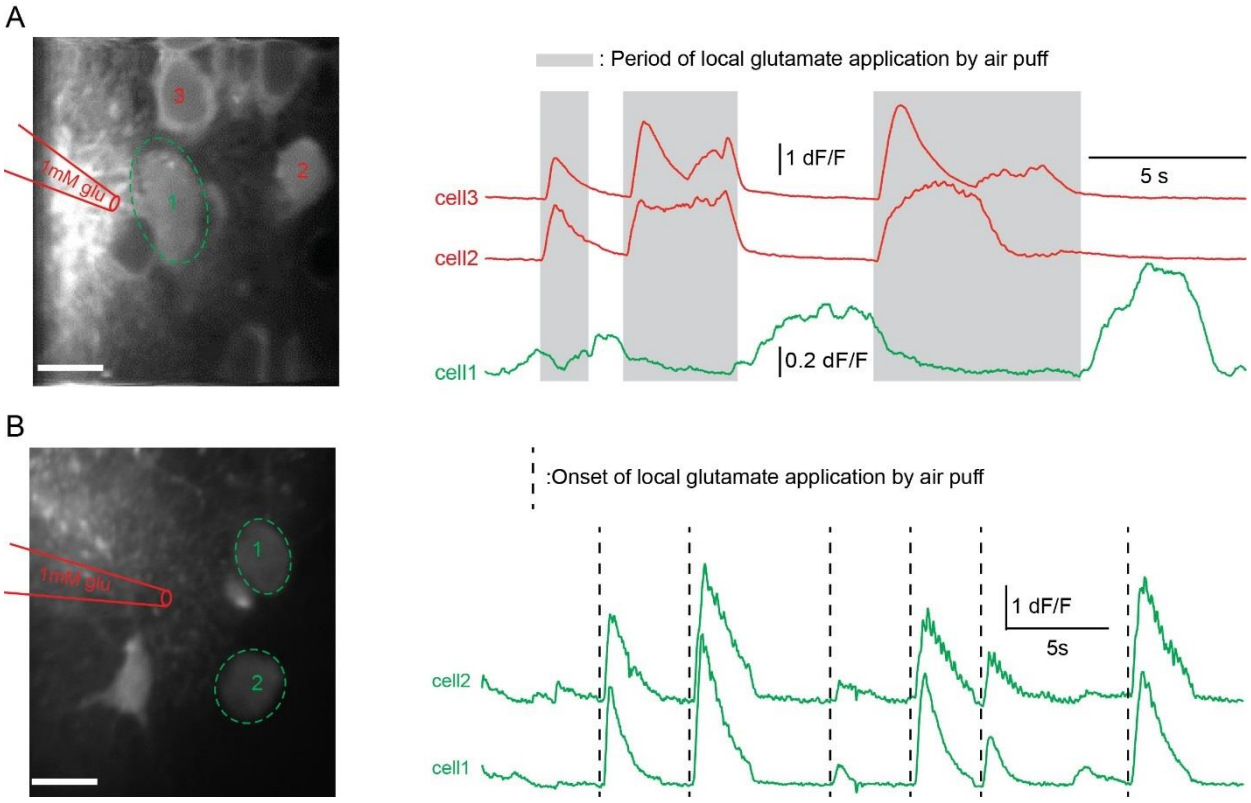

Figure 28. Local glutamate application affects 5HT3aR+ interneurons in different ways

(**A**) Left: *In vivo* two-photon image of cortical neurons in layer 2/3 of the V1 stained with the fluorescent calcium indicator dye Cal-520 AM. An EGFP expressing 5HT3aR+ interneuron is indicated by a green dashed line. Two EGFP negative cells are indicated by red dashed lines. Right: Calcium transients evoked by local glutamate application. Glutamate application periods are indicated by the gray regions. (**B**) Left: In vivo two-photon image of two EGFP-expressing 5HT3aR+ interneurons in layer 1 of the primary visual cortex stained with the fluorescent calcium indicator dye Cal-520 AM. Interneurons are indicated by green dashed lines. Right: Calcium transients evoked by local glutamate application. Onsets of glutamate application are indicated by black dashed line.

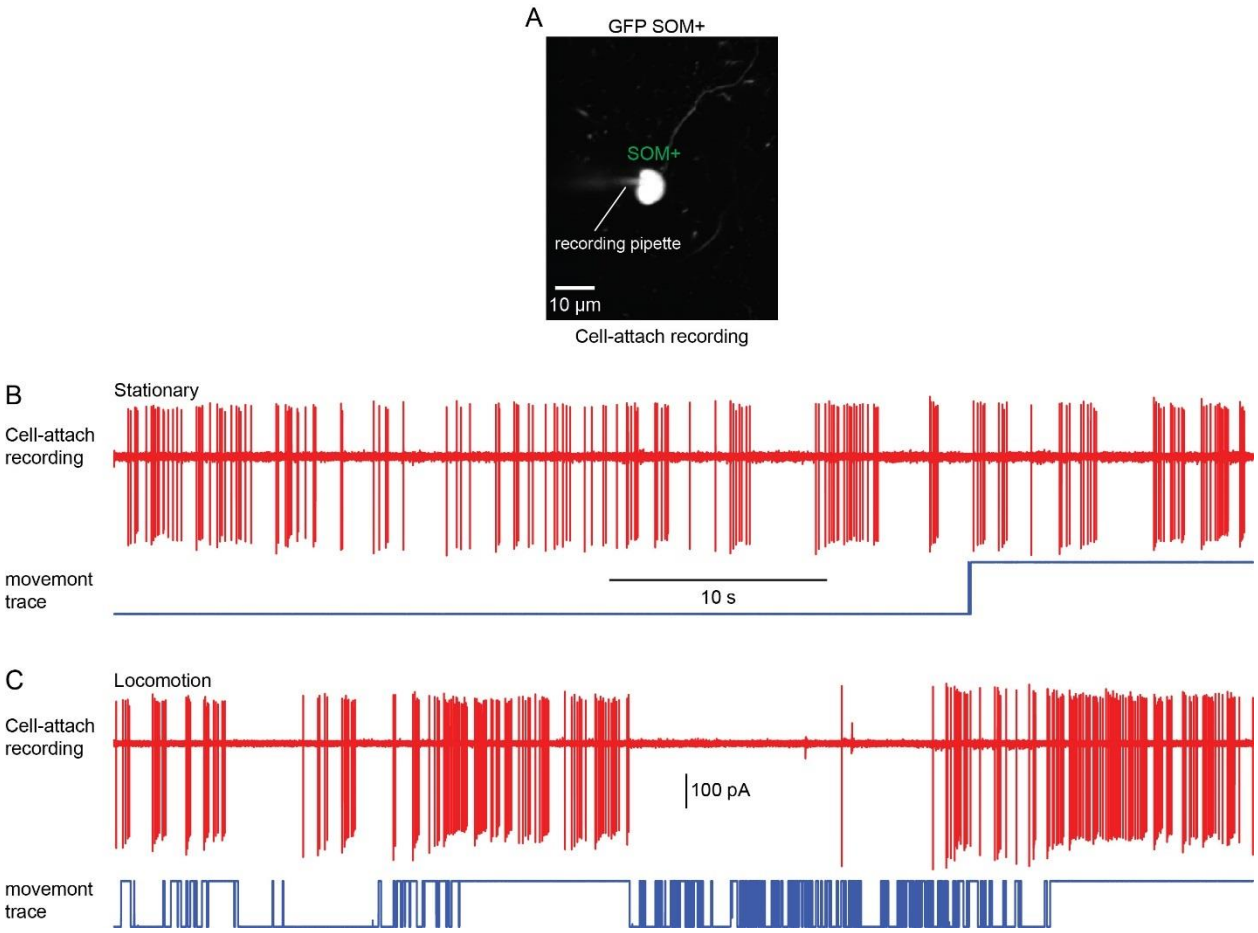

Figure 29. Decreased activity of a SOM+ interneuron during locomotion

(**A**) *In vivo* two-photon image of a GFP-expressing SOM+ interneuron. The cell-attached Recording pipette was filled with 50 µM Alexa 488 dissolved in normal Ringer solution. (**B**) Cell-attached recording from the SOM+ interneuron in the stationary state. (**C**) The firing rate was reduced when the mouse was running**.**

To find out whether the suppression of the 5HT3aR+ interneuron's activity by local network activation is a common feature of all 5HT3aR+ interneurons or not, we repeated the experiment with other randomly selected 5HT3aR+ interneurons. We found that glutamate can efficiently excite these randomly selected 5HT3aR+ interneurons as indicated by reliably evoked calcium transients in these cells (Figure 27B). These data represent evidence that the 5HT3aR+ interneurons in which the activity was reduced during locomotion belong to a unique subgroup. We conclude that the reduction of activity

of these interneurons during locomotion occurs because of the activation of the local network surrounding them.

3.4.3. Effects of locomotion on SOM+ interneuron

We successfully performed cell-attached recordings from four SOM + interneurons during running periods. In two of these cells, a decrease in their firing rate was observed. Figure 29A shows one of these experiments. When the mouse was stationary, the spontaneous firing rate was 4.19 Hz (Figure 29B), whereas, when the mouse was running, the cell's firing rate decreased to 0.75 Hz (Figure 29C). The mean value of spontaneous firing rate of SOM+ cells was 5.55 ± 1.01 Hz during the stationary period (n = 3 periods from 2 cells), whereas, when the mouse started running, the spontaneous firing rate significantly decreased to 2.48 ± 2.16 Hz ($p < 0.05$, paired t-test). In two other SOM+ cells, the firing rate was not affected by locomotion. The mean spontaneous firing rate of these two cells was not significantly different between the stationary state (8.66 ± 4.14 Hz) and the locomotion (8.94 ± 4.39 Hz; $p = 0.35$, paired t-test).

In summary, we found that locomotion has two opposite effects on PV+ interneurons and 5HT3aR+ interneurons. Whether this divergence is dependent on the identity of a specific subgroup of these interneurons is still unclear. Besides, more experiments on SOM+ interneurons are required to tackle this question.

3.4.4. Effects of locomotion on the neuronal activity of pyramidal cells

For pyramidal cells, it was found that locomotion can enhance their visual responses (Niell & Stryker, 2010). Here, we present data obtained with 25 pyramidal cells in which activities was affected by locomotion. In 18 of these cells, the activity was increased during locomotion. One example cell is presented in Figure 31A. The cell was highly orientation selective when the mouse was stationary. Locomotion increased the cell's responses both to the preferred orientation and non-preferred orientation with a more prominent increase in response to the preferred orientation (Figure 31B).

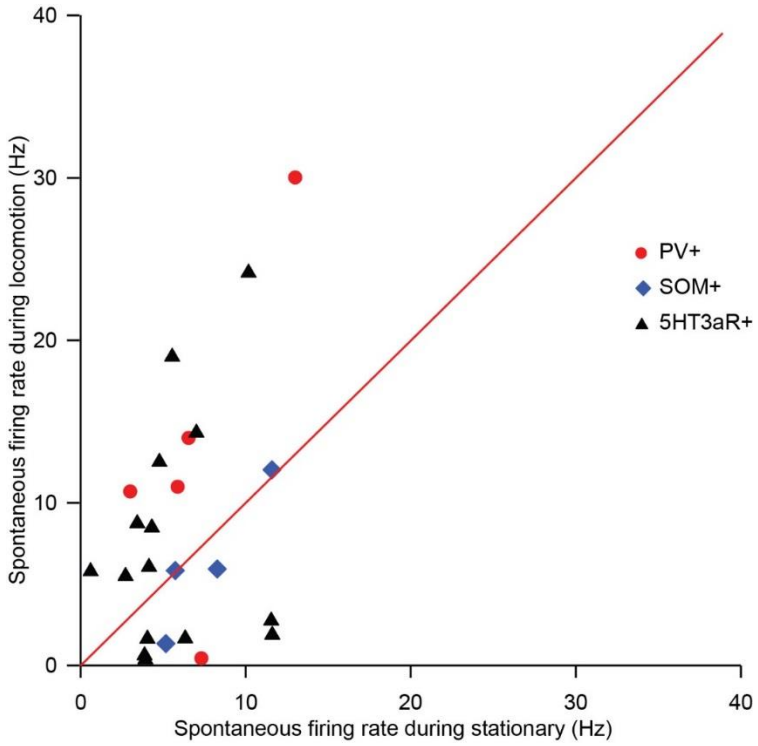

Figure 30. Firing rates during stationary periods plotted against firing rates during the locomotion periods for PV+ (red dot), SOM+ (blue diamond) and 5HT3aR+ (black triangle) interneurons.

Thus, consistent with the earlier work of others (Niell & Stryker, 2010), we found that locomotion increased the responsiveness of the cell but kept their tuning properties unaltered (Figure 31C). We also found seven cells in which the activity was reduced during locomotion. One example experiment is shown in Figure 32. There, two cells in one field of view were affected in distinct ways by locomotion. One cell (cell 1 in Figure 32A) responded to one direction of the drifting grating in a weak and unreliable way. However, it responded to the same direction very strongly during locomotion (Figure 32B top panel). The other cell (cell 2 in Figure 32A) was highly orientation selective during the stationary period and during locomotion, the response to the drifting grating was strikingly

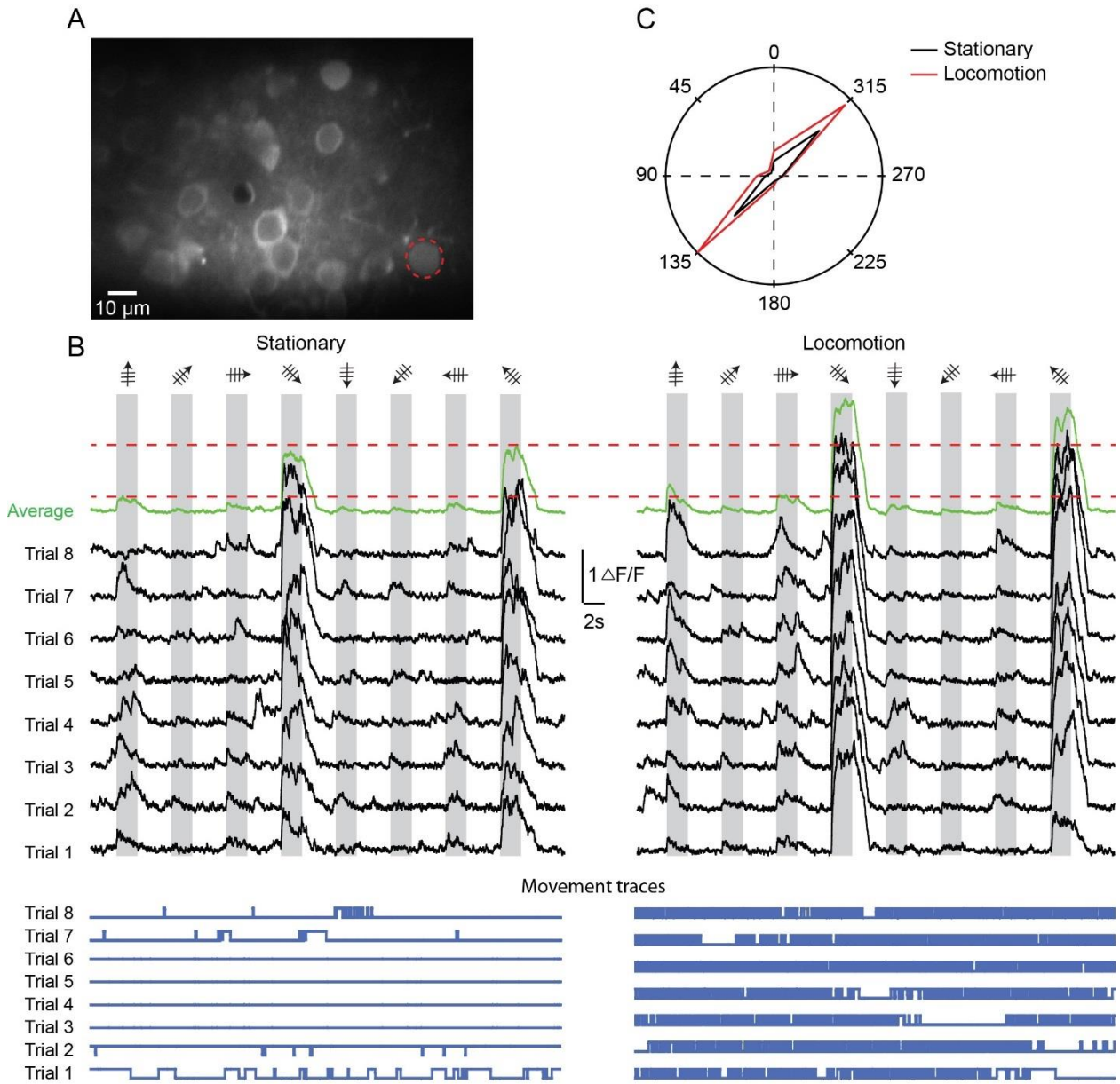

Figure 31. Locomotion increases visual stimulus-evoked responses in pyramidal neurons

(**A**) *In vivo* two-photon image of cortical neurons in layer 2/3 of the V1 stained with Cal-520 AM. An example cell is indicated by red dashed line. (**B**) Upper: Calcium transients evoked by visual stimulation of the example cell during the stationary (left panel) and the locomotion (right panel). Single trials are represented with black lines, and the average of all trials are shown in green. Bottom: Movement traces corresponding to the stationary (left panel) and locomotion (right panel).

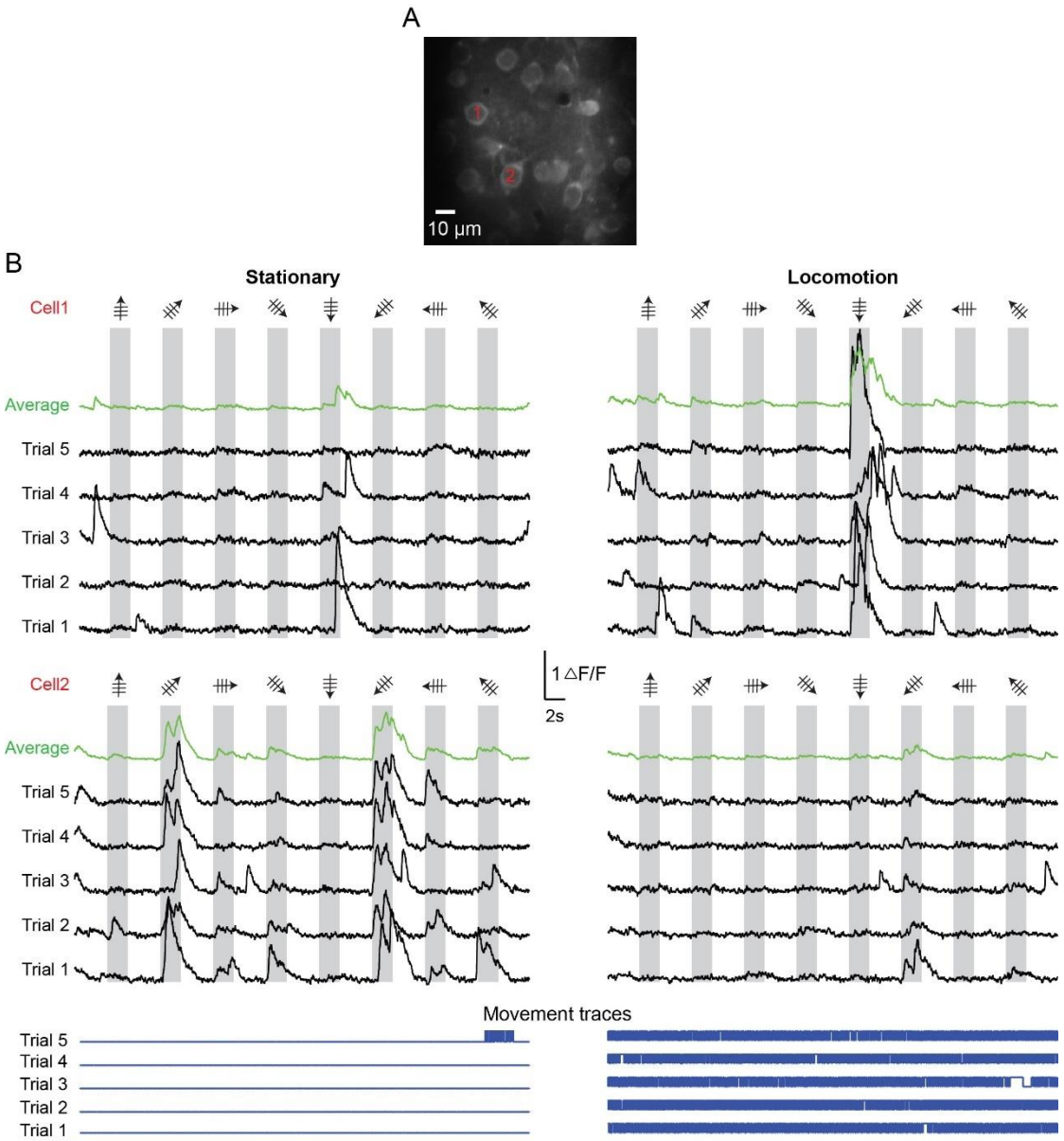

Figure 32: Visual stimulus-evoked response decreased by locomotion

(**A**) *In vivo* two-photon image of cortical neurons in layer 2/3 of the V1 stained with the fluorescent calcium indicator dye Cal-520 AM. Two example cells are indicated by red dashed lines. (**B**) Upper: Example cell showed increased responses to its preferred direction during locomotion (right panel) compared to that during stationary state (left panel). Middle: Example cell showed a decreased response to its preferred direction of the drifting grating during locomotion (right panel) compared that during stationary state (left panel) Bottom: Movement traces corresponding to stationary (left panel) and locomotion (right panel).

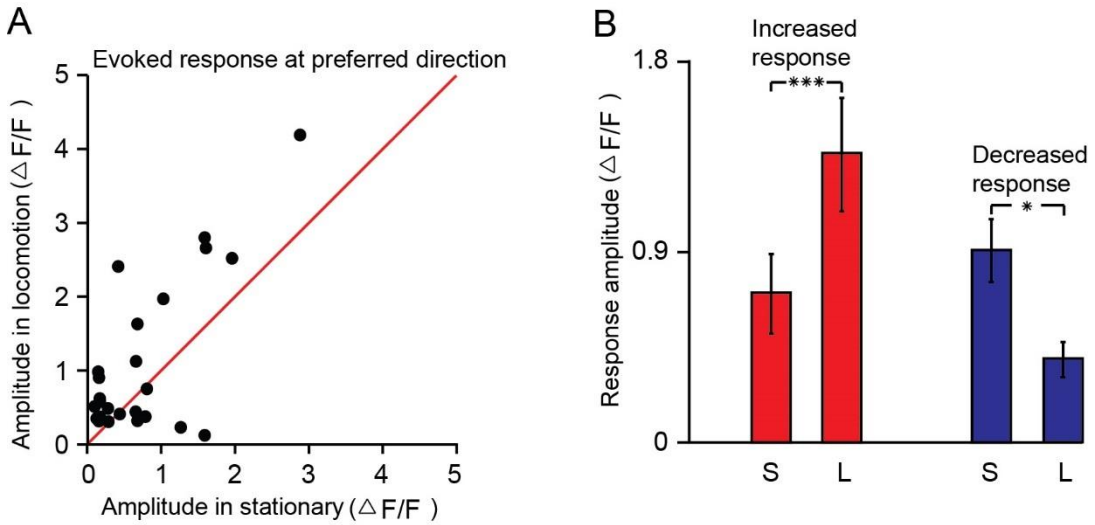

Figure 33. Locomotion affects neuronal responses to visual stimulation in different ways. (**A**) Plots of evoked calcium transients of layer2/3 neurons to the preferred direction during stationary periods versus locomotion periods. (**B**) Mean amplitudes of evoked calcium transients during stationary periods and locomotion periods for those neurons showing increased responses during locomotion periods (n = 18 cells) and neurons showing decreased responses during locomotion periods (n = 7 cells). S: stationary, L: locomotion. Error bar, SEM. * $p < 0.05$, *** $p < 0.0001$. Paired t-test.

reduced (Figure 32B middle panel). Since in most of our population imaging experiments, we did not confirm the cell types of the recorded cells, the possibility that some of them belonged to an interneuron group with high orientation selectivity in the awake state cannot be excluded. However, the data presented here indicate that there are two different effects of locomotion on neuronal activity of primary visual cortex (Figure 33A). On average, for those neurons with increased activity during locomotion, the calcium transients increased from ΔF/F = 0.70 ± 0.19 in stationary to 1.37 ± 0.27 in locomotion with a significant difference (n = 18, $p < 0.01$, paired t-test. Figure 33B). For those neurons with decreased activity, the calcium transients decreased from ΔF/F = 0.89 ± 0.15 in stationary to 0.39 ± 0.07 in locomotion with a significant difference (n = 7, $p < 0.05$, paired t-test. Figure 33B).

4. Discussion

In this study, we performed a cell type-specific characterization of the response properties of morphologically and molecularly defined interneurons and pyramidal neurons in layer 2/3 of the primary visual cortex of awake head-restrained mice. By using two-photon calcium imaging combined with various forms of patch-clamp recordings, we discovered a new type of interneuron that fulfills the role of a hub control unit of layer 2/3 neurons and characterized its morphological, functional and immunohistochemical properties. Furthermore, we determined that the response properties of the three major groups of cortical interneurons were distinctly different regarding baseline firing rates, sensory stimulation-evoked firing rates, peak response latencies, and orientation selectivity indices in the awake state. Moreover, we identified a new class of 5HT3aR positive interneurons, which was characterized by a unique and highly distinct activity profile. Morphological analyses demonstrated that this is a new type of giant basket cell (GBC) of the mouse visual cortex, which receives synaptic input from cortical layers 1 and 2/3 and provides a synaptic output through a huge axonal arbor exclusively to layer 2/3 neurons. The immunohistochemical analysis demonstrated that GBCs are positive not only for 5HT3aR but also for Vasoactive intestinal peptide (VIP), Reelin and Cholecystokinin (CCK). Besides, by comparison of the tuning property of single neurons during distinct cortical states, we found that behavior state had different impacts on a different type of neurons. In conclusion, this study demonstrates that the structural diversity of inhibitory interneurons is associated with highly distinct functional features. This functional diversity was not anticipated in previous studies and emphasizes the need for systematic structure-function analyses of neurons in awake, behaving animals.

4.1. Impairment of neuronal direction/orientation tuning by anesthesia

Starting with the study of Wurtz (Wurtz, 1969), in which the author demonstrated that the selective properties of neurons in the V1 were similar in alert and anesthetized primates, it is now widely accepted that general anesthesia has no significant impact on the neuronal responses to sensory stimuli. Recently, researchers in the field of vision research performed experiments in the mouse visual cortex and also found that tuning properties in the awake animal were similar to those in anesthetized animals (Niell & Stryker, 2010; Durand et al., 2016). However, our present findings are in striking contrast to the conclusion of those reports (see the second part of the results section). We used a highly controlled approach in which we determined the tuning properties of the same neurons repeatedly in the awake and anesthetized states. Instead of finding a similarity of the neuronal activity in the awake and anesthetized state, we found a distinct difference in the awake and anesthetized states among different groups of neurons in the mouse primary visual cortex.

For the PV+ interneurons, the reduced baseline firing and evoked firing activities in the anesthetized state were in agreement with the general idea that anesthetics mainly target on $GABA_A$ receptors and thus enhanced the inhibition (Campagna et al., 2003). For the SOM+ interneurons, in contrast to the robust responses to the visual stimulus in the awake state, we found that most tested SOM+ interneurons (5/6) ceased firing in the anesthetized state, only one cell (1/6) showed a weak response to the drifting grating. These findings were in general consistent with previous studies which demonstrated that the activity of the SOM+ interneurons was strongly suppressed by anesthesia (Kerlin et al., 2010; Adesnik et al., 2012). Two possible mechanisms can explain this. First, it is known the activity of SOM+ interneuron is largely dependent on cholinergic activity in the cortex (Fanselow et al., 2008), since the cholinergic activity decreased in the cortex during anesthesia, the SOM+ interneurons' activity would also decrease. Second, SOM+ interneurons typically receive strongly facilitating synaptic input from pyramidal neurons. Therefore, a high cortical network activity state, like wakefulness, can more likely excite the SOM+ interneuron, whereas, in a low cortical network activity state like anesthesia,

SOM+ cells cannot be activated. On the other hand, other studies in the urethane-anesthetized mice showed a delayed and weak but selective response of the SOM+ interneuron to sensory stimulus in the primary visual cortex and also the primary auditory cortex (Ma et al., 2010; Li et al.,2015). The discrepancy of these data indicates an anesthetics-specific effect on the activity of the SOM+ interneurons.

It is interesting to note that GBCs showed contrary response patterns in the different states. One possible explanation for this conversion could be a decrease of the inhibitory inputs in the anesthetized state. We presumed that these decreased inputs could be from the reduced activities of the SOM+ interneurons based on the following cues. First, unlike the fast and transient response of PV+ interneurons, SOM+ showed a robust and sustained response to the visual stimulus. Moreover, SOM+ interneuron's activities during the gray period were less than PV+ interneurons. Correspondingly, the GBCs' activities were strongly suppressed during the drifting periods but recovered during gray periods. Second, most of the SOM+ interneurons ceased firing or only showed a weak response to visual stimulus in the anesthetized state. These changes could induce the decrease of the inhibitory input to the GBCs, and thus enable the GBCs to show an evoked firing to the visual stimulus in the anesthetized state. On the other hand, since PV+ interneurons' responses to visual stimulus did not change too much, they might not be a critical factor in determining the conversion of GBCs response in the two different brain states. Third, previous studies from slice work have shown that in the layer 2/3 of the primary visual cortex, different subtypes of interneurons can interact with each other (Jiang et al., 2013, 2015; Karnani et al.,2016). Besides, it was shown that PV+ interneurons preferentially inhibited one another but not the other type of interneurons, whereas SOM+ interneurons avoided one another and inhibited all other kinds of interneurons (Pfeffer et al., 2013). This finding further supports our presumption of the SOM+ interneurons as a potential candidate to account for the changes of the GBCs' activities in different brain states.

These changes of the interneurons' activities due to the anesthesia will affect, in turn, the performance of the pyramidal cells in the cortical network. In our study of population calcium imaging, we found nearly 60% of the recorded neurons showed decrease in

response amplitudes to preferred orientation but kept their tuning unchanged. These changes in response amplitude can be attributed to an enhanced inhibition, generated by the effect of the anesthetics on GABA receptors (Campagna et al., 2003). We also found that around 16% of the cells responded only in the anesthetized state, which was consistent with the results from one recent study (Kimura et al., 2014). Besides, our finding that a portion of cells in the mouse primary visual cortex changed their tuning properties in different states challenged the conclusion that tuning properties were similar in different states from previous studies (Niell & Stryker, 2010; Durand et al., 2016). The most likely explanation for this discrepancy is that all other authors compared data recorded from different cohorts of animals during wakefulness and anesthesia respectively, so it is impossible to learn whether single neurons changed tuning or not in various states. However, by taking advantage of two-photon calcium imaging, we can compare tuning properties of the same cell in different states and thus make a more accurate assessment of how the brain states can affect cortical neurons' activity.

4.2. Response properties of the interneurons in the V1 of the awake mice

Cortical GABAergic interneurons can be classified as three non-overlapped groups according to the molecular marker they expressed (Rudy et al.,2010). In the awake mice, we found different response properties of the interneurons compared to that reported in the anesthetized mice (Ma et al., 2010; Mesik et al., 2015). In our study, SOM+ rather than PV+ interneurons showed the strongest response to the drifting gratings. Moreover, both SOM+ and PV+ interneurons showed poor orientation selectivity. Our data were in contradiction with one previous study which demonstrated that PV+ neurons showed fast, strong and poor tuned response, whereas SOM+ neurons showed a selective but delayed and weak response to the visual stimulus (Ma et al., 2010).

We found PV+ interneurons showed the highest spontaneous activities among the three interneuron groups. One previous study from slice work has shown that PV+ interneuron was enriched with potassium channel Kv3.1b which can mediate rapid action potential repolarization, fast after-hyperpolarization, and brief refractory period. Thus,

these properties enable PV+ interneurons to generate high-frequency spikes (Massengill et al.,1997). Besides, we found that PV+ interneurons showed a fast and transient response to visual stimulus. These data are consistent with previous *in vitro* work which revealed that during thalamocortical activation fast-spiking interneurons were only transiently activated because of rapid depression of their thalamocortical inputs (Tan et al., 2008).

One previous study has reported that SOM+ interneurons completely lacked surround suppression. However, PV+ interneurons and pyramidal cells in layer 2/3 of the V1 showed marked surround suppression with larger stimuli. (Adesnik et al., 2012). In our study, we found that SOM+ interneurons showed highest evoked firing rate among the three interneuron groups. This could be because in our experiment, the visual stimulus covered a large visual field of the animal (~70°× 50°), which may excite SOM+ interneurons but suppress other cells because of the surround suppression. Besides, we found that SOM+ interneurons showed a delayed response to visual stimulus compared to the PV+ interneurons. These data were consistent with previous findings from slice work which revealed that SOM+ interneurons were robustly and persistently activated after a delay (Tan et al., 2008). A similar finding was also reported in the anesthetized mice (Ma et al., 2010).

In our study, we found that 5HT3aR+ interneurons showed the lowest baseline firing and evoked firing among the three interneuron groups. Moreover, they showed the most delayed response to the visual stimulus. These response properties can be attributed to two factors. First, 5HT3aR+ interneurons received weak direct thalamic inputs only in deep layer 3 and layer 4 (Lee et al., 2010). In the superficial layer, they were biased to receive stronger inputs from other cortical areas (Lee et al.,2013; Zhang et al.,2014), thus, resulting in a delayed response compared to other neurons which received direct thalamic inputs. Second, it has been shown that the visual stimulus can elicit the release of acetylcholine in the V1 (Laplante et al.,2005). The released acetylcholine, in turn, can activate 5HT3aR+ interneurons via the nicotinic receptors (Lee et al., 2010; Fu et al.,

2014). Thus, the delayed responses of the 5HT3aR+ interneurons could be a reflection of the acetylcholine release in the V1.

Most of the Interneurons in V1 were unselective to orientation (Kerlin et al.,2010; Polack et al.,2013; Sohya et al., 2007), while a subset of interneurons showed high orientation selectivity (Ma et al., 2010; Runyan et al., 2010). In our study, we found that all recorded interneurons showed poor orientation selectivity. This was inconsistent with some studies which reported highly selective interneuron subtypes (Ma et al., 2010; Runyan et al., 2010). There are two possible explanations for this discrepancy. First, our study was performed on the awake mice, while these experiments were done in the anesthetized animal (Ma et al., 2010, Runyan et al., 2010). Since some of the ion channels like $GABA_A$ receptors, nicotinic acetylcholine receptors, 5HT3a receptors are sensitive to various anesthetics (Campagna et al., 2003), the high orientation selectivity of the interneurons could result from the effects of anesthetics. Second, due to the existence of a vast diversity of GABAergic interneurons in the cortex, it is possible that some subtype of the interneurons reported in previous studies were missing in our current data set. Interestingly, we also found a new subtype of interneuron in the 5HT3aR+ interneuron group, which, to our knowledge has not been reported before. We defined this subtype of interneuron as giant basket cell (GBC), based on their morphological and immunohistochemical characteristics. Different from other interneurons which showed evoked responses to the drifting gratings, the GBCs showed suppressed responses to the drifting gratings. There are several possibilities to account for this unique functional property of GBCs in awake mice. First, the excitatory inputs of GBC may decrease during the visual stimulus. Second, a previous study has shown that the cannabinoid receptor CB1 is selectively expressed by CCK-containing interneurons (Freund et al., 2003). The decreased activity of the GBCs during the visual stimulus could be a cannabinoid receptor mediated Long-lasting self-inhibition on these cells (Bacci et al., 2004). Third, the inhibitory inputs of GBC may increase during the visual stimulus. We presumed that SOM+ interneurons might be a candidate account for the increased inhibition. In the cortex, balanced inhibition might serve to increase the temporal precision and thereby

reduce the randomness of cortical operation (Wehr & Zador, 2003; Okun & Lampl, 2008). The suppressed responses of these interneurons may break the balance of excitation and inhibition, favor excitation and thereby enhance the neuron's response. Interestingly, in the somatosensory cortex, SOM+ but not 5HT3aR+ interneurons also showed the suppressed response to whisking (Gentet et al., 2012), indicating a modality specific of the function diversity.

Previous studies have shown that each of the three major interneuron groups can be further divided into several subgroups based on the properties of the morphological and immunohistochemical markers. For example, the PV+ group includes basket and chandelier cells; the SOM+ group includes Martinotti and non-Martinotti cells, and the 5HT3aR+ group can be segregated into VIP-positive and non-VIP positive cells. These subgroups were different in many aspects, including their functions in the local networks, the expressed markers such as PV, SOM or 5HT3aR seemed to be the only common feature between each interneuron subgroups (Tremblay et al., 2016). Therefore, it is necessary to do the systematic structure-function analyses of these neurons in awake, behaving animals.

4.3. Locomotion-dependent binary responses of the neurons in mouse V1

In this study, we determined the effects of locomotion on spontaneous firing rates in identified interneurons and on the visual response of putative pyramidal cell in layer 2/3 of mouse primary visual cortex. Our data revealed both in interneurons and pyramidal cells, the effect of locomotion on the neuronal activity was binary. Some neurons increased activity while others decreased activity during the locomotion.

In the past few years, many studies investigated possible mechanisms of the modulation of visual response by locomotion. At the cellular level, recent studies have shown that the neurons' membrane potential became more depolarized during locomotion. This depolarization enhanced the gain and improved the signal-to-noise ratio of the neurons while running. Moreover, noradrenergic rather than cholinergic input was

essential for the depolarization of excitatory neurons during running (Bennett et al., 2013; Polack et al., 2013).

The cellular mechanism of the decreased activity of the neurons during locomotion could be different in pyramidal cells and interneurons. For the pyramidal cells, a reduction in membrane potential variability which reduces the probability of membrane potential reaching the action potential threshold (Chance et al.,2002; Fellous et al., 2003), could be the reason for the decreased neuronal activity during locomotion (Schneider et al., 2014). However, it needs to be noted here is that for the increased firing pyramidal cells, the variation was also decreased (Bennett et al., 2013; Polack et al., 2013). Thus, the result of the counteraction between membrane potential depolarization and less variation may determine whether a pyramidal cell increase or decrease firing during locomotion. In the somatosensory cortex, SOM+ interneurons hyperpolarized and reduced action potential firing during whisking or running (Gentet et al., 2012; Reimer et al., 2014). It is unclear whether the decreased activity of the SOM+ interneurons in the primary visual cortex during locomotion could be due to the hyperpolarization of their membrane potential or not. Also, since currently there are no studies, to our knowledge, which report the cellular mechanisms of the locomotion related to a decreased firing of the PV+ and the 5HT3aR+ interneurons, more experiments need to be done to learn possible cellular mechanisms accounting for this.

At the circuit level, Fu et al. firstly proposed an inhibition-disinhibition circuit consisting of VIP+ and SOM+ interneurons mediated the enhancement of V1 responses by locomotion (Fu et al., 2014). However, this disinhibitory model was challenged by the finding that the activities of the interneurons during locomotion were indeed context-dependent and cell type specific (Dipoppa et al., 2016; Pakan et al., 2016). In many cases of our study, we recorded the ‘binary effects’ generated by locomotion in the same neuronal subgroups from the same animals. Since all recordings were performed in the same condition, these findings cannot be explained by the context-dependent theory. Instead, we presumed that more complex inhibition-disinhibition circuits existed in the brain to modulate neuronal responses to the stimulus from the external world.

4.4. Outlook

Interneurons represent a small but essential fraction of all cortical neurons with key roles in brain function (10%– 15% in rodents; Meyer et al., 2011). They are highly diverse regarding their morphology, connectivity, and physiological properties. Although interneurons can be divided into three non-overlapping major groups, more and more lines of evidence indicate that even individual groups of interneurons, as defined by molecular markers, are still extremely heterogeneous in terms of morphology and *in vivo* functions. Therefore, it is not feasible to assess the role of the interneurons in a local network by globally manipulating their activities using molecular genetics without considering their cell-specific functional diversity. The method devised in this study of 'reversed engineering', in which the first step is the in vivo functional characterization, followed secondarily by a morphological and immunohistochemical analysis, provides a tedious but effective strategy for a comprehensive analysis of functionally distinct neurons in the brain. An important next step will be the identification of the cell-specific synaptic circuitry in such functionally diverse neurons by using, for example, single cell rabies virus tracing methods (Wertz et al., 2015). A comprehensive understanding of the entire spectrum of in vivo cell-specific neuronal functions is the basis for understanding behavior-related neuronal codes of distinct neuronal networks.

5. References

Adesnik, H., Bruns, W., Taniguchi, H., Huang, Z.J., and Scanziani, M. (2012). A neural circuit for spatial summation in visual cortex. Nature *490*, 226-231.

Anderson, S.A., Eisenstat, D.D., Shi, L., and Rubenstein, J.L. (1997). Interneuron migration from basal forebrain to neocortex: dependence on Dlx genes. Science *278*, 474-476.

Azouz, R., Gray, C.M., Nowak, L.G., and McCormick, D.A. (1997). Physiological properties of inhibitory interneurons in cat striate cortex. Cereb Cortex *7*, 534-545.

Bacci, A., Huguenard, J.R., and Prince, D.A. (2004). Long-lasting self-inhibition of neocortical interneurons mediated by endocannabinoids. Nature *431*, 312-316.

Bennett, C., Arroyo, S., and Hestrin, S. (2013). Subthreshold mechanisms underlying state-dependent modulation of visual responses. Neuron *80*, 350-357.

Bonhoeffer, T., and Grinvald, A. (1991). Iso-orientation domains in cat visual cortex are arranged in pinwheel-like patterns. Nature *353*, 429-431.

Campagna, J.A., Miller, K.W., and Forman, S.A. (2003). Mechanisms of actions of inhaled anesthetics. N Engl J Med *348*, 2110-2124.

Cardin, J.A., Palmer, L.A., and Contreras, D. (2007). Stimulus feature selectivity in excitatory and inhibitory neurons in primary visual cortex. J Neurosci *27*, 10333-10344.

Chance, F.S., Abbott, L.F., and Reyes, A.D. (2002). Gain modulation from background synaptic input. Neuron *35*, 773-782.

Chen, X., Leischner, U., Rochefort, N.L., Nelken, I., and Konnerth, A. (2011). Functional mapping of single spines in cortical neurons in vivo. Nature *475*, 501-505.

DeFelipe, J., Lopez-Cruz, P.L., Benavides-Piccione, R., Bielza, C., Larranaga, P., Anderson, S., Burkhalter, A., Cauli, B., Fairen, A., Feldmeyer, D.*, et al.* (2013). New insights into the classification and nomenclature of cortical GABAergic interneurons. Nat Rev Neurosci *14*, 202-216.

Deisseroth, K., and Schnitzer, M.J. (2013). Engineering approaches to illuminating brain structure and dynamics. Neuron *80*, 568-577.

Dipoppa M, Ranson A, Krumin M, Pachitariu M, Carandini M, Harris KD. Vision and locomotion shape the interactions between neuron types in mouse visual cortex. BioRxiv 058396; doi: https://doi.org/10.1101/058396

Dombeck, D.A., Khabbaz, A.N., Collman, F., Adelman, T.L., and Tank, D.W. (2007). Imaging large-scale neural activity with cellular resolution in awake, mobile mice. Neuron *56*, 43-57.

Drager, U.C. (1975). Receptive fields of single cells and topography in mouse visual cortex. J Comp Neurol *160*, 269-290.

Durand, S., Iyer, R., Mizuseki, K., de Vries, S., Mihalas, S., and Reid, R.C. (2016). A Comparison of Visual Response Properties in the Lateral Geniculate Nucleus and Primary Visual Cortex of Awake and Anesthetized Mice. J Neurosci *36*, 12144-12156.

Fanselow, E.E., Richardson, K.A., and Connors, B.W. (2008). Selective, state-dependent activation of somatostatin-expressing inhibitory interneurons in mouse neocortex. J Neurophysiol *100*, 2640-2652.

Fellous, J.M., Rudolph, M., Destexhe, A., and Sejnowski, T.J. (2003). Synaptic background noise controls the input/output characteristics of single cells in an in vitro model of in vivo activity. Neuroscience *122*, 811-829.

Fenno, L., Yizhar, O., and Deisseroth, K. (2011). The development and application of optogenetics. Annu Rev Neurosci *34*, 389-412.

Franks, N.P. (2006). Molecular targets underlying general anaesthesia. Br J Pharmacol *147 Suppl 1*, S72-81.

Freund, T.F., Katona, I., and Piomelli, D. (2003). Role of endogenous cannabinoids in synaptic signaling. Physiol Rev *83*, 1017-1066.

Fu, Y., Tucciarone, J.M., Espinosa, J.S., Sheng, N., Darcy, D.P., Nicoll, R.A., Huang, Z.J., and Stryker, M.P. (2014). A cortical circuit for gain control by behavioral state. Cell *156*, 1139-1152.

Garaschuk, O., Milos, R.I., and Konnerth, A. (2006). Targeted bulk-loading of fluorescent indicators for two-photon brain imaging in vivo. Nat Protoc *1*, 380-386.

Gentet, L.J., Avermann, M., Matyas, F., Staiger, J.F., and Petersen, C.C. (2010). Membrane potential dynamics of GABAergic neurons in the barrel cortex of behaving mice. Neuron *65*, 422-435.

Gentet, L.J., Kremer, Y., Taniguchi, H., Huang, Z.J., Staiger, J.F., and Petersen, C.C. (2012). Unique functional properties of somatostatin-expressing GABAergic neurons in mouse barrel cortex. Nat Neurosci *15*, 607-612.

Goldey, G.J., Roumis, D.K., Glickfeld, L.L., Kerlin, A.M., Reid, R.C., Bonin, V., Schafer, D.P., and Andermann, M.L. (2014). Removable cranial windows for long-term imaging in awake mice. Nat Protoc *9*, 2515-2538.

Haider, B., Hausser, M., and Carandini, M. (2013). Inhibition dominates sensory responses in the awake cortex. Nature *493*, 97-100.

Hajos, N., Acsady, L., and Freund, T.F. (1996). Target selectivity and neurochemical characteristics of VIP-immunoreactive interneurons in the rat dentate gyrus. Eur J Neurosci *8*, 1415-1431.

Horikawa, K., and Armstrong, W.E. (1988). A versatile means of intracellular labeling: injection of biocytin and its detection with avidin conjugates. J Neurosci Methods *25*, 1-11.

Hubel, D.H., and Wiesel, T.N. (1959). Receptive fields of single neurones in the cat's striate cortex. J Physiol *148*, 574-591.

Hubel, D.H., and Wiesel, T.N. (1962). Receptive fields, binocular interaction and functional architecture in the cat's visual cortex. J Physiol *160*, 106-154.

Hubel, D.H., and Wiesel, T.N. (1968). Receptive fields and functional architecture of monkey striate cortex. J Physiol *195*, 215-243.

Hubel, D.H., Wiesel, T.N., and Stryker, M.P. (1977). Orientation columns in macaque monkey visual cortex demonstrated by the 2-deoxyglucose autoradiographic technique. Nature *269*, 328-330.

Inta, D., Alfonso, J., von Engelhardt, J., Kreuzberg, M.M., Meyer, A.H., van Hooft, J.A., and Monyer, H. (2008). Neurogenesis and widespread forebrain migration of distinct GABAergic neurons from the postnatal subventricular zone. Proc Natl Acad Sci U S A *105*, 20994-20999.

Jeon, C.J., Strettoi, E., and Masland, R.H. (1998). The major cell populations of the mouse retina. J Neurosci *18*, 8936-8946.

Jiang, X., Shen, S., Cadwell, C.R., Berens, P., Sinz, F., Ecker, A.S., Patel, S., and Tolias, A.S. (2015). Principles of connectivity among morphologically defined cell types in adult neocortex. Science *350*, aac9462.

Jiang, X., Wang, G., Lee, A.J., Stornetta, R.L., and Zhu, J.J. (2013). The organization of two new cortical interneuronal circuits. Nat Neurosci *16*, 210-218.

Karnani, M.M., Jackson, J., Ayzenshtat, I., Tucciarone, J., Manoocheri, K., Snider, W.G., and Yuste, R. (2016). Cooperative Subnetworks of Molecularly Similar Interneurons in Mouse Neocortex. Neuron *90*, 86-100.

Kerlin, A.M., Andermann, M.L., Berezovskii, V.K., and Reid, R.C. (2010). Broadly tuned response properties of diverse inhibitory neuron subtypes in mouse visual cortex. Neuron *67*, 858-871.

Kimura, R., Safari, M.S., Mirnajafi-Zadeh, J., Kimura, R., Ebina, T., Yanagawa, Y., Sohya, K., and Tsumoto, T. (2014). Curtailing effect of awakening on visual responses of cortical neurons by cholinergic activation of inhibitory circuits. J Neurosci *34*, 10122-10133.

Kitamura, K., Judkewitz, B., Kano, M., Denk, W., and Hausser, M. (2008). Targeted patch-clamp recordings and single-cell electroporation of unlabeled neurons in vivo. Nat Methods *5*, 61-67.

Krubitzer, L., and Kaas, J. (2005). The evolution of the neocortex in mammals: how is phenotypic diversity generated? Curr Opin Neurobiol *15*, 444-453.

Laplante, F., Morin, Y., Quirion, R., and Vaucher, E. (2005). Acetylcholine release is elicited in the visual cortex, but not in the prefrontal cortex, by patterned visual stimulation: a dual in vivo microdialysis study with functional correlates in the rat brain. Neuroscience *132*, 501-510.

Lee, S., Hjerling-Leffler, J., Zagha, E., Fishell, G., and Rudy, B. (2010). The largest group of superficial neocortical GABAergic interneurons expresses ionotropic serotonin receptors. J Neurosci *30*, 16796-16808.

Lee, S., Kruglikov, I., Huang, Z.J., Fishell, G., and Rudy, B. (2013). A disinhibitory circuit mediates motor integration in the somatosensory cortex. Nat Neurosci *16*, 1662-1670.

Li, L.Y., Xiong, X.R., Ibrahim, L.A., Yuan, W., Tao, H.W., and Zhang, L.I. (2015). Differential Receptive Field Properties of Parvalbumin and Somatostatin Inhibitory Neurons in Mouse Auditory Cortex. Cereb Cortex *25*, 1782-1791.

Ling, C., Schneider, G.E., and Jhaveri, S. (1998). Target-specific morphology of retinal axon arbors in the adult hamster. Vis Neurosci *15*, 559-579.

Ma, W.P., Liu, B.H., Li, Y.T., Huang, Z.J., Zhang, L.I., and Tao, H.W. (2010). Visual representations by cortical somatostatin inhibitory neurons--selective but with weak and delayed responses. J Neurosci *30*, 14371-14379.

Ma, Y., Hu, H., Berrebi, A.S., Mathers, P.H., and Agmon, A. (2006). Distinct subtypes of somatostatin-containing neocortical interneurons revealed in transgenic mice. J Neurosci *26*, 5069-5082.

Markram, H., Toledo-Rodriguez, M., Wang, Y., Gupta, A., Silberberg, G., and Wu, C. (2004). Interneurons of the neocortical inhibitory system. Nat Rev Neurosci *5*, 793-807.

Massengill, J.L., Smith, M.A., Son, D.I., and O'Dowd, D.K. (1997). Differential expression of K4-AP currents and Kv3.1 potassium channel transcripts in cortical neurons that develop distinct firing phenotypes. J Neurosci *17*, 3136-3147.

Matyas, F., Freund, T.F., and Gulyas, A.I. (2004). Convergence of excitatory and inhibitory inputs onto CCK-containing basket cells in the CA1 area of the rat hippocampus. Eur J Neurosci *19*, 1243-1256.

Mesik, L., Ma, W.P., Li, L.Y., Ibrahim, L.A., Huang, Z.J., Zhang, L.I., and Tao, H.W. (2015). Functional response properties of VIP-expressing inhibitory neurons in mouse visual and auditory cortex. Front Neural Circuits *9*, 22.

Metin, C., Godement, P., and Imbert, M. (1988). The primary visual cortex in the mouse: receptive field properties and functional organization. Exp Brain Res *69*, 594-612.

Meyer, A.H., Katona, I., Blatow, M., Rozov, A., and Monyer, H. (2002). In vivo labeling of parvalbumin-positive interneurons and analysis of electrical coupling in identified neurons. J Neurosci *22*, 7055-7064.

Meyer, H.S., Schwarz, D., Wimmer, V.C., Schmitt, A.C., Kerr, J.N., Sakmann, B., and Helmstaedter, M. (2011). Inhibitory interneurons in a cortical column form hot zones of inhibition in layers 2 and 5A. Proc Natl Acad Sci U S A *108*, 16807-16812.

Miyoshi, G., Hjerling-Leffler, J., Karayannis, T., Sousa, V.H., Butt, S.J., Battiste, J., Johnson, J.E., Machold, R.P., and Fishell, G. (2010). Genetic fate mapping reveals that the caudal ganglionic eminence produces a large and diverse population of superficial cortical interneurons. J Neurosci *30*, 1582-1594.

Nassi, J.J., and Callaway, E.M. (2009). Parallel processing strategies of the primate visual system. Nat Rev Neurosci *10*, 360-372.

Niell, C.M., and Stryker, M.P. (2008). Highly selective receptive fields in mouse visual cortex. J Neurosci *28*, 7520-7536.

Niell, C.M., and Stryker, M.P. (2010). Modulation of visual responses by behavioral state in mouse visual cortex. Neuron *65*, 472-479.

Ohki, K., Chung, S., Ch'ng, Y.H., Kara, P., and Reid, R.C. (2005). Functional imaging with cellular resolution reveals precise micro-architecture in visual cortex. Nature *433*, 597-603.

Ohki, K., Chung, S., Kara, P., Hubener, M., Bonhoeffer, T., and Reid, R.C. (2006). Highly ordered arrangement of single neurons in orientation pinwheels. Nature *442*, 925-928.

Ohki, K., and Reid, R.C. (2007). Specificity and randomness in the visual cortex. Curr Opin Neurobiol *17*, 401-407.

Okun, M., and Lampl, I. (2008). Instantaneous correlation of excitation and inhibition during ongoing and sensory-evoked activities. Nat Neurosci *11*, 535-537.

Oliva, A.A., Jr., Jiang, M., Lam, T., Smith, K.L., and Swann, J.W. (2000). Novel hippocampal interneuronal subtypes identified using transgenic mice that express green fluorescent protein in GABAergic interneurons. J Neurosci *20*, 3354-3368.

Pakan, J.M., Lowe, S.C., Dylda, E., Keemink, S.W., Currie, S.P., Coutts, C.A., and Rochefort, N.L. (2016). Behavioral-state modulation of inhibition is context-dependent and cell type specific in mouse visual cortex. Elife *5*.

Petilla Interneuron Nomenclature, G., Ascoli, G.A., Alonso-Nanclares, L., Anderson, S.A., Barrionuevo, G., Benavides-Piccione, R., Burkhalter, A., Buzsaki, G., Cauli, B., Defelipe, J.*, et al.* (2008). Petilla terminology: nomenclature of features of GABAergic interneurons of the cerebral cortex. Nat Rev Neurosci *9*, 557-568.

Pfeffer, C.K., Xue, M., He, M., Huang, Z.J., and Scanziani, M. (2013). Inhibition of inhibition in visual cortex: the logic of connections between molecularly distinct interneurons. Nat Neurosci *16*, 1068-1076.

Pi, H.J., Hangya, B., Kvitsiani, D., Sanders, J.I., Huang, Z.J., and Kepecs, A. (2013). Cortical interneurons that specialize in disinhibitory control. Nature *503*, 521-524.

Polack, P.O., Friedman, J., and Golshani, P. (2013). Cellular mechanisms of brain state-dependent gain modulation in visual cortex. Nat Neurosci *16*, 1331-1339.

Pronneke, A., Scheuer, B., Wagener, R.J., Mock, M., Witte, M., and Staiger, J.F. (2015). Characterizing VIP Neurons in the Barrel Cortex of VIPcre/tdTomato Mice Reveals Layer-Specific Differences. Cereb Cortex *25*, 4854-4868.

Purves D, Augustine GJ, Fitzpatrick D, HALL WC, Lamantia AS, Mcnamara JO, Williams SM. Functional Specialization of the Rod and Cone Systems. Neuroscience. 3rd edition, 2004.

Reimer, J., Froudarakis, E., Cadwell, C.R., Yatsenko, D., Denfield, G.H., and Tolias, A.S. (2014). Pupil fluctuations track fast switching of cortical states during quiet wakefulness. Neuron *84*, 355-362.

Rudy, B., Fishell, G., Lee, S., and Hjerling-Leffler, J. (2011). Three groups of interneurons account for nearly 100% of neocortical GABAergic neurons. Dev Neurobiol *71*, 45-61.

Runyan, C.A., Schummers, J., Van Wart, A., Kuhlman, S.J., Wilson, N.R., Huang, Z.J., and Sur, M. (2010). Response features of parvalbumin-expressing interneurons suggest precise roles for subtypes of inhibition in visual cortex. Neuron *67*, 847-857.

Schneider, D.M., Nelson, A., and Mooney, R. (2014). A synaptic and circuit basis for corollary discharge in the auditory cortex. Nature *513*, 189-194.

Sellers, K.K., Bennett, D.V., Hutt, A., Williams, J.H., and Frohlich, F. (2015). Awake vs. anesthetized: layer-specific sensory processing in visual cortex and functional connectivity between cortical areas. J Neurophysiol *113*, 3798-3815.

Sofroniew, N.J., Flickinger, D., King, J., and Svoboda, K. (2016). A large field of view two-photon mesoscope with subcellular resolution for in vivo imaging. Elife *5*.

Sohya, K., Kameyama, K., Yanagawa, Y., Obata, K., and Tsumoto, T. (2007). GABAergic neurons are less selective to stimulus orientation than excitatory neurons in layer II/III of visual cortex, as revealed by in vivo functional Ca2+ imaging in transgenic mice. J Neurosci *27*, 2145-2149.

Steriade, M., Amzica, F., and Contreras, D. (1996). Synchronization of fast (30-40 Hz) spontaneous cortical rhythms during brain activation. J Neurosci *16*, 392-417.

Steriade, M., Nunez, A., and Amzica, F. (1993). A novel slow (< 1 Hz) oscillation of neocortical neurons in vivo: depolarizing and hyperpolarizing components. J Neurosci *13*, 3252-3265.

Stern, E.A., Kincaid, A.E., and Wilson, C.J. (1997). Spontaneous subthreshold membrane potential fluctuations and action potential variability of rat corticostriatal and striatal neurons in vivo. J Neurophysiol *77*, 1697-1715.

Stosiek, C., Garaschuk, O., Holthoff, K., and Konnerth, A. (2003). In vivo two-photon calcium imaging of neuronal networks. Proc Natl Acad Sci U S A *100*, 7319-7324.

Tada, M., Takeuchi, A., Hashizume, M., Kitamura, K., and Kano, M. (2014). A highly sensitive fluorescent indicator dye for calcium imaging of neural activity in vitro and in vivo. Eur J Neurosci *39*, 1720-1728.

Tan, Z., Hu, H., Huang, Z.J., and Agmon, A. (2008). Robust but delayed thalamocortical activation of dendritic-targeting inhibitory interneurons. Proc Natl Acad Sci U S A *105*, 2187-2192.

Tremblay, R., Lee, S., and Rudy, B. (2016). GABAergic Interneurons in the Neocortex: From Cellular Properties to Circuits. Neuron *91*, 260-292.

Van Hooser, S.D. (2007). Similarity and diversity in visual cortex: is there a unifying theory of cortical computation? Neuroscientist *13*, 639-656.

Wang, X.D., Chen, C., Zhang, D., and Yao, H. (2014). Cumulative latency advance underlies fast visual processing in desynchronized brain state. Proc Natl Acad Sci U S A *111*, 515-520.

Wang, Y., Toledo-Rodriguez, M., Gupta, A., Wu, C., Silberberg, G., Luo, J., and Markram, H. (2004). Anatomical, physiological and molecular properties of Martinotti cells in the somatosensory cortex of the juvenile rat. J Physiol *561*, 65-90.

Wehr, M., and Zador, A.M. (2003). Balanced inhibition underlies tuning and sharpens spike timing in auditory cortex. Nature *426*, 442-446.

Wertz, A., Trenholm, S., Yonehara, K., Hillier, D., Raics, Z., Leinweber, M., Szalay, G., Ghanem, A., Keller, G., Rozsa, B.*, et al.* (2015). PRESYNAPTIC NETWORKS. Single-cell-initiated monosynaptic tracing reveals layer-specific cortical network modules. Science *349*, 70-74.

Wurtz, R.H. (1969). Visual receptive fields of striate cortex neurons in awake monkeys. J Neurophysiol *32*, 727-742.

Xu, Q., Cobos, I., De La Cruz, E., Rubenstein, J.L., and Anderson, S.A. (2004). Origins of cortical interneuron subtypes. J Neurosci *24*, 2612-2622.

Xu, X., and Callaway, E.M. (2009). Laminar specificity of functional input to distinct types of inhibitory cortical neurons. J Neurosci *29*, 70-85.

Yavorska, I., and Wehr, M. (2016). Somatostatin-Expressing Inhibitory Interneurons in Cortical Circuits. Front Neural Circuits *10*, 76.

Zhang, S., Xu, M., Kamigaki, T., Hoang Do, J.P., Chang, W.C., Jenvay, S., Miyamichi, K., Luo, L., and Dan, Y. (2014). Selective attention. Long-range and local circuits for top-down modulation of visual cortex processing. Science *345*, 660-665.

6. Acknowledgements

In the first place, I would like to thank my supervisor, Prof. Arthur Konnerth. Thank you for giving me this opportunity to work in your lab. Also, thank you for putting so much time, energy and patience into my training and learning. Under your guidance, I have got a great ability-promotion in many aspects.

Many thanks to Prof. Thomas Misgeld and Prof. Helmuth Adelsberger as members of my thesis committee to provide me a lot of supports and valuable comments on my project study.

Many thanks to Dr.Valérie Bonfardin and Dr. Monika Brill for their contributions to the immunohistochemical experiments presented in this thesis.

Special thanks to Dr. Jana Hartmann for her valuable suggestions on improving my presentation as well as writing skills.

I would like to say thanks to Dr.Tatsuo Sato, Dr.Beomjong Song, Dr.Hongbo Jia, Dr.Zsuzsanna Varga, and Yang Chen, Antje Birkner, Carsten Tischbirek for their contributions and helps in my study.

Special thanks to Prof. Dr. Xiaowei Chen (Brain Research Institute, Third Military Medical University, Chongqing, China) for his generous help and assistant during my Ph.D. study. Also, he has always been a good example for me to follow.

I would like to say thanks to the excellent technical assistance team in this institute: Dietmar Beyer, Felix Beyer, Christian Obermayer, Christine Karrer, Andreas Fohr, Rosa Karl and Petra Apostolopoulos. Thanks all of you for your strong and efficient support.

In the end, I would like to express my deepest gratitude to my parents WanBang Zhang and Xiao’e Hu, also to my wife and my daughter, you sacrifice and endure a lot to help me to finish my study. Thank you!

7. Publications

Chen XW, Förster R, Zhang K, He WJ, Ding R, Wang YH, Yang ZQ, **Zhang YH**, Stobart J, Weber B, Adelsberger H and Konnerth A. (2017) Fear learning-dependent memory trace in a neuron-glia circuit. (Under revision).